

Book of Abstracts

XIV Annual Meeting of the Italian Chapter of the European Society of Biomechanics

18-19 | June | Palermo | 2025

Organizing Committee

Luca Faes
Vincenzo La Carrubba
Salvatore Pasta
Diana Massai

Scientific Committee

Alessandra Aldieri, Alberto Audenino, Francesca Berti, Maria Cristina Bisi, Simone Borrelli, Ludovica Cacopardo, Alessandro Caimi, Federica Caselli, Chiara Catalano, Gerardo Catapano, Simona Celi, Claudio Chiastra, Monika Colombo, Michele Conconi, Michele Conti, Anna Corti, Luca Cristofolini, Enrico Dall'Ara, Francesco De Gaetano, Giuseppe De Nisco, Cristina Falcinelli, Benedetta Fantaci, Francesco Fontana, Stefano Gabetti, Diego Gallo, Pierfrancesco Gaziano, Alessio Gizzi, Julius Guccione, Emanuela Jacchetti, Luigi La Barbera, Emanuele Luigi Carniel, Giulia Luraghi, Michele Marino, Diana Massai, Valentina Mazzi, Francesco Migliavacca, Umberto Morbiducci, Salvatore Pasta, Francesco Pasqualini, Gianni Pedrizzetti, Marco Palanca, Giancarlo Pennati, Marco Pensalfini, Selene Pirola, Giovanni Putame, Riccardo Reale, Francesco Sturla, Mara Terzini, Silvia Todros, Giuseppe Vario, Emanuele Vignali, Emiliano Votta, Elisabetta Zanetti

Sponsor

exemplar solutions for complexity

Abbott

pyroscience sensor technology

MP strumenti

Patronage

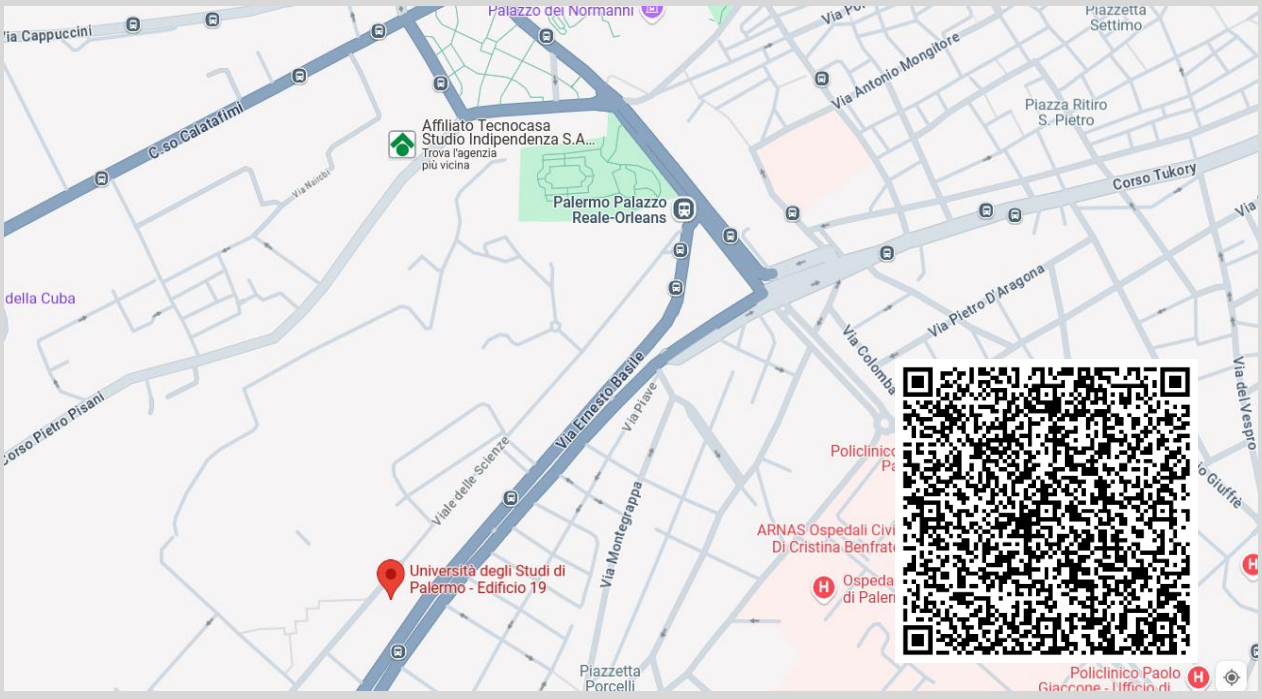
European Society of Biomechanics

Università degli Studi di Palermo

Congress Venue

Campus of the University of Palermo, Building 8 and 19, Viale delle Scienze, next to the Department of Engineering





Keynote Speakers



Stephane Avril,

Centre Ingénierie et Santé

Ecole des Mines de Saint-Etienne

Saint-Etienne

France

Title of lecture: “Benefits and impact of digital twins in vascular mechanobiology”



María Ángeles Pérez Ansón,

Instituto de Investigación en Ingeniería de Aragón
Universidad de Zaragoza
Zaragoza
Spain

Title of lecture: “Tissue engineering approaches for cancer research”

INTERVERTEBRAL DISC GEOMETRY AFFECTS VERTEBRAL STRAINS IN MULTI-VERTEBRAE FINITE ELEMENT MODELS

Alessandra Aldieri (1), Arianna Rota (1), Luca Cristofolini (2), Marco Palanca (2), Marco Viceconti (2)

1. PolitoBIOMed Lab, Department of Mechanical and Aerospace Engineering, Politecnico di Torino, Italy; 2. Department of Industrial Engineering, University of Bologna, Italy;

Introduction

In light of the limited predictive accuracy demonstrated by the clinical gold standards employed to assess the risk of vertebral fractures [l], its accurate estimation *in silico* would be crucial to prevent such events, which have implications on the quality of life as well as on healthcare systems. Physiological boundary conditions can be included in Computed tomography (CT)-based multi-vertebrae finite element (FE) models thanks to the intervertebral discs' (IVD) inclusion. However, the IVD contours can hardly be isolated from other surrounding soft tissues in CT images taken *in vivo*, so that no information concerning IVD geometry besides material properties can be obtained from CT. The aim of this work was to assess the impact of geometrical assumptions regarding the IVDs on the vertebral strains in a multi-vertebrae FE model built starting from the CT of a cadaver specimen.

Methods

CT images of a cadaver thoracolumbar four-vertebrae human spine segment were acquired. Due to the absence of other soft tissue around the spine segment, the IVDs contours were clearly visible in the images and their geometry could thus be realistically reconstructed. Hence, two different CT-based FE models were generated: a so called realistic model (M_R), where the IVDs shape was reconstructed faithfully to their appearance in the CT, and a so called idealized model (M_I), where the IVDs geometry was reconstructed by simply connecting the upper and lower vertebral endplates without considering the IVDs real shape and external bulging as visible in the CT (Fig. 1). Vertebrae were modelled with a 10-node tetrahedral mesh and with HU-based heterogenous material properties [2],[3]. The IVDs were modelled with a 20-node hexahedral mesh and adopting literature-based constitutive laws as shown in Table 1. Applied boundary conditions replicated experimental compression-flexion tests which had been performed on the same specimen, as shown in Fig. 1 [4].

Model #	*Anulus constitutive model*	*Nucleus constitutive model*
1	GOH [5]	Linear elastic [5]
2	GOH [6]	Linear elastic [6]
3	GOH [7]	Mooney-Rivlin [7]

Table 1. Overview of the literature-based constitutive laws employed to model the IVD. GOH: Gasser-Ogden-Holzapfel

Experimental displacement and strain fields were computed on the surfaces of the two central vertebral bodies (T11: control, T12: metastatic) employing a 4-camera DIC set-up (GOM Aramis 12M). Hence, FE-predicted displacements and principal deformations could also be compared to the full-field DIC experimental values.

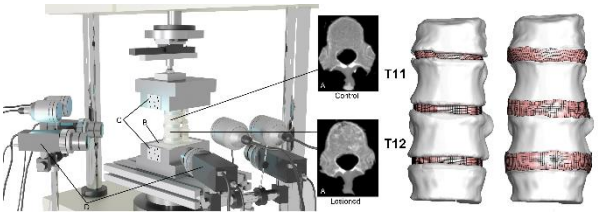


Figure 1. Experimental set-up (left) and the CT-based M_I and M_R models (right).

Results

In Fig. 2 the minimum principal strains on T11 and T12 vertebrae as detected by DIC and predicted by the models are shown. Statistically significant differences according to Mann-Whitney test ($p<0.05$) were always identified between M_R and M_I independently from how the IVD anulus and nucleus were modelled. Interestingly, with M2 strains being the closest to the experimental ones, the inclusion of the IVD realistic geometry always moved the predictions closer to the experiments.

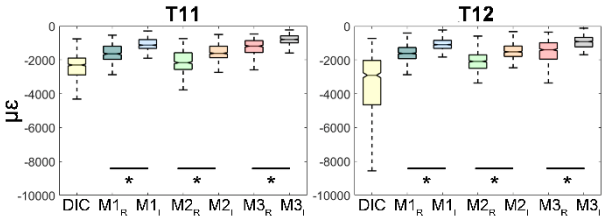


*Figure 2. DIC and FE-predicted minimum principal strains (με) on the surface of T11 and T12 vertebrae. *p<0.05.*

Discussion

Herein, the significant effect the inclusion of subject-specific information about the IVD has on CT-based FE multi-vertebrae models predictions was demonstrated, focusing specifically on IVD geometry. The possibility to draw such data from other imaging techniques (e.g., MRI) or from statistical shape models for instance, considering MRI could not be easily available, should be investigated.

References

1. Kim et al, Sci Rep, 11(1): 5553, 2021. **2.** Taddei et al, Med Eng Phys. 29(9): 973-9, 2007. **3.** Morgan et al, J Biomech, 36: 897–904, 2003. **4.** Palanca et al, Bone 151: 116028, 2021. **5.** Cavalcanti et al., ENBENG 2013. **6.** Vinyas et al., Cogent Eng 10(1): 2184446, 2023. **7.** Godinho et al., Clin Biomech, 90: 105490, 2021.

NUMERICAL SIMULATIONS TO ASSES FENESTRATED STENT-GRAFT PERFORMANCE IN AORTIC ARCH ANATOMIES

Anna Ramella (1), Giulia De Campo (1), Sara Barati (1), Virginia Fregona (1), Jasper de Kort (2), Ludovic Canaud (3), Giulia Luraghi (1), Santi Trimarchi (2,4), Francesco Migliavacca (1)

1. Politecnico di Milano, Italy; 2. IRCCS Ospedale Policlinico di Milano, Italy; 3. Centre Hospitalier Universitaire de Montpellier, France; 4. Università degli Studi di Milano, Italy

Introduction

Thoracic Endovascular Aortic Repair (TEVAR) is a minimally invasive technique to treat thoracic aorta and aortic arch pathologies by deploying a self-expandable stent-graft at the affected region. In particular, for conditions involving the aortic arch where supra-aortic vessels are located, the adoption of fenestrated stent-grafts (fen-SG) is on the rise [1]. This approach helps maintain blood flow to the upper body and arms while avoiding supra-aortic vessel bypass surgery. In the recent literature, there has been an increase in the use of numerical models in the TEVAR field. However, there remains a gap in studies that numerically assess the mechanical performance of fen-SG in patient-specific anatomies. This study aims to fill it by developing a comprehensive numerical workflow that integrates validated Finite Element Analysis (FEA)[2] and Computational Fluid Dynamics (CFD) simulations to thoroughly assess the biomechanical behavior of fen-SGs in patient-specific scenarios.

Materials and Methods

Clinical data. Three patient-specific aortic geometries with pathology at the aortic arch level are collected from Policlinico di Milano Hospital and Centre Hospitalier Universitaire de Montpellier. The patients were treated using the Canaud technique to create fen-SG[3]. Canaud fen-SGs are manually fabricated from Medtronic Valiant Captivia stent-grafts and are composed of two fenestrations [Fig.1-top]: a larger proximal one for the brachiocephalic and left common carotid arteries, and a smaller reinforced one for the left subclavian artery.

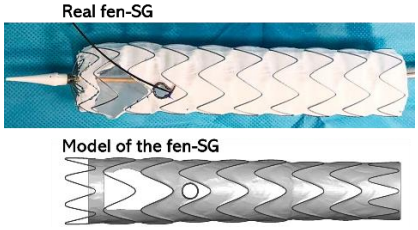


Figure 1: Real (top) and numerical (bottom) models of the Canaud fenestrated stent-graft (fen-SG).

Numerical models. Aortic anatomies are segmented from pre-operative Computed Tomography (CT) images. The fen-SG numerical model has been recreated modifying the mesh of an already validated one [Fig.1-bottom][3]. The aorta and stent-graft discretization technique and material properties are taken from previous studies [2,4]: linear elastic shell elements and zero-pressure inclusion for the aorta; fabric PET material and membrane elements for the graft; beam elements and nitinol material for the stent. The validated tracking FEA simulation [2] replicates the fen-SG implantation. FEA results are compared against post-op CT images for validation. Then, the output of the structural model is used as input for CFD simulations to assess blood flow after the procedure. An inlet velocity waveform and 3-elements WK circuits at the outlets are imposed as boundary conditions. Blood is treated as Newtonian. Fen-SG and aorta interactions are assessed by analysing vessel wall stress maps. The device apposition to the aortic wall and proximal sealing are assessed by calculating distances from structural modelling (contact maps) and extracting CFD blood flow paths.

Results

The FEA validation results [Fig.2-a] reached a good overlap between simulated and real fen-SG with an error of 6% on average. Fig.2-b depicts an example of FEA contact map and CFD blood flow at a systolic peak for the same patient.

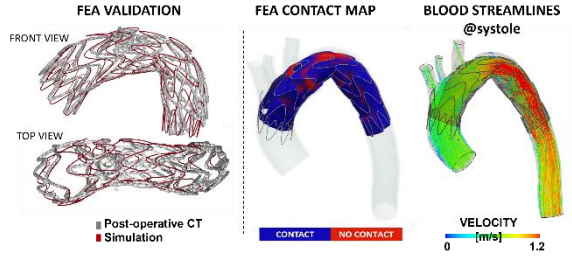


Figure 2: FEA and CFD results for one patient as example. (a) Fenestrated TEVAR simulation validation (red:simulation; grey:segmentation form post-op CT). (b) Post-processing analysis of the device sealing.

Discussion

This study developed and validated a methodology for replicating fen-SG implantation for the first time in the literature, enabling a novel combined FEA and CFD approach. It enhances the assessment of sealing performance towards predicting fenestrated TEVAR complications.

References

1. Nation et al. *Semin Intervent Radiol* 2015;**32**(3):265–71.
2. Ramella et al. *Ann Biomed Eng* 2022;**50**(12):1941–53.
3. Canaud L et al. *J Endovasc Ther* 2024;**31**(1):89–97.
4. Ramella et al. *Biomech Mod Mechanobiol* 2024;**23**(2):525

Acknowledgements

This work was carried out within the MUSA: "Multilayered Urban Sustainability Action" and "PRIN 2022 Mission 4, Component 1: 2022L3JC5T" projects, funded by the European Union – NextGenerationEU, under the National Recovery and Resilience Plan (NRRP).

BIOMECHANICAL EFFECTS OF CORNEAL COLLAGEN CROSSLINKING IN PORCINE MODELS

Anna Pia Bonuomo (1,2) , Ibrahim Seven (3), Pat Lopath (3), Federica Boschetti (2), Anna Pandolfi (1)

[1] Civil and Environmental Engineering Department, Politecnico di Milano, Milan, Italy,
[2] Chemistry, Materials, and Chemical Engineering Department, Politecnico di Milano, Milan, Italy,
[3] TECLens, Inc. (9 Riverbend Dr S, Stamford, CT 06907, USA).

Introduction

Corneal collagen crosslinking (CXL) is a leading therapeutic approach to strengthen the corneal stroma and address ectatic disorders such as keratoconus and post-LASIK ectasia [1,2]. CXL enhances corneal biomechanical stability and halts disease progression by inducing covalent bonds within the stromal collagen matrix [2,3]. Traditional epi-off protocols achieve high efficacy but entail significant patient discomfort and extended recovery periods. Epithelium-preserving (epi-on) CXL protocols aim to reduce invasiveness while maintaining therapeutic outcomes [4]. This study investigates the biomechanical impact of epi-on CXL using porcine corneas, focusing on the effects of varying UV-A exposure durations. The goal is to optimize CXL protocols by balancing biomechanical efficacy with patient comfort and enabling customized treatments tailored to individual needs by varying UV-A exposure durations.

Methods

Fresh porcine corneas were harvested and mounted onto an anterior inflation chamber pressurized to 4 mmHg. Inflation tests were conducted on excised epi-on porcine corneas, monitoring the corneal dome's configuration change at specific pressures. After preconditioning with cyclic pressure (4–20 mmHg), corneal thickness was assessed via optical coherence tomography (OCT). Only corneas with thicknesses between 600 µm and 800 µm were included. Riboflavin 0.5 mL and NaCl 0.1 g were introduced via a reservoir lens for 30 minutes under 12 mmHg. This combination was used because riboflavin alone caused swelling due to differences in osmolarity between riboflavin and the porcine cornea. Hydration and osmotic balance were maintained using Hanks' Balanced Salt Solution (HBSS). Epi-on CXL was performed under 12 mmHg with UV-A irradiation at 4 mW/cm² for 10, 20, or 30 minutes. Pre- and post-crosslinking stiffness was evaluated through pressure cycling and 3D OCT imaging.

Results

Preliminary results showed a clear stiffening effect of the corneas post-CXL compared to pre-CXL until physiological intraocular pressure levels. The observed reduction in apex displacement after crosslinking suggests an improvement in stromal biomechanical properties (*Figure 1)*. Tests conducted so far have been performed using 30 minutes of UV-A exposure, demonstrating the potential of this duration to achieve significant stiffening. This trend is consistent with past studies highlighting the relationship between UV-A exposure and corneal stiffening [3]. While detailed analysis is ongoing, it is hypothesized that the stiffening effect is influenced by both the duration of UV-A exposure and the depth of riboflavin penetration. Further studies are required to validate these findings and to optimize the parameters of the epi-on CXL protocol for consistent and effective outcomes.

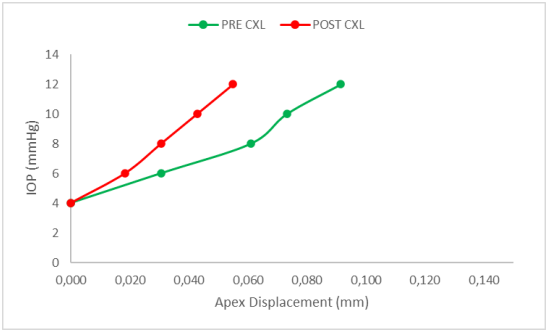


Figure 1: Inflation tests for the cornea groups irradiated for 30 minutes. IOP versus apex displacement: comparison between the untreated (PRE CXL) corneas and the treated (POST CXL) corneas.

Discussion

This study highlights epi-on CXL as a less invasive alternative. Preliminary results show significant post-CXL corneal stiffening, even at physiological IOP, validating the 30-minute UV-A exposure. Key strengths include epithelium preservation and CXL at physiological IOP, enhancing clinical relevance. Riboflavin and NaCl countered osmolarity-induced swelling, ensuring proper stromal penetration. Integrating experimental findings into FEA models will support personalized treatment planning.

References

1. Pandolfi et al., Biomech. Model. Mechanobiol, 5(3), 237–246, 2006.
2. Cornaggia et al., Mech. Soft Mater, 2, 15, 2020.
3. Boschetti et al., PLoS ONE, 16(4), e0249949, 2021.
4. Bonfanti et al., Proc. R. Soc. A, 479(2279), 2023.

MECHANICAL CHARACTERIZATION OF 3D-PRINTED STENT-GRAFTS: EFFECTS OF DESIGN AND PRINTING PARAMETERS THROUGH EXPERIMENTAL TESTING AND COMPUTATIONAL SIMULATIONS

Luca Battaglia (1), Giovanni Spinella (2) , Franca Scocozza (3) e Michele Conti (3)

1. Dipartimento di Medicina Sperimentale, Università di Genova, Genova, Italia 2. Dipartimento di Chirurgia vascolare ed endovascolare, Ospedale Policlinico San Martino, Genova, Italia 3. Dipartimento di Ingegneria Civile e Architettura, Università di Pavia, Pavia, Italia

Introduction

The treatment of aortic diseases requires innovative solutions to improve the effectiveness and safety of surgical interventions [1]. Off-the-shelf (OTS) endografts often lack the compliance needed to adapt to patient-specific anatomies, increasing procedural risks. Additive Manufacturing (AM) and numerical simulations offer transformative opportunities by enabling the customization of 3D-printed endografts with tailored morphological and mechanical properties. Advanced methods, such as finite element analysis (FEA), facilitate accurate predictions of stent behavior under physiological conditions, optimizing both design and performance. The aim of this study is to predict the behavior of customized endografts, 3D-printed with specific variations in their morphological and mechanical characteristics (Fig. 1).

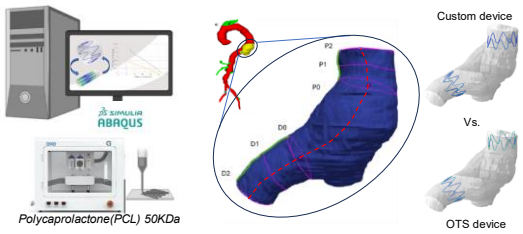


Figure 1: From CAD model to 3D printing and FEA simulation

Methods

To evaluate the feasibility of producing customized endografts using 50 kDa polycaprolactone (PCL), Chronic Outward Force (COF) was assessed through numerical crimping simulations validated against experimental data. Endograft rings were designed using CAD models derived from Valiant™ Captivia™ OTS devices, with configurations featuring eight (N8) or five (N5) ridges, a nominal diameter of 30 mm, a wire diameter (dw) of 0.5 mm, and a height of 15 mm. These rings were 3D-printed using a pneumatic extrusion system (Axolotl Axo A3), calibrated to deposit planar W-shaped PCL rings with a 0.5 mm nozzle. Post-printing, rings were thermally welded to achieve their final geometry, ensuring fidelity to CAD dimensions. Micro-CT imaging and compression tests were employed to validate shape fidelity and mechanical performance. Rings were compressed uniaxially at defined speeds using an MTS machine and analyzed for Reaction Forces within clinically relevant oversizing ranges (10–20%), referred to as RF_{ovs}. An FEA simulation using Abaqus/CAE with material-specific parameters, integrating morphological deviations from micro-CT imaging, validated the mechanical response of PCL. The same FEA model was applied to nitinol analogs, simulating crimping-induced deformation and release in patient-specific aortic proximal and distal Landing Zones (LZs).

Results

Compression tests on 3D-printed rings (N8 and N5) revealed average RF_{ovs} of 1.8×10^{-3} N (N8) and 2.2×10^{-3} N (N5). Numerical simulations validated these results, predicting 1.9×10^{-3} N (N8) and 2.0×10^{-3} N (N5), with RF_{ovs} falling within ±10% of experimental data. Validated crimping and release simulations confirmed significant RF reductions for PCL compared to nitinol (4 to 50 times lower). However, design parameters were shown to influence COF. An optimized N6 ring with dw = 0.8 mm achieved RF_{ovs} comparable to nitinol OTS devices, reaching 1 N, demonstrating feasibility for endovascular applications (Fig. 2).

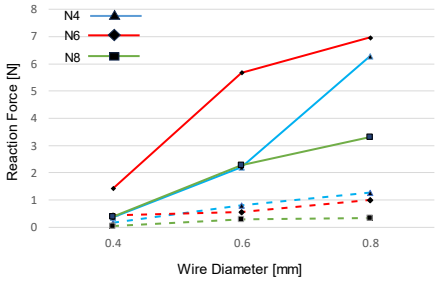


Figure 2: RF_{ovs} values as a function of d_w and N_r for both nitinol rings (solid line) and PCL rings (dashed line).

Discussion

This study highlights the potential of AM and numerical simulations to optimize the design and performance of endografts. The numerical and experimental workflow proved effective in predicting the mechanical behavior of 3D-printed rings, confirming that wire diameter is the primary determinant of radial force. The PS release simulation provided promising data for customizing 3D-printed devices, highlighting improved placement and stress distribution. While PCL rings exert less force, their RF values can be tuned through design parameters to meet endovascular application requirements.

References

1. Spinella G, et al. Assessment of geometrical remodeling of the aortic arch after hybrid treatment. Eur J Cardiothorac Surg. 2019 Jun 1;.

THE IMPACT OF BICUSPID VALVE MORPHOLOGY ON THE SELECTION OF TAVI DEVICES: AN IN-SILICO STUDY

Benedetta Grossi (1,2), Giulia Luraghi (1), Sara Barati (1), Ottavia Cozzi (2), Letizia Maria Perri (1), Gianluigi Condorelli (2), Giulio Stefanini (2), Francesco Migliavacca (1)

1. Department of Chemistry, Materials and Chemical Engineering, Politecnico di Milano, Milan, Italy;
2. Department of Biomedical Sciences, Humanitas University, Pieve Emanuele, Milan, Italy

Introduction

Type 1 bicuspid aortic valve (BAV) represents a challenge for transcatheter aortic valve implantation (TAVI), raising concerns about procedural risks. In such challenging anatomies, it is crucial to provide the clinician a comprehensive understanding of patient characteristics. Additionally, there is a knowledge gap regarding the procedural implications of using different self-expandable devices in BAV cases. In this context, patient-specific simulations of the TAVI procedure represent a powerful tool for gaining predictive insights. The aim of this study is to investigate how BAV and tricuspid aortic valve (TAV) morphologies affect the selection of prosthetic devices and the potential development of conduction disturbances, using a novel and validated in-silico approach[1].

Methods

This is a prospective, single-center, observational cohort study. Five patients with BAV undergoing TAVI were enrolled. Tricuspid aortic valves were virtually modeled within each BAV patient-specific anatomy, resulting in ten virtual patients. Both Acurate Neo2 and Evolut R implantations were subsequentially simulated across all cases (Figure 1). To ensure the accuracy of the simulated positioning of the prosthetic device, a quantitative validation of BAV simulations was performed against post-operative angiographies. Post-implantation stresses exerted on both the stent and aortic root were measured, allowing a comparative analysis of the impact of the two valve morphologies on stent expansion and potential development of conduction disturbances.

Results

Superimposing the final configuration of the implanted stents on patients' post-procedural angiographies, a percentage difference lower than 10% was observed in all cases. In patients implanted with Acurate Neo2, peak stresses acting on the stent implanted in bicuspid cases are greater than tricuspid ones. On the other hand, in patients who received the Evolut R device, the stress magnitude acting on the prosthetic device assumes comparable values. Specifically, comparing stent stresses between BAV and TAV configurations, the stress gap increased by 21.96 ± 5.35 % ($p = 0.01$) in Acurate Neo2 cases ($n = 6$) compared to Evolut R cases ($n = 4$). The analysis of aortic root stresses showed no significant differences between BAV ($n = 5$) and TAV ($n = 5$) configurations, with a mean stress difference of 5.1 ± 8.17 % ($p > 0.05$).

Discussion

This work presents a computational investigation of the influence of different native valve morphologies on TAVI. Acurate Neo2 implantation in bicuspid cases shows increased resistance to stent deployment, thus preventing its complete expansion. On the contrary, high radial force devices are less influenced by native valve morphology. Furthermore, the implantation of self-expandable devices in BAV patients does not seem to translate into a heightened risk of post-TAVI conduction abnormalities, regardless of the selected device. In conclusion, our patient-specific model shows that the Evolut R demonstrates consistent anchoring regardless of valve morphology, without increasing the risk of post-implantation conduction disturbances, annulus rupture, or stent migration, hence resulting more suitable for BAV cases. Through the achieved results, this study underlines the importance of patient-specific numerical simulations in BAV cases, particularly in the selection of the appropriate bioprosthetic valve.

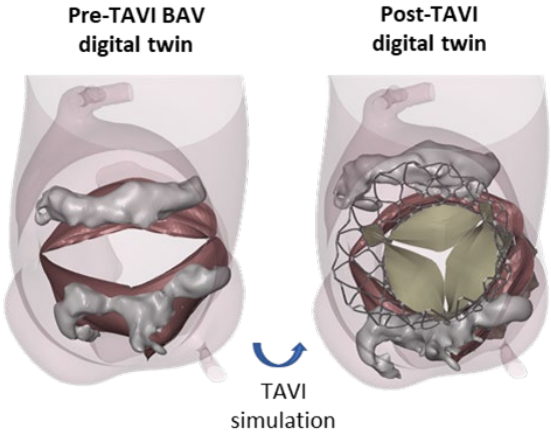


Figure 1: Illustration showing the pre-TAVI model of a BAV patient and its post-implantation configuration.

References

1. Grossi et al, Comput Biol Med 182, 2024.

Acknowledgements

The study is supported by a research grant of the Italian Ministry of University and Research (PRIN 2022 PNRR, grant P20227KTBZ). G.L, L.P. and F.M. are supported by the European Research Council (ERC, project PROTEGO, G.A. 101162753).

A COMPREHENSIVE IN-SILICO PIPELINE FOR THE PREVENTION AND TREATMENT OF ATRIAL FIBRILLATION PATIENTS

Benigno Marco Fanni (1), Ilaria Verdirame (1,2), Francesca Danielli (3), Emanuele Gasparotti (1), Francesca Berti (3), Sergio Berti (4), Giancarlo Pennati (3), Lorenza Petrini (5), Simona Celi (1)

1. BioCardioLab, Bioengineering Unit, Fondazione Monasterio, Italy; 2. Department of Information Engineering, University of Pisa, Pisa, Italy; 3. Department of Chemistry, Materials and Chemical Engineering, Politecnico di Milano, Italy; 4. Adult Cardiology Unit, Fondazione Monasterio, Italy; 5. Department of Civil and Environmental Engineering, Politecnico di Milano, Italy.

Introduction

In patients with non-valvular atrial fibrillation (AF), the left atrial appendage occlusion (LAAO) represents a key treatment option for patients with contraindications to anticoagulation therapies, due to the thrombogenic risk associated to the LAA [1]. However, complications such as peri-device leakage and device-related thrombosis can arise post-procedure [1, 2]. Computational modeling offers a valuable approach to assess thromboembolic risk before and after the procedure [3]. Currently, the entire numerical workflow based on device deployment and hemodynamics evaluation has never been presented and investigated. For the first time, this work presents an in-silico pipeline that integrates computational fluid dynamics (CFD) and finite element (FE) models to simulate hemodynamics in both pre- and post-LAAO scenarios on patients' anatomies.

Methods

The proposed pipeline employs a sequential workflow: (*i*) CFD simulation of left atrial (LA) hemodynamics before the intervention (CFD-pre); (*ii*) FE simulation of the LAAO procedure (FE-LAAO); (*iii*) CFD simulation of post-LAAO hemodynamics (CFD-post). From pre-operative CT images, the LA model is segmented to simulate baseline hemodynamics and the LAAO intervention (Figure 1a). FE results are then used to generate a post-LAAO CFD model, enabling assessment of residual stroke risk. This methodology (Figure 1b) was applied to two patients whose pre-operative CT datasets were available. The CFD simulations were carried out using Ansys Fluent (Ansys, USA). Boundary conditions were set according to [3], by adjusting a generic mitral flow waveform according to patient's heart rate and stroke volume. The package Abaqus (Dassault Systèmes, USA) was used for the FE analyses. A Watchman FLX occluder model [4] was virtually implanted, with device size (35 mm) based on LAA ostium measurements. Moreover, LAAO simulations accounted for the patient's fossa ovalis position to accurately constrain the delivery system during device deployment. FE simulations were run with different LA wall stiffness (WS) properties and catheter types (single and double curve) for each patient to also evaluate their effect on post-LAAO hemodynamics. The resulting deformed LA and device geometries were used for post-LAAO CFD simulations under the same conditions as CFD-pre models. In particular, a volume subtraction between the volume meshes of deformed LA and device was performed to obtain the CFD-post domain.

Results

Velocity fields and hemodynamic indices were obtained for both CFD-pre and CFD-post simulations for all configurations (different WS values and catheter types). In one patient, complete LAA occlusion was achieved (Figures 1d-e). In the second, a gap between the device and LAA wall led to peri-device leakage, as observed in the CFD-post evaluation (Figures 1f-g).

Discussion

This work presents a comprehensive in-silico pipeline to simulate the clinical workflow for AF patients undergoing LAAO. The cascade process, from CFD-pre, through FE-LAAO, to CFD-post, enables quantitative assessment of device-related effects and residual risk. This tool has the potential to inform pre-operative planning, optimize device selection, and enhance patient-specific outcomes in LAAO.

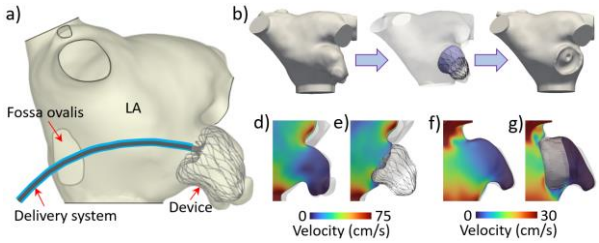


Figure 1: (a) Device deployment in patient-specific anatomy; (b) In-silico pipeline: CFD-pre, FE-LAAO (b) and CFD-post (c) models; (d-e) Velocity maps at LAA for the first analyzed case, resulting in a complete occlusion, and second one (f-g), presenting instead a peri-device leakage.

References

1. Alkhouli et al, JACC, 1(5), 100136, 2022.
2. Friedman et al, JACC, 9(1):108–110, 2023.
3. Fanni et al, Applied Sciences, 10(4), 1448, 2020.
4. Danielli et al, Int J Numer Meth Bio, e3814, 2024.

Acknowledgements

This work is part of the project "PLACE – Planning LAa ClosurE" (RF-2021-12375208), funded by the Italian Ministry of Health.

A COMBINED IN VITRO AND IN SILICO PIPELINE FOR THE CHARACTERIZATION OF DRUG-COATED BALLOON COATINGS

Francesca Berti (1), Martina Clerici (1), Ivan Dell'Acqua (1), Elena Bianchi (1), Dimitrios Zantzas (1), Efstathios Stratakos (1), Giancarlo Pennati (1)

1. LaBS, DCMC, Politecnico di Milano, Piazza Leonardo da Vinci 32, 20133 Milano, Italy

Introduction

Drug-coated balloons (DCBs) offer a promising alternative to treat cardiovascular diseases, but face challenges due to limited and poorly understood drug-coating transfer mechanisms [1]. Many factors influence coating transfer effectiveness, among which the contact pressure (CP) exerted by the balloon on the arterial wall during inflation at the target site. This work aims to elucidate the correlation between CP and the transfer and retention of drug coating to the arterial tissue. To achieve this, a comprehensive pipeline is developed for characterizing DCBs, focusing on: i) the amount of coating transferred to the artery during the balloon inflation, and ii) the extent of coating washed off from the arterial wall by the blood flow. In essence, we aim to propose simplified and cost-effective in vitro frameworks, which are designed and supported by computational simulations, to evaluate their performances under controlled conditions.

Methods

A dedicated compression setup, referred to as a *stamping* setup, was developed and 3D printed to simulate the DCB-vessel interaction during inflation at the target site in a reproducible and simplified mechanical process using a tensile testing machine MTS Synergie (100 N load cell) (Fig. 1a). Cylindrical DCB slices were created by resin inflation and cutting of a single commercial device (Pearlflow, L2MTech GmbH) [2], allowing to increase the number of specimens for testing. Swine arterial strips were prepared as counterparts for the *stamping* experiments. CP values were influenced by strip thickness and Young's modulus (denoted as h and E, unknown a priori). To address this, each stamping test was articulated in two phases: i) once the strip was mounted on the machine, a first compression test was performed at its lateral ends, allowing to measured h and assessed E through a surrogate modeling approach based on the local force-displacement curve; ii) without repositioning the strip, the central portion underwent the effective *stamping* test with the DCB slice, applying a calibrated force to achieve the desired interfacial CP value. This force value was, in turn, identified from another surrogate model taking as input the newly obtained h and E (Fig. 1b). Three different CP values of 20, 50, and 80 KPa were selected for the *stamping* tests. After *stamping*, samples were dried for 24 hours and then inspected by optical microscopy to quantify the coating transferred area by image segmentation. Since drying is a destructive condition applicable once in the specimen's lifetime, some of the tests at 50 KPa were immediately used for subsequent tests. Indeed, a custom-made millifluidic device was designed to house post-stamping arterial strips, which were then subjected to a 60-second water flow simulating the restored bloodstream at two different flow rates. Two strips were tested per each flow condition and then dried for 24 hours to optically quantify the remaining coated area, assuming as the initial condition the results from the stamping tests at the same prescribed CP.

Results

The *stamping* protocol consistently achieved transferred coating areas ranging from 15.6% to 55.4% from 20 to 80 KPa. A linear relationship between the applied CP and the % coating transferred area onto the arterial surface was found regardless of variations in arterial properties (Fig. 1c), demonstrating the effectiveness of the surrogate modeling approach. Such repeatability allowed us to rely on a predictable amount of coating lost during washing-off, which was proportional to the applied flow rate.

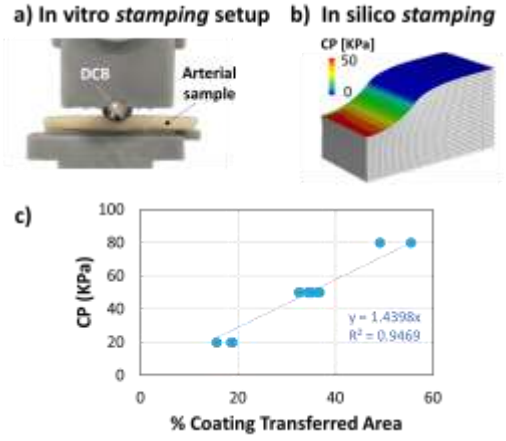


Figure 1: Key elements of the in vitro-in silico pipeline

Discussions and Conclusions

By combining in silico and in vitro approaches the proposed pipeline establishes a new standard for DCB coating characterization.

References

1. Marzlin et al, J Interv Cardiol, e5175607, 2022.
2. Stratakos et al. Ann Biomed Eng, 2024

Acknowledgments

This project has received funding from the European Union's Horizon 2020 research and innovation programme under the Marie Skłodowska-Curie grant agreement No 956470.

IN SILICO DESIGN OF EXPERIMENTS TO CALCULATE STRESS CONCENTRATION FACTORS FOR CROSS-CURVED BONE PLATES

Federico A. Bologna, Ulyana Konopada, Dario Carbonaro, Alberto L. Audenino, Mara Terzini

Department of Mechanical and Aerospace Engineering, Politecnico di Torino, Turin, Italy
Polito^{BIO}Med Lab, Politecnico di Torino, Turin, Italy

Introduction

In bone surgery, osteosynthesis plates have evolved from simple straight designs to more complex, anatomically tailored cross-curved shapes [1]. The complexity of these geometries commonly requires Finite Element (FE) analyses to evaluate stress distribution in bone plates, particularly around holes or notches. While FE analyses offer detailed simulations, they are computationally demanding [2]. Analytical methods, on the other hand, typically provide only basic stress evaluations on straight plates [3].
Stress Concentration Factors (here denoted as *Kt*) from literature are often applied to account for the presence of screw holes in the critical sections of plates. However, these factors are typically based on limited data and do not account for the cross curvature of the plate.
This study aims to provide accurate *Kt* values for bone plates by accounting for cross curvature and expanding on existing empirical data. To achieve this, an *in silico* Design of Experiments (DOE) approach is employed to generate results, which will inform development of user-friendly surrogate polynomial (SP) models. The ultimate goal is to enhance the prediction of bone plate performance, thereby improving their design and reliability.

Methods

Thirteen bone plates with diverse cross-sectional geometries were selected, representing various anatomical regions such as the wrist, malleolus, clavicle, tibia, and femur. The primary dimensions of the plates, including thickness (t), width (w), hole diameter (d), and curvature radius (r), were extracted. A parametric FE model was then developed using Ansys Workbench.
A perpendicular force of 10 N was applied to one side of the plate, while the opposite side was constrained.
To cover a wide range of geometries, full factorial designs [4] with six levels were implemented, encompassing configurations with three or four parameters (t, w, d, and r). The DOE was developed in three phases. In the first phase, 216 rectangular flat plates without curvature were analyzed. In the second phase, the curvature radius was introduced, generating curved geometries to evaluate the maximum distance between the extrados surface and the centroid. Finally, a comprehensive DOE combining all parameters was created, resulting in 1296 unique configurations.
Two distinct SP models were created: one for flat plates and another for curved plates. These models were validated using the dimensions of the thirteen selected commercial plates, comparing the results with those obtained from FE simulations.

Results

In the case with maximum cross curvature (Figure 1A), an increase of almost 5% (Kt = 1.95) was observed with respect to the flat rectangular plate (Figure 1B).
The SP models that exhibited coefficients of determination (R^2) greater than 0.95 in both the implementation and assessment phases were the third-order model for rectangular plates, in accordance with [5], and the second-order model for cross-curved plates. Maximum stress values predicted using the SP models were compared to FE simulations (Figure 1C), resulting in errors below 15% for all plates.

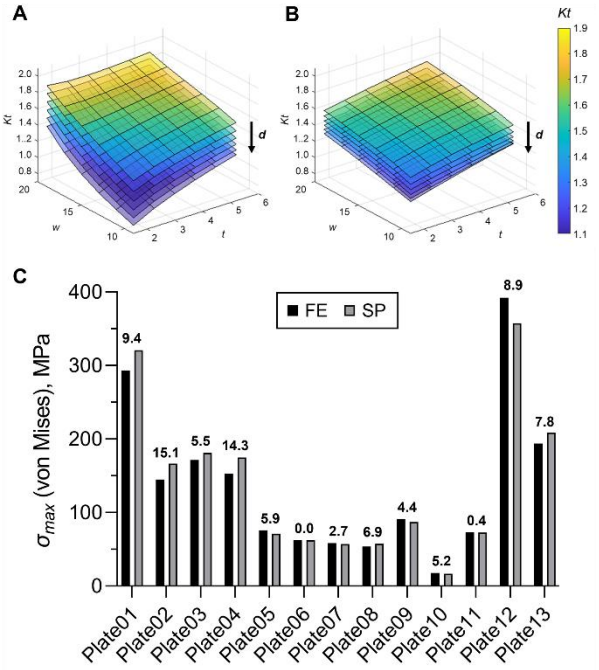


Figure 1: Response surfaces of the simulated Kt for (A) high cross-curved and (B) flat plates with a circular opening as a function of width and thickness for increasing hole diameters. (C) Maximum stress and % error of the SP model compared to the FE analysis.

Discussion

The SP models provide accurate and computationally efficient methods for predicting *Kt* in both flat and curved plates, offering significant potential for optimizing bone plates geometrical designs.

References

1. Burny et al, Med. Eng. Phys, 22:469–479, 2000.
2. Terzini et al, Front Bioeng Biotechnol, 8: 1–11, 2020.
3. Kenedi et al, J Braz Soc Mech, 39:645–659, 2017.
4. Draper and Lin, Response Surface Designs, 1996.
5. Reissner, J App Mech, 12:A69-A77, 1945.

SPINAL SAGITTAL ALIGNMENT IN MUSCULOSKELETAL MODELS: RETHINKING ITS RELEVANCE IN LOAD TRANSMISSION ESTIMATION

Simone Borrelli (1,2), Valentina Benna (2), Alberto L. Audenino (1,2), Mara Terzini (1,2)

1. Polito^{BIO}Med Lab, Politecnico di Torino, Turin, Italy; 2. Department of Mechanical and Aerospace Engineering, Politecnico di Torino, Turin, Italy.

Introduction

Chronic Low Back Pain (cLBP) affects over 15% of the European population with a concerning prevalence in women (53.3%) [1]. Clinical studies indicate that spinal sagittal alignment (SSA) is a key factor in cLBP onset [2] and understanding how SSA affects the load transmission to intervertebral joints could help elucidate the complex etiology of cLBP and support rehabilitation trials. However, subject-specific musculoskeletal (MSK) modeling with personalised SSA remain limited, also due to the lack of tools able to automatically integrate SSA into MSK models. To address this gap, the authors have developed a free-access standalone tool (soon to be published under CC BY-NC-SA), conceived to integrate specific SSA. This study presents this tool, to (i) evaluate the impact of specific SSA on subject-specific models with generic spine profile, and (ii) analyse how different SSA affect load transmission along the thoracolumbar segment.

Methods

A total of 122 upper-body subject-specific female models (mass: P_{50} 39.6 kg, P_{25}-P_{75} 35.5-46.7 kg; height: 56.8 ± 3.4 cm) were extracted from the Framingham Heart Study [3] and revised for a more recent MSK model [4] (OpenSim4.4). These reference models (M_{ref}) presented articulated thoracolumbar segment with spherical joints, and cubic non-linear rotational stiffnesses were added to include intervertebral joint passive reactions. The tool (Matlab2024, Figure 1) permitted to create for each M_{ref} 12 new models with a specific SSA (M_{SSA}). All SSAs were randomly generated, spanning the curvature physiological ranges and classified in accordance with Roussouly types (RT1-RT4) [5], characterized by an increasing sacral slope (RT1: <35°, RT2: 28°-35°, RT3: 43°-76°, RT4: >45°), lordosis (RT1: 41°-64°, RT2: 44°-58°, RT3: 35°-45°, RT4 >60°), and a cranial motion of the apex of the lordosis (RT1: L5, RT2, RT3: L4, RT4: L3). The physiological orientation range of single vertebral levels was used as control of the resulting SSAs. A total of 1586 models were simulated in upright posture and intervertebral joint reactions were analysed. The Wilcoxon Signed-Rank paired test (M_{ref}, M_{SSA}) was conducted. The average intra-subject variability of intervertebral joint compression (ΔC_{SSA}) was computed as the coefficient of variation of the RMSD between M_{ref} and the twelve M_{SSA}. The Kruskal Wallis with Dunn-Sidak post-hoc tests were used to assess the statistical significance of the intervertebral joint reactions normalized for the mass ($IVJR_N$) between the RTs.

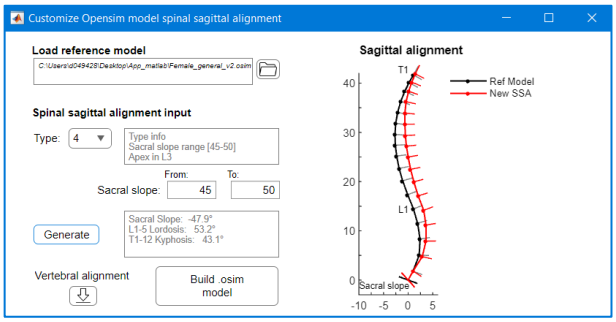


Figure 1: User interface of the developed tool to create and assign specific SSA to musculoskeletal models.

Results

All models were successfully created with no simulation failures. Across the 122 subjects, the average ΔC_{SSA} remained above 10% along the entire segment. The most affected levels were L5-S1 (25.5 ± 5.6%) and T11-T12 (18.2 ± 5.9%). More than 70% of M_{SSA}'s intervertebral joint reactions distributions differed significantly from their respective M_{ref} (α <0.05). $IVJR_N$ in RT1 and RT4 was always different below T5-T6 (p <0.01), while RT2 and RT3 showed comparable $IVJR_N$, reflecting their morphological similarity. Figure 2 returns the relationship between increased lumbar curvature (RT1< RT4) and the craniocaudal rise in $IVJR_N$, and viceversa.

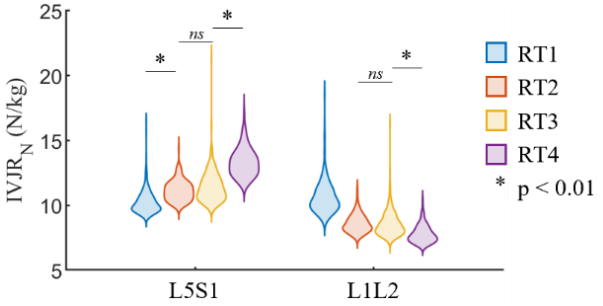


Figure 2: $IVJR_N$ density distribution for RT1-RT4.

Discussion

Results highlight the need to move beyond a single generic spine profile in MSK modeling. The presented tool shows promise in facilitating this transition. Despite using simple neutral standing simulations, it allowed the estimation of how different physiological SSAs affect load distribution along the thoracolumbar segment.

References

1. Ferreira et al., *The Lancet Rheumatology*, 5:316-329, 2023.
2. Rahman et al., *Physical Therapy in Sport*, 59:60-72, 2023.
3. Mokhtarzadeh et al., *J Bone Miner Res,* 36:704-711, 2021.
4. Burkhart et al, *J Biomech,* 112, 2020.
5. Roussouly et al., *Spine (Phila. Pa 1976)*, 30:346-353. 2005.

ENHANCING PERSONALIZED MANDIBULAR RECONSTRUCTION PLATES: IN SILICO MODELING AND EXPERIMENTAL VALIDATION

Camilla Gironi (1), Federico Parisini (1), Laura Cercenelli (1), Gregorio Pisaneschi (2), Mattia Mele (2), Francesco Ceccariglia (3,4), Achille Tarsitano (3,4), Emanuela Marcelli (1, 5)

1. eDIMES Lab – Laboratory of Bioengineering, Department of Medical and Surgical Sciences (DIMEC), University of Bologna, Italy; 2. Department of Industrial Engineering (DIN), University of Bologna, Italy; 3. Oral and Maxillo-Facial Surgery Unit, IRCCS Azienda Ospedaliero-Universitaria di Bologna, Italy; 4. Maxillofacial Surgery Unit, Department of Biomedical and Neuromotor Sciences (DIBINEM), University of Bologna, Italy; 5. PRO (Preclinical and translational Research in Oncology) Research Platform, IRCCS Azienda Ospedaliero-Universitaria di Bologna, Italy

Introduction

Mandibular reconstruction is a standard surgical procedure performed to restore the continuity of the mandible subjected to tumors, trauma, or infections. The fibular free-flap technique is commonly used for mandibular reconstruction, typically involving the fixation of a titanium plate and screws [1]. Recent advances in virtual surgical planning and computer-aided design and manufacturing (CAD/CAM) technologies offer the potential for more precise and efficient surgical procedures [2]. Alongside these innovations, finite element (FE) modeling has emerged as a powerful tool for simulating the biomechanics of the reconstructed mandible, allowing for the optimization of surgical strategies [3]. However, thorough validation of such models remains a challenge [4]. This study aims to experimentally validate an in silico FE model for the design of personalized mandibular reconstruction plates, focusing on its accuracy in predicting the mechanical behavior of the plates under clenching loads to and assessing its potential to optimize the plates design.

Methods

A patient-specific in silico model for mandibular reconstruction was developed from high-resolution CT scans using Mimics 26.0 (Figure 1). The mandible and fibula were segmented, and a 3D model was imported into ANSYS software for FE analysis. A custom CAD/CAM titanium reconstruction plate previously designed for implantation, was replicated in FE model. Isotropic, linear elastic material properties were assigned to the mandible, fibula, and plate. The mandible was constrained to enable condylar hinge rotation and limit vertical incisal tooth displacement, while forces were applied to replicate the effect of clenching muscles.

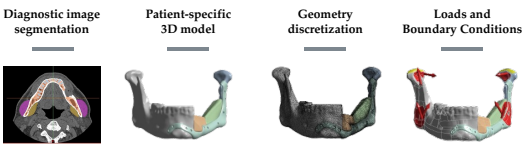


Figure 1. *In silico model for mandibular reconstruction.*

Experimental validation was performed using a 3D-printed mandible made from Rigid 10K resin via SLA technology, and a titanium alloy plate fabricated using DMLS technology (Figure 2). A custom-designed setup was developed to securely position the mandible and plate during testing. Mechanical loading was applied through a bar designed to replicate the muscle resultant force generated during incisal clenching, thereby simulating physiological masticatory loads.

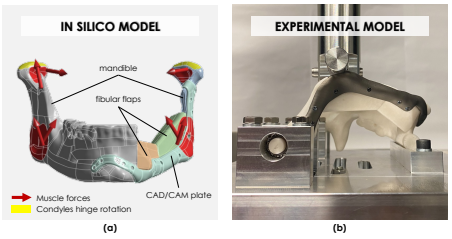


Figure 2. *In silico model (a) and experimental model (b) of the mandible and plate under clenching conditions.*

Results

The experimental validation demonstrated a good correlation between the in silico model and the 3D-printed mandible and titanium plate under the reproduced clenching loads. Both the simulation and experimental setups displayed comparable stress patterns, with peak stresses concentrated at areas of high mechanical loading, confirming the model's accuracy in replicating real-world conditions.

Discussion

The validated in silico model shows significant potential to enhance the design of patient-specific mandibular reconstruction plates by providing a more precise and tailored approach to surgery. Integrating this model into clinical practice could optimize surgical outcomes and reduce operative times. Future advancements may involve incorporating more complex loading scenarios and expanding the model's application to a wider range of maxillofacial patient-specific implants, further improving personalization and surgical efficiency.

References

1. Kumar et al, J Maxillofac Oral Surg, 15: 425-441 2016
2. Yang et al, Ann Surg Oncol, 28: 363–375, 2021
3. Aftabi et al, Comput Biol Med, 169, 2024
4. Merema et al, Oral Dis, 27:42-51, 2021

OPTIMIZING BONE HEALING IN MANDIBULAR RECONSTRUCTION: A MECHANOBIOLOGICAL APPROACH TO FIXATION STRATEGIES

Camilla Gironi (1), Alessandro Borghi (2), Federica Ruggiero (3), Laura Cercenelli (1), Silvia Schievano (4, 5), Fabrizio Neri (3), Anna Maria Baietti (3), Achille Tarsitano (6, 7), Emanuela Marcelli (1, 8)

1. eDIMES Lab – Laboratory of Bioengineering, DIMEC, University of Bologna, Italy; 2. Department of Engineering, Durham University, UK; 3. Maxillofacial Surgery Unit, Bellaria-Maggiore Hospital, AUSL di Bologna, Italy; 4. Craniofacial Unit, Great Ormond Street Hospital for Children, UK; 5. Great Ormond Street Institute of Child Health, University College London, UK; 6. Oral and Maxillo-Facial Surgery Unit, IRCCS Azienda Ospedaliero-Universitaria di Bologna, Italy; 7. Maxillofacial Surgery Unit, DIBINEM, University of Bologna (Italy); 8. PRO Research Platform, IRCCS Azienda Ospedaliero-Universitaria di Bologna, Italy

Introduction

Mandibular reconstruction after tumor resection, trauma, or infection is crucial for restoring function and aesthetics. The fibular free-flap technique, using fibula segments secured with titanium plates, is the gold standard. However, challenges remain, with non-union rates between the grafted fibula and native mandible reported up to 20% [1]. Despite advancements in Virtual Surgical Planning (VSP) and computer aided design and manufacturing (CAD/CAM) technologies, optimizing bone healing at intersegmental gaps remains an open issue. Secondary bone healing, which involves callus formation and remodeling, is significantly influenced by mechanical factors such as interfragmentary movement and the stability of fixation [2]. While mechanical strains play a key role in bone regeneration, optimal fixation conditions are still unclear [3]. This study aims to develop a mechanobiological model to simulate bone healing at intersegmental gaps following mandibular reconstruction, with a focus on callus ossification and the role of mechanical strain. By assessing different CAD/CAM fixation strategies—reconstruction plates and miniplates—this model aims to optimize fixation designs and improve clinical outcomes.

Methods

Post-operative DICOM images from two mandibular reconstruction patients—one with a reconstruction plate (Figure 1a) and the other with miniplates (Figure 1b)—were used to create 3D models for Finite Element (FE) analysis in ANSYS.

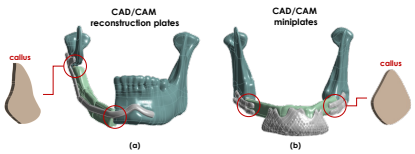


Figure 1. *3D models of patients: (a) with a reconstruction plate and (b) with miniplates.*

Material properties were assigned, and the mandible was constrained to allow condylar rotation, restrict vertical tooth displacement, and simulate clenching forces. A tissue differentiation model was developed to simulate bone healing process, using mechanical stimuli (volumetric and distortional strains) to drive the callus ossification process [2, 4]. Regions of the callus meeting osteogenesis thresholds were selected for ossification, and in subsequent iterative simulation steps, the selected elements were progressively stiffened to simulate the ossification process, while other regions maintained granulation tissue properties. This iterative process allowed the model to evolve, providing a dynamic representation of how mechanical factors and fixation strategies influence bone healing.

Results

Results revealed that ossification in the callus occurred earlier in the patient treated with miniplates compared to the patient with a reconstruction plate (Figure 2).

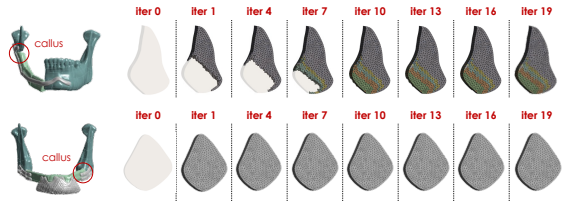


Figure 2. *Callus mesh elements undergoing ossification at specific iterations for patients with reconstruction plate (top) and miniplates (bottom).*

This earlier initiation of ossification suggests a potentially more favorable clinical outcome for the patient treated with miniplates, as the mechanical environment may have facilitated more rapid bone formation and healing.

Discussion

These preliminary findings highlight the impact of fixation strategy on bone healing, indicating that fixation strategies with lower stiffness, such as miniplates, may promote accelerated healing during the early stages of bone repair. Future studies should investigate various fixation techniques and biomechanical parameters to enhance treatment strategies for mandibular reconstruction.

References

1. Yoda et al, Med Eng Phys, 56:1-8, 2018
2. Claes et al, J Biomechanics, 32:255-266, 1995
3. Kreutzer et al, J Cran Maxil. Surgery, 51:621-628, 2023
4. Reina-Romo et al, J Biomechanics, 44:917-923, 2011

Advanced *in silico* musculoskeletal model of the lumbar spine: a finite element method for load sharing analyses

Linda Carpenedo, Luigi La Barbera

LaBS – Department of Chemistry, Materials and Chemical Engineering "G. Natta", Politecnico di Milano

Introduction

Load sharing among musculoskeletal structures is critical for spinal stability, with muscles playing a central role. Imbalances in the distribution of loads may lead to pathologies like low-back pain, a global health issue. Due to challenges in measuring spinal loads experimentally, computational methods are a valuable alternative. Multibody models enable efficient simulations but lack tissue-specific detail, while Finite Element (FE) models provide greater detail, but face limitations in integrating the active action of muscles and are computationally demanding.
This study presents a parametric FE model of the lumbar spine that incorporates muscle architecture to enable detailed evaluation of load sharing across spinal structures. Its development, validation, and application to study load sharing are discussed.

Material and Methods

The geometry is derived from a previously validated CAD parametric model of the spine with all structures defined as continuous deformable bodies in Abaqus [1]. Body weight contributions are represented as percentages of total weight distributed eccentrically to vertebral centroids, while head-neck and arms are integrated by their center-of-mass forces. Eight muscle groups are modelled with fascicles as uniaxial connectors with stiffness $k=qF/l$ (28 on each side), with q=20 (based on preliminary sensitivity analyses), F and l the force and the rest length of each fascicle (Fig. 1a). Muscle forces are provided as an input in terms of percentage of maximal activity (max fascicle stress set to 0.6MPa). The muscle pattern proposed by El-Rich et al. [2] for standing is taken as an initial reference and further adjustments on muscle forces are made to find a kinematics compatible with standing, thus minimizing the range of motions (RoMs).

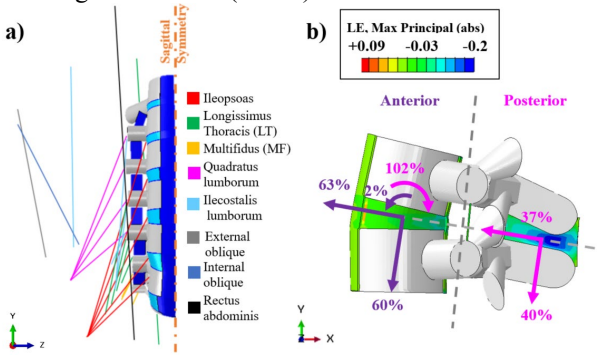


Figure 1: a) muscle architecture, b) LE max principal on L3-L4 soft tissues, with CFs, SFs and BMs on the anterior (in purple) and posterior (in magenta) column.

As more muscle patterns led to similar RoMs, an energy criterion on the sum of cubed muscle stresses is minimized to find the optimal solution. Intradiscal pressures (IDPs) and muscle patterns are used for validation. Compressive (CFs) and shear forces (SFs) and bending moments (BMs) in soft tissues are quantified to assess load sharing.

Results

The optimal solution identified for standing (Table I) is based on a 10% abdominal activation, with MF and LT fascicles at L5 being the most active (over 30%).
CFs are primarily supported by the anterior column (annulus, nucleus, and longitudinal ligaments), which carries approximately 80% of total CF (range: 60-100%, Fig.1b). The posterior column (capsular, flaval, interspinous, supraspinous, and intertransverse ligaments) supports an average of 90% of BMs, with the capsular ligament contributing most (up to 125% of extension). SFs are distributed between the anterior column (average 66%, range: 50-90%) and posterior column (average 34%, range: 10-50%).

Level	RoM [°]	IDP [MPa]	CF [N]	SF [N]	BM [Nm]
T12-L1	0.57	0.59	473	150	1.69
L1-L2	-0.25	0.55	494	147	-2.32
L2-L3	-0.90	0.49	525	75	-5.88
L3-L4	-0.48	0.38	545	-40	-7.52
L4-L5	-0.62	0.46	540	-197	-5.76
L5-S1	0.74	0.54	503	-317	-2.17

Table 1: RoMs, IDPs, total CF, SF and BM for standing. (RoM>0, BM>0 in flex; CF>0 in compress; SF>0 posterior).

Discussion

Muscle forces and IDPs are coherent with experimental *in vivo* data for standing, while RoMs fall within the range of the neutral zone. Moreover, the calculated load sharing aligns with the one estimated through *in vitro* experiments [3]. Therefore, the model can be considered validated and credible. By incorporating deformable components, this approach also allows to visualize continuous strains distributions on any structure of interest (Fig. 1b). This kind of quantification makes this method a source of insights that can't be derived from state-of-the-art multibody models. Future developments may include automatization of the optimization algorithm, sensitivity analyses on muscle attachment points and spinal alignment.

References

1. Bellina et al, J Biomech, 111951, 2024.
2. El-Rich et al, 29:2633-2642, 2004.
3. Adams et al, Spine, 5(3):245-253, 1980.

SURGICAL MESHES MESOSCALE FINITE ELEMENT MODELS FROM 2D IMAGE-BASED GEOMETRY RECONSTRUCTION

Vittoria Civilini (1)(2), Alessandra Aldieri (1)(2), Dario Carbonaro (1)(2), Vincenzo Giacalone (1)(2), Alberto Audenino (1)(2), Mara Terzini (1)(2)

1. Department of Mechanical and Aerospace Engineering, Politecnico di Torino, 10129 Turin, Italy;
2. Polito^{BIO}Med Lab, Politecnico di Torino, 10129 Turin, Italy;

Introduction

The *in vivo* behavior of synthetic surgical meshes is challenging to evaluate experimentally. Moreover, the loading patterns these devices are subjected can vary significantly depending on the implantation region [1], [2]. In this context, *in silico* models can facilitate the analysis of surgical mesh behavior under complex loading conditions that are impossible to replicate experimentally. However, the complex morphology of meshes is rarely incorporated into computational model. Considering the known influence of knitted structures on the mechanical behavior of textile devices, incorporating these information would provide valuable insights. Specifically, pore characteristics – such as shape, orientation, and dimensions – are critical parameters for tissue ingrowth, directly influencing patient comfort and surgical outcomes [3]. This study presents a framework for implementing a mesoscale finite element (FE) model for a surgical mesh. The process includes: geometry reconstruction, optimization of constitutive material models, and models validation.

Methods

The pores perimeters of eight meshes – four lightweight, LW and four standard weight, SW – were extracted from 2D high-resolution images to reconstruct a mesh unit cell as a porous surface in Rhinoceros 3D (v6.0, Robert McNeel & Associates, USA). The unit cell was then meshed with shell element in Hypermesh (v2019, Altair Hyperworks, USA). The test condition of uniaxial tensile tests, previously performed in our laboratory, were replicated in terms of specimens shape and dimension and boundary conditions in Abaqus/CAE (v6.19, Dassault Systèmes, USA)[4]. Three different constitutive material models were optimized by minimizing the squared error between ten points on the experimental and computational force-displacement curves in both principal directions using the HyperStudy software. Initially, a linear elastic model was implemented to assess its ability to replicate the anisotropic behavior characteristic of the in vitro mechanical response of these textile devices, leveraging the porous geometry that mirrors the morphology of the meshes. Then, two isotropic hyperelastic material models (i.e., Neo-Hookean and Mooney-Rivlin) were optimized to better capture the non-linearity of the force-displacement curves. Finally, the behaviour of the porous models under multidirectional loads was investigated by replicating the conditions of the ball burst test. The force-displacement curves, obtained from *in vitro* and *in silico* analyses, were compared to validate the models.

Results

The geometry reconstruction was effectively conducted for all the meshes. Figure 1 illustrates two examples, showcasing the reconstructed geometry alongside contour plot of the the final displacement obtained from uniaxial tensile and ball burst test simulations using the Mooney-Rivlin material definition.

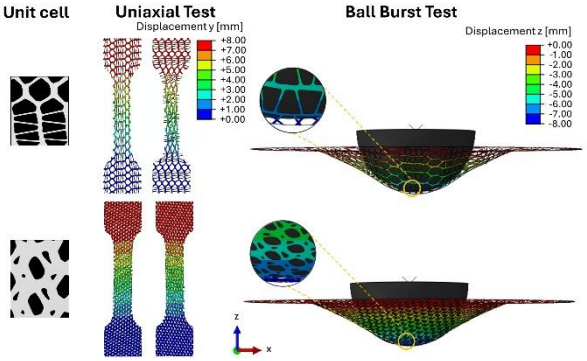


Figure 1: Unit cell, specimen shape, and displacement along the z-direction after the imposed penetration of the sphere: LW mesh results are shown in the first row, and SW mesh results are in the second row.

The linear elastic material definition enables the simulation of small displacement (ds=2.8 mm) under uniaxial tensile test conditions. In contrast, the adoption of hyperelastic material allow for simulation with displacement up to 10 mm. Preliminary results obtained for two LW and two SW meshes indicate minimal differences in the accuracy of the hyperelastic constitutive models, suggesting comparable performance across both material definitions.

Conclusion

The FE models, developed by reconstructing pore geometry from 2D images, accurately identify the strong and weak directions in anisotropic meshes using isotropic material definitions. Furthermore, these models provide valuable insights into the mesh response to multidirectional loading, including details on local behavior such as pores deformation. The ongoing project aims to aims to expand on these findings through FE models developed for all eight reconstructed meshes.

References

1. K. Junge et al, *Hernia*, 5(3): 113–118, 2001.
2. Y. Ozog et al, *Int. Urogynecol. J.*, 25(4): 499–506, 2014.
3. S. P. Lake et al, *J. Mech. Behav. Biomed. Mater.*, 42: 186–197, 2015.
4. V. Civilini et al, *J. Mech. Behav. Biomed. Mater.*, 144, 2023.

EXPERIMENTAL AND NUMERICAL ANALYSIS OF PERIPHERAL NERVES REGENERATED IN HYDROGEL-BASED CONDUITS

Marta Confalonieri (1,2), Silvia Spadoni (1), Silvia Todros (1), Elena Stocco (2), Silvia Barbon (2), Cesare Tiengo (3), Andrea Porzionato (2), Piero Pavan (1, 4)

1. Department of Industrial Engineering, University of Padova, Italy; 2. Department of Neurosciences, Section of Human Anatomy, University of Padova, Italy; 3. Department of Neurosciences, Clinic of Plastic Surgery, University of Padova, Italy; 4. Fondazione Istituto di Ricerca Pediatrica Città della Speranza, Padova, Italy

Introduction

Over the past decades, nerve conduits (NCs) have emerged as a promising alternative to nerve autografts, the current gold standard for treating peripheral nerve injuries with substance loss. The efficacy evaluation of these devices usually involves functional, histological, electrophysiological, and imaging assessments; yet, the mechanical properties of the regenerated nerves are often overlooked. This study investigates the mechanical behavior of nerves regenerated in oxidized polyvinyl alcohol (OxPVA) conduits, comparing them to healthy nerves. Additionally, a computational model is developed to simulate the *in vivo* mechanics of the device and its interaction with the injured nerve.

Methods

The OxPVA solution was synthesized through an oxidative reaction of native polyvinyl alcohol (oxidation degree: 1%) [1]. Rectangular samples (34×8×0.6 mm^3) were obtained by pouring the solution into 3D-printed molds, while NCs, with an internal diameter of 0.7 mm and a wall thickness of 1.2 mm, were fabricated using a cast-molding technique [1]. The physical cross-linking process was achieved through six freeze-thawing (FT) cycles (F: –20 °C for 6 h; T: RT for 1 h).

First, suture retention (SR) tests were performed on rectangular samples (n = 4), where each sample was sutured with a 9-0 caliber thread fixed to the grip of the testing apparatus, while the opposite edge was clamped. Additionally, to evaluate the ability of OxPVA conduits to support nerve regeneration, the device was implanted in an animal model of disease (3 Sprague Dawley rats) to bridge a 5 mm nerve gap (Authorization n. 837/2019-PR, 09 December 2019). After six weeks, regenerated nerves including the implanted NCs were harvested for mechanical testing, alongside sciatic nerves from 16 healthy rats as controls (healthy nerves). All the nerves were tested in uniaxial tensile mode. Both tensile and SR tests were carried out on the Bose ElectroForce® Planar Biaxial Test Bench instrument (TA Instruments, New Castle, USA) at a strain rate of 0.5% s^{-1} up to 100% strain in hydrated conditions.

A Finite Element Method (FEM) model was built based on a typical geometry where a NC is symmetrically sutured around two nerves. The OxPVA was modeled as an isotropic elastic material, while an isotropic hyperelastic constitutive model was used to describe the nerves. The experimental data of the stiffer nerve among the ones tested were used to fit the constitutive model, in order to consider the worst possible effect in terms of force applied to the sutures. Numerical analyses are performed using ABAQUS Standard (Simulia, Dassault Systèmes, France) to simulate a tensile loading of the nerve-NC complex corresponding to 20% elongation of the total initial length. Numerical results allow to evaluate the maximum force acting on the sutures and to compare it with experimental SR force values.

Results and discussion

The SR tests showed SR peak force at suture pullout ranging from 0.23 to 0.27 N (Figure 1a). These values are consistent with those reported in the literature [2]. The value of maximum force acting on the suture estimated numerically (about 0.15 N) from the stress distribution (Figure 1a) is lower than the experimental SR peak force. This suggests that the implant can bear physiological loads in the short term after surgical implantation. Both healthy and regenerated nerves were found to withstand the applied strain far beyond the upper limit of physiological strain [3] (Figure 1b). Healthy nerves exhibited significant variability in mechanical behavior across subjects. The regenerated nerve tissue showed higher stiffness with respect with healthy nerves. This can be explained by the higher content of fibrotic tissue found in the early phase of regeneration.

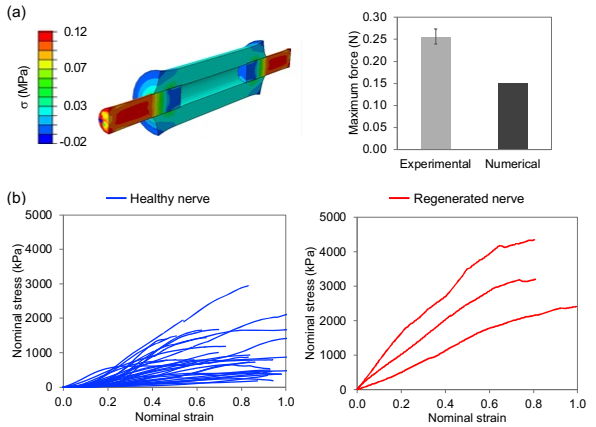


Figure 1: (a) Longitudinal normal stress at 20% elongation of the nerve-NC complex, comparison of experimental SR peak force and maximum force estimated by FEM model; (b) Uniaxial tensile behavior of healthy and regenerated nerves.

References

1. Stocco et al, Sci Rep, 8(1):604, 2018.
2. Kim et al, Adv Healthc Mater, 13(20):e2400142, 2024.
3. Boyd et al, J Orthop Res, 23(4):764-70, 2005.

A COMBINED NUMERICAL-EXPERIMENTAL APPROACH TO STUDY FLUID AND SOLUTE TRANSPORT PHENOMENA THROUGH THE RETINA

Alessandro Conte (1), Riccardo Tripputi (1), Diego Albani (2), Carmen Giordano (1), Federica Boschetti (1)

1. *Department of Chemistry, Materials and Chemical Engineering "Giulio Natta", Politecnico di Milano, Milan, Italy.*
2. *Istituto di Ricerche Farmacologiche Mario Negri IRCCS, Department of Neuroscience, Milan, Italy.*

Introduction

Transport phenomena in the retina involve complex interactions among fluid flow, molecular diffusion, and cellular activity. These processes are critical for maintaining retinal homeostasis and are disrupted in the case of retinal pathologies, such as age-related macular degeneration (AMD), in which drusen accumulate between the retinal pigment epithelium (RPE) and Bruch's membrane, and interfere with nutrient and oxygen transport, exacerbating retinal dysfunction [1,2]. In this work, a fluid and solute transport model in the retina and a retina-on-a-chip model are developed. Interestingly, retinal and cerebral tissues share similar pathological processes, including inflammation and protein aggregation, pointing to the existence of the brain-retina axis [3].

Materials & Methods

The simulation domain includes the RPE, Bruch's membrane, and adjacent retinal layers. The macular region is modeled as in [2]. A transition zone between the parafoveal and foveal regions is modeled with a gradual thinning of the retinal layers. Brinkman's law governs fluid flow, while Fick's law is used to model solutes advection-diffusion. We assume that both the retinal membrane (RM) and the RPE layer are permeable to the fluid. The permeabilities (k) of the RM, of the RM-RPE complex, and of the RM-RPE-choroid complex are measured in pig retinas using a custom-made device, which allows the application of a known pressure head and the measurement of the flow rate. Water flux through RM and RPE is regulated by Starling's law [1]. For this preliminary model, we assumed that the transport of proteins across the RM is governed by a concentration difference between the vitreous and the choroid. The retina-on-a-chip system includes a co-culture chamber fabricated using Biomed Clear Resin with a stereolithographic 3D printer (Formlabs 3B+). The chamber integrates a scaffold mimicking the structure and properties of the native Bruch's membrane, seeded with human RPE cells [4] and dividing the system into two chambers: an apical chamber, which will support the growth of photoreceptors seeded into a 3D-printable bio-ink [5], and a basal chamber to emulate the choroid tissue.

Results

We are testing our model with physiological values of pressures and concentrations. Preliminary results are obtained considering the diffusion coefficient of albumin [1]. Our ongoing simulations focus on the effect of interstitial fluid flow and local diffusivity variations on solute transport. The increase in the height of the parafoveal region causes, for a given velocity flow, an increase in the permeability and therefore a reduction in the pressure gradient (Figure 1).

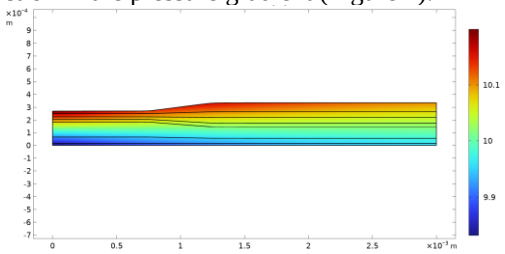


Figure 1. Model simulation showing fluid pressure [Pa].

Discussion

The mathematical model and the retina-on-a-chip model are meant to interact both in the simulation phase, in which the in vitro model will help to determine parameters that cannot be derived from literature, such as the diffusion coefficient of β-amyloid and in the validation phase, in which we will measure physical quantities (pressures and concentrations) in the retinal and choroidal layers and compare them to the predicted ones.

Conclusion

Our combined experimental and numerical method is providing an initial framework for studying the complex transport phenomena in the retina, and the mechanisms of drusen accumulation in disrupting retinal physiology.

References

1. Ruffini et al, IOVS, 65: 19-25, 2024.
2. Vercellin, et al, *Math. Biosciences*, 339: 108650, 2021.
3. Alber et al, Alzheimer's and Dementia, 20: 728–740, 2024.
4. Belgio et al, Bioengineering, 8:18, 2021.
5. Belgio et al, Applied Sciences, 14:6980, 2024.

THE IMPACT OF THE INTERCONNECTION MECHANISM MODELLING ON GLOBAL STIFFNESS AND FATIGUE BEHAVIOR OF SPINAL FIXATORS

Roberta Cromi, Francesca Berti, Luca Ciriello, Luigi La Barbera, Giancarlo Pennati, Tomaso Villa

Department of Chemistry, Materials and Chemical Engineering "Giulio Natta" (LaBS) – Politecnico di Milano

Introduction

Posterior spinal fixation systems are widely recognized as the gold standard for treating various spinal disorders. Within these devices, the interconnection mechanism (IM) plays a crucial role in securing the pedicle screw to the spinal rod. However, to the best of the authors' knowledge, the interaction among the components is often neglected: the IM has been biomechanically studied only by Ciriello et al. [1] who examined its static behavior. Nevertheless, the incidence of fatigue-induced IM failure has been reported to reach up to 11.2% and among these, fretting fatigue must be considered. Fretting occurs when two surfaces experience relative tangential micromovements, due to oscillating forces, leading to a reduction in the material's expected fatigue life. In this scenario, the present work aims to investigate the nut-rod interaction in spinal fixation devices and to declinate the critical role of micromovements in device failure, implementing fretting fatigue criteria and evaluating the system's resistance. To assess the reliability of spinal fixation devices it is essential to investigate their strength and fatigue behavior: (i) the estimation of the system's overall stiffness demands an appropriate description of the interaction between the components; (ii) an accurate investigation of fretting fatigue requires a detailed study of the mesh in contact areas where micromovements occur.

Methods

A Finite Element (FE) model of the IM was developed and validated based on simplified tests, designed to individually analyze each component. The nut was first compressed between two rigid plates until a force comparable to a typical tightening torque [1] was achieved, and then unloaded. The same set-up was computationally replicated meshing the titanium nut with three different hexahedral element sizes. The *in vitro* and *in silico* nut displacement and stiffness were compared to validate the FE model. A sensitivity analysis was also conducted on the rod, modelled as a titanium half-cylinder (*Figure 1*), focusing on proper discretization. The validated nut-rod interaction was subsequently tested to simulate the worst-case loading scenario for the fixation system. Specifically, the nut was statically pushed against the rod, as occurs after tightening, while the rod was subjected to cyclic longitudinal load σ_N [3] (*Figure 1*). Four different fretting fatigue criteria were implemented and validated through comparison with Namjoshi's study [2]. Among them, the Findley Parameter (FP) was chosen to be faced with the Sines stress to determine on the rod the difference in fatigue life predictions when fretting is considered in such devices.

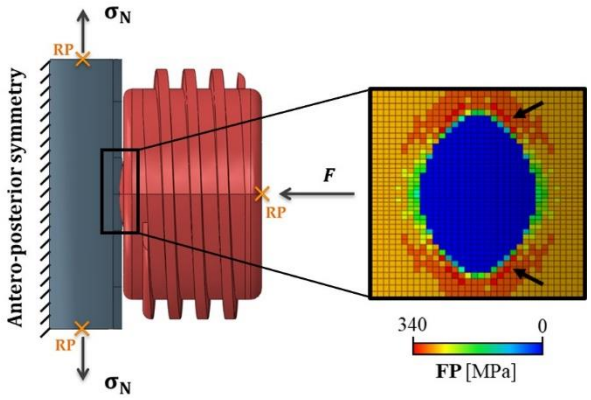


Figure 1: Loads and boundary conditions of the nut-rod FE model. The FP values on the rod's surface are highlighted.

Results

The computational model, showing all discrepancies lower than 5% with respect to the experimental tests, is validated. The meshes able to properly describe the components' interface are characterized by an element size of $75\mu m$ and $50\mu m$ for the nut and rod respectively. The implementation of the fretting criteria shows that the FP is the most independent from the shape of the pad and the type of cyclical load applied to the rod. The maximum Sines stress value identified on the rod is lower than the titanium limit, indicating no risk of fatigue fracture. In contrast, the rod's contact surface shows a maximum FP (*Figure 1, black arrows*), implying a rupture at about 1000 load cycles.

Discussion

The mesh elements are comparable to the grain size of the material for both the nut and rod, as required for an accurate fretting analysis [2]. The comparison between the Sines stress and the FP maximal values highlights that fretting is a non-negligible factor in the study of spinal fixation systems' causes of failure, due to its important reduction in fatigue expected life. Moreover, this demonstrates that fretting analysis needs critical plane-based approaches because of the non-proportional loading conditions given by the micromotions.

References

1. Ciriello et al, J Mech Behav Biomed Mater., 135:105460, 2022 Nov.
2. Namjoshi et al, Fatigue & Fracture of Engineering Materials & Structures, 25: 955-964, 2002.
3. La Barbera et al, Proceedings of the IMechE - Part H, 2017;231(2):176-185.

Acknowledgements

Thanks are due to M. Morandi for his technical support.

INTEGRATING MOTION CAPTURE AND ROBOTICS FOR USABILITY TESTING OF A VIDEO LARYNGOSCOPE

Marco Daghero (1,3), Simone Borrelli (1,3), Giovanni Putame (1,3), Taian M. Vieira (2,3), Mara Terzini (1,3)

1. Department of Mechanical and Aerospace Engineering, Politecnico di Torino, Turin, Italy; 2. LISiN-Department of Electronics and Telecommunications, Politecnico di Torino, Turin, Italy; 3. Polito^{BIO}Med Lab, Politecnico di Torino, Turin, Italy.

Introduction

The EU Medical Device Regulation requires manufacturers to minimize use errors and ensure the safety and performance of medical devices for their intended users, as outlined in the General Safety and Performance Requirements [1]. Within a risk management framework, quantifying the loads transmitted through medical devices by users during intended use would enable the identification and mitigation of risks associated with use errors, thereby ensuring the devices' safety and effectiveness under all intended conditions of use [2]. However, recording loads during the operation of handheld devices presents significant challenges. Hence, this preliminary study introduces a novel testbench for usability testing, which consists in recording medical maneuvers with motion capture and replicating them with a sensorized robotic arm. The study focuses on the application of this testbench to mock intubation with a video laryngoscope.

Methods

The movement of an innovative video laryngoscope, devised with a steerable tip for improved visualization and airway management (Medsniper srl), was recorded using a 12-camera motion capture system (Vicon Nexus, Figure 1A) while performing a typical intubation procedure into a commercial phantom (Airway Management Trainer, BT Inc.). The movement was divided in two phases: (1) the insertion of the laryngoscope in the phantom airways, recorded with four reflective markers attached to the laryngoscope handle, and (2) the rotation of the lever controlling the laryngoscope tip, captured using three markers attached to the lever. For the maneuver replication (Figure 1B), the laryngoscope was mounted on a Doosan H2515 cobot using a pneumatic gripper (Schunk srl). Phase (1) was replicated by imposing the pose coordinates to the cobot's end-effector while the lever rotation in phase (2) was driven by two servo motors (Figure 1B, Tower Pro Pte. Ltd.) controlled via an Arduino board. A 6-axis load cell (Schunk srl FT-axia 80) measured the forces exerted on the laryngoscope during both phases.

Results

The motion of the laryngoscope captured by the motion tracking system was remarkably similar to that replicated by the robotic arm (Figure 1C), yielding residuals lower than 10% of the ROM in 95% of the samples. During phase (1), peak force in the plane of movement (y-z) amounted to 32.1 N and -24.6 N in the y and z directions respectively; accordingly, the peak torque around the x axis was 1.32 Nm (Figure 1D). Regarding phase (2), the residual of the lever rotation (θ) was less than 9% of the ROM, and the peak torque measured around the axis of rotation (x) was 0.61 Nm.

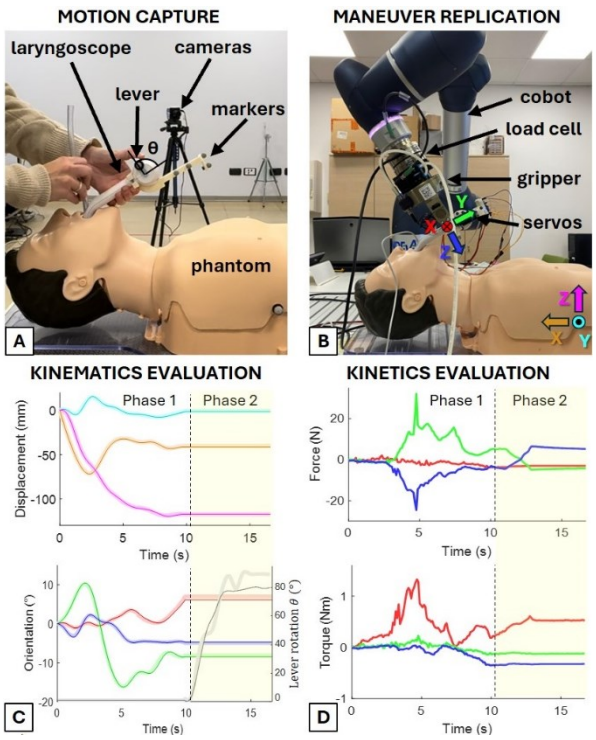


Figure 1: A-B) Experimental setup. C) Captured (light, thick) and replicated (dark, thin) laryngoscope's motion (color) and lever rotation (gray). D) Measured loads.

Discussion

This study presents a novel testbench combining motion capture and robotics to test the usability of a video laryngoscope during intubation procedure. Preliminary results confirm the method accuracy in reproducing a complex maneuver, while also providing synchronized 6-axis force measures, thereby demonstrating the approach's potential for evaluating medical devices' performance and ensuring regulatory compliance.

References

1. MDR 2017/745, OJEU, L117, 2017, (Annex I - GSPR).
2. IEC 62366-1:2015.

Acknowledgements

This publication is part of the project PNRR-NGEU which has received funding from the MUR – DM 351/2022.

Comparison of Methods for Estimating Neuromuscular Control Patterns Using a Muscle-Driven 6DOF Knee Model

Maria Dalle Vacche (1), Giulio Rigoni (1), Davide Pavan (1), Fabiola Spolaor (1), Zimi Sawacha (1)

1. *Department of Information Engineering, University of Padua, Padua, Italy*

Introduction

In high-intensity sports, rapid movements and demanding play make Anterior Cruciate Ligament injuries the most common knee injuries. Drop landing (DL), a frequent maneuver in these sports, places significant stress on the knee due to sudden impacts and high forces on ligaments, muscles, and tendons [1]. Developing accurate musculoskeletal models (MSMs) that simulate these tasks and account for ligament roles is essential, along with reliable methods for estimating internal parameters, especially under dynamic conditions. In this regard, Static Optimization (SO) is commonly used to estimate muscle activations (MA) and forces (MF), however the lack of information about subject specific motor control, might lead to poor prediction when pathological or elite athletes are the object of the investigation. To improve estimates of internal parameters via MSMs electromyography (EMG)-informed methods have been developed. Among them EMG-informed Computed Muscle Control (CMC) [2] and Moco [3] showed the ability to provide estimates of muscle excitations closer to experimental surface EMG (sEMG).

The aim of this study is to compare the performance of these two methods with the SO one applied to a 6-degree-of-freedom (DOF) musculoskeletal knee model [1], focusing on their ability to estimate MA and MF.

Methods

Ten healthy subjects (mean age and BMI: 26.1 ± 1.5 years, 22.6 ± 2.0 kg/m²) were acquired through six BTS cameras (60 Hz), synchronized with two Bertec force platforms (960 Hz) and an 8-channel sEMG system (1000 Hz) during three DLs. sEMG sensors were placed bilaterally on the Vastus Lateralis, Rectus Femoris, Tibialis Anterior and Gastrocnemius Lateralis muscles. Thirty reflective markers were positioned following the IORGait protocol [4]. Data were processed in OpenSim (Inverse Kinematics, Inverse Dynamic, SO) using a 6DOF knee MSM to generate input files for Moco EMG-driven analysis and constrain muscle excitations for the CMC. Moco EMG-driven was then applied to estimate MA and MF. sEMG envelope peaks were calculated via bandpass filtering (10–450 Hz) with a fifth-order Butterworth filter. To assess the impact of incorporating sEMG data into MSMs, the root mean square error (RMSE) and coefficient of multiple correlation [5] between muscle activations estimated through the different approaches and experimental sEMG were computed. Paired t-tests using SPM [6] were conducted across all methods.

Results

Results of the present study showed that Moco EMG-driven estimates are closer to the experimental sEMG (correlation > 0.98 and RMSE < 0.02).

Figure 1 compares the right and left leg across the hip, knee, and ankle joints. In *Figure 2*, the comparison between SO, CMC and Moco's MA can be observed.

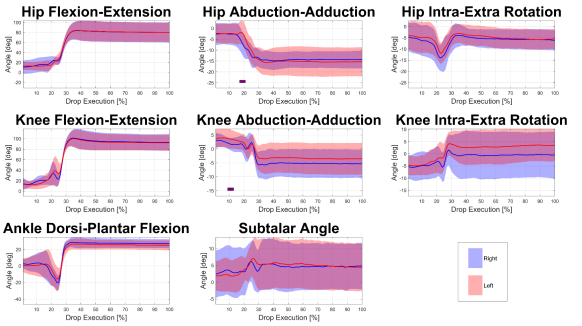


*Figure 1: Lower limbs's joint kinematics comparison between right (blue) and left (red) leg: mean ± std. *statistical significance (p<0.05)*

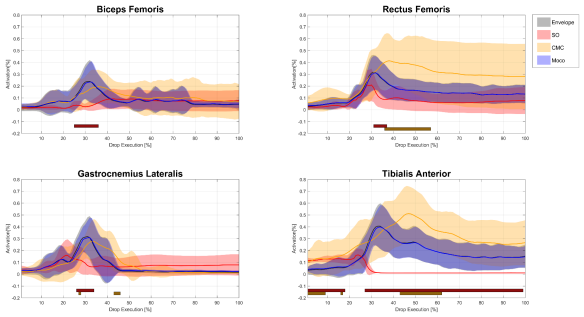


*Figure 2: Comparison among experimental sEMG and SO, CMC, Moco estimates: mean ± std. *statistical significance (p<0.05)*

Discussion

Given that MF cannot be experimentally measured, our results suggest that MF estimated through Moco EMG-driven should be preferred in the context of a 6DOF knee model.

References

1. Pavan D, PhD Dissertation, 2020
2. Roelker S et al., J Appl Biomech, 36:1-20, 2020.
3. Dembia CL et al., PLoS Comput, 16:e1008493, 2020.
4. Leardini A et al., Gait Posture, 26:560-571, 2007.
5. Ferrari A et al., Gait Posture, 31:540-542, 2010.
6. Pataky TC, Comput Methods Biomech Biomed Engin, 15:295-301, 2012.

INVESTIGATION OF STRAIN-RATE INFLUENCE ON THE MECHANICAL BEHAVIOR OF RETINA

Damiano Bertolo (1), Francesca Berti (1), Beatrice Belgio (1), Anna Pandolfi (2), Federica Boschetti (1)

1. Department of Chemistry, Materials and Chemical Engineering "Giulio Natta" (LaBS), Politecnico di Milano, Milano, Italy;

2. Department of Civil and Environmental Engineering, Politecnico di Milano, Milano, Italy

Introduction

Inherited Retinal Diseases (IRDs) are one of the leading causes of blindness among working-age adults. As of now, the best option for treatment is represented by retinal gene therapy, delivered by subretinal injection. Still, many aspects of the procedure have not been extensively studied, and they are mostly left to the surgeon experience. To develop a model of the retina to describe its behavior when subjected to subretinal injection, experimental studies have been carried out. Most studies have investigated the elastic properties of the retinal tissue under uniaxial tensile test [1]. While tensile tests are simple to perform, they fail to recreate a load configuration like what happens in vivo or during surgery. For this reason, small punch tests represent an interesting alternative since they subject the retina to biaxial deformation. One previous work has already analyzed the elastic behavior of retina performing small punch tests. The aim of this study is to explore whether strain rate influences the response of the retina under this load configuration, investigating its viscoelastic behavior. The experimental results were then compared with a finite element model to determine the constitutive parameters of the retina.

Material and methods

To investigate the mechanical behavior of the retina, porcine retinas have been employed due to their similarities with human ones and their high availability. The extraction protocol was taken from a previous work, and it is designed to mechanically isolate the retina without altering its properties [2]. The experimental tests were carried out with a small punch test configuration performed with EnduraTEC ELF 3200 (BOSE) machine test as described in previous work [2]. The displacement measurements were recorded with the machine LVDT transducer while the load was measured with a 1.5 N load cell. The retina sample was fixated between two 3D-printed dies designed with a central hole for the passage of a stainless-steel head punch during the test. Each retina sample was subjected to three precondition cycles with a displacement rate of 0.1 mm/s up to 1 mm. After that, three loading/unloading cycles were performed, each at a different rate, up to 2 mm. The displacement rates selected for this work are 0.01 mm/s, 0.1 mm/s and 1 mm/s. The finite element model employed for the fitting of the experimental data designed in Abaqus CAE models the head punch as a linear elastic material with stainless steel properties (E = 200 GPa, ν = 0.33), while the retina was modeled as a hyperelastic material with a Neo-Hookean constitutive model.

Results

The comparison between the force-displacement curves obtained for each strain rate shows no significant difference. Figure 1 shows a comparison between the average experimental curves for each strain rate tested.

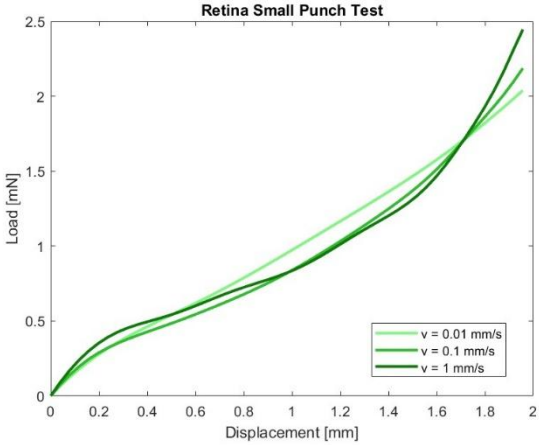


Figure 1: Load-displacement curve of the retina tested with small punch test under different strain-rate.

Different constitutive parameters were tested in the finite element simulation of the small punch test and the best-fit parameters are indicated in Table 1. The results shown in terms of Young's modulus and Poisson's ratio for the average experimental curve are similar to what was found in previous studies [2]. A T-test conducted to compare the Young's Modulus of each strain-rate group demonstrated no statistically significant difference for the range of strain-rate tested in this work.

Parameter	Result	UOM
C10	1.135	KPa
D1	8.837×10^{-3}	1/KPa
E	6.787	KPa
ν	0.495	

Table 1: Best-fit Neo-Hooke parameters and resultant Young's modulus and Poisson's Ration.

References

1. Ferrara et al, Biomechanical properties of retina and choroid: a comprehensive review of techniques and translational relevance. Eye. 35:1818-1832, 2021.
2. Belgio et al, A combined experimental-computational approach for retinal characterization. Experimental Eye Research. 251, 2025.

ANALYSIS OF THE CORRELATION BETWEEN CEREBRAL ANEURYSM SHAPE AND COILING OUTCOMES

Dario Tarantino (1), Salvatore Pasta (1,2), Beatrice Bisighini (3), Alessandra Corvo (3)

1. Department of Engineering, Università degli Studi di Palermo, Viale delle Scienze Ed.8, Palermo, Italy;

2. Department of Research, IRCCS ISMETT via Tricomi, 5, Palermo, Italy; 3. Mines Saint-Etienne, Saint-Etienne, France

Introduction

Intracranial aneurysms (IAs) are pathological conditions characterized by the weakening of the cerebral arterial wall, leading to abnormal dilation. If untreated, IA rupture can cause subarachnoid haemorrhage with high mortality risk. Endovascular coiling is a minimally invasive treatment that has proven effective in reducing rupture risk [1], however, the complex geometry of aneurysms and the unpredictable mechanical behaviour of coils make it challenging to predict treatment outcomes. This study developed a fully automated workflow to investigate the relationship between aneurysm geometry and coil embolization outcomes using advanced finite element (FE) simulations.

Methods

The workflow involved aneurysm geometry analysis, parametric modelling, and numerical simulation of coiling with both rigid and deformable walls. Data were extracted from the open-source clinical database AneuX, and 132 aneurysms were selected based on morphological criteria to create representative models. Three key geometric parameters were identified: maximum diameter (Dmax), neck diameter (Dn), and height (H). These parameters were used to construct a parametric aneurysm model in Grasshopper, enabling the generation of 500 synthetic models sampled via Latin Hypercube Sampling (LHS).

Then, finite element simulations were conducted using Abaqus Explicit. Two simulation sets were performed for each model: one with rigid walls and one with deformable walls, to assess the impact of wall deformability on coil behavior. Simulations employed a standard coil model reflecting clinical properties [2]. Key mechanical outputs, contact pressure (Cpress), reaction force and strain energy, were extracted due to their clinical relevance according to literature.

Finally, Spearman's correlation analysis was used to evaluate relationships between geometric parameters (Dmax, Dn, H) and coiling outcomes.

Results

The workflow successfully simulated coil deployment across all 500 aneurysm models for both rigid and deformable wall scenarios. Variability in final coil configurations was observed, even among aneurysms with similar shape, underscoring the complexity of predicting coil behavior.

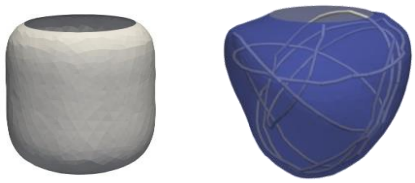


Figure 1: Representations of the same aneurysm in its untreated configuration and after coil deployment.

Correlation analysis revealed weak trends but no strong statistical correlations between aneurysm geometry and coiling outcomes. A weak negative correlation was observed between Dmax and coiling outcomes, suggesting reduced coil effectiveness in larger aneurysms. Similarly, a weak inverse correlation was found between H and mechanical outputs. These findings highlight potential challenges in treating larger or taller aneurysms. No correlation was observed between Dn and the outcomes.

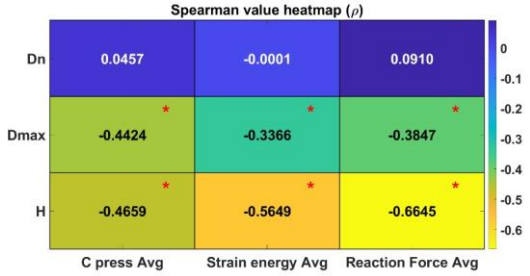


Figure 2: Spearman correlation value heatmap for deformable wall simulations.

Discussion

The study's novel fully automated workflow minimized manual intervention and reduced simulation preparation time while ensuring consistency. This approach improves reproducibility and offers a flexible platform for further exploration of geometric and biomechanical scenarios. While no strong correlations were identified between geometric parameters and coiling outcomes, this study highlights the importance of considering complex biomechanical factors, such as wall properties and blood flow dynamics, in future research. The workflow represents an important step toward personalized surgical planning and improved prediction of coil embolization success, potentially reducing recurrence and complications.

References

1. Zhao, Junjie, et al., Angiology 69.1 (2018): 17-30.
2. Damiano, R. J., Ma, D., Xiang, J., Snyder, K. V., Meng, H., & Kolega, J., *PLoS ONE*, 14(12), e0226421, 2019.

EFFECT OF DIFFERENT BONE MATERIAL FAILURE MODELS ON PROXIMAL FEMUR CRACK PROPAGATION SIMULATIONS

Davide Bentivoglio, Cristina Curreli, Fabio Baruffaldi and Antonino Amedeo La Mattina

Laboratorio di Tecnologia Medica, IRCCS Istituto Ortopedico Rizzoli, Bologna, Italy

Introduction

Femur fractures represent one of the major causes of disability and mortality in the elderly population [1]. The importance of preventing mechanical instability was a crucial aspect from a clinical point of view. CT-based subject-specific finite-element (FE) femur models were developed with the aim of accurately assessing femur fracture risk. However, several materials models and failure criteria have been proposed in the literature based on both strain [2] and stress [3][4][5], with no clear superiority of one over the others. The aim of this study is to investigate the impact of different material failure models on femur crack propagation and fracture load, which have been rarely explored in the literature.

Methods

A proximal femur geometry was derived from a CT scan. A 10-node tetrahedral mesh with element edges of 2.5 mm was generated, and material properties of bone were assigned element-wise, varying the Young modulus with the bone mineral density estimated from the CT scan [6]. A FE simulation (Ansys Mechanical APDL, version 2023R2) was performed for each yield relation [2][3][4][5]; crack propagation and macroscopic fracture were modelled through deactivation of the elements whose von Mises stress/strain overcame its yield value All degrees of freedom of nodes were locked in the lowest part of proximal femur, and a distributed force was applied on the upper surface of the femur head. The load was applied with the following temporal pattern: force was incremented until elements started to fail; the load was then kept constant until no more elements were deactivated; force load was then increased until other elements failed. The analysis continued until numerical divergence occurred, due to rigid body motion of the bone fragments; the last force applied was interpreted as failure load. Other model outputs considered were the first load which deactivated elements (trigger force), and the failed elements, representing the crack line.

Results

Figure 1 shows the force applied through load steps in a femur model: failure and trigger forces were different for each yield relation. In addition, the number of load steps applied until divergence and the crack path obtained with the diverse yield criteria were different. In some cases, the failure and trigger forces were the same (i.e., Kaneko and Schileo).

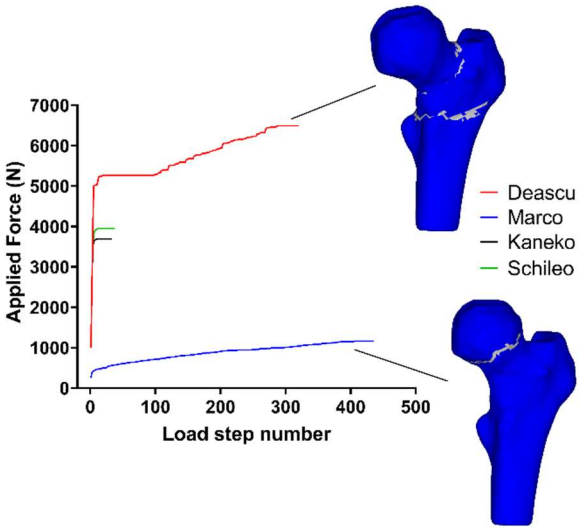


Figure 1: Mechanical response of a proximal femur model with different yield criteria and examples of crack paths obtained using two different models.

Discussion

The analysis performed showed a strong dependence between femur mechanical response and material failure criterion. Different failure relationships influence results in FE simulations in terms of failure initiation, ultimate femur strength and crack propagation. Great care should be taken in the choice of the failure criterion used in FE simulations. Future large-scale high-resolution experimental studies (*e.g.*, organ-scale DVC from micro-CT scans) could help in the development of better materials models.

References

1. Cooper et al., *Osteoporosis Int* **2**, 285–289 (1992).
2. Schileo et al., J Biomech, 41(2):356-367, 2008.
3. Dragomir-Daescu et al., Ann Biomed Eng. 39(2):742-755, 2011.
4. Kaneko et al., J Biomech, 37(4):523-530, 2004.
5. Marco et al., Comput Methods Programs Biomed, 173:67-75, 2019.
6. F. Taddei et al., Medical Engineering and Physics, (29):973-9, Nov 2007.

Acknowledgements

This research was funded by the Italian Ministry of Health — 5 × 1000 Anno 2021, Redditi 2020 "Valutazione motoria strumentale in anziani fragili dopo frattura del collo del femore"

ASSESSING CALCIFICATION EFFECTS IN TEVAR PROCEDURES: A COMPUTATIONAL ANALYSIS

Giulia De Campo (1), Anna Ramella (1), Sara Barati (1), Giulia Luraghi (1), Virginia Fregona (1), Maurizio Domanin (2,3), Robin Heijmen (4) Santi Trimarchi (2,3), Francesco Migliavacca (1)

1.Department of Chemistry, Materials and Chemical Engineering, Politecnico di Milano, Italy

2. IRCCS Ospedale Policlinico di Milano, Italy; 3. Università degli Studi di Milano, Italy 4. Department of Cardiothoracic Surgery, Radboud University Medical Centre, Nijmegen, The Netherlands

Introduction

Thoracic endovascular aneurism repair (TEVAR) is a mini-invasive technique which consists of a placement of a stent-graft in the pathological tract to replace the blood fluid dynamics [1]. TEVAR guidelines discourage the procedure when high calcified aortas are present, in particular in the landing zone regions, due to the possibility of developing endoleak; however, clinicians, sometimes, proceed with the operation off-label despite these recommendations [2]. This study analyzes, in-silico, the effects of the calcification on a patient-specific anatomy after a TEVAR procedure, testing different calcification geometries and mechanical properties.

Methods

A patient-specific anatomy without calcification from Professor Hejimen of Radboud University Medical Center, Netherlands, was taken into consideration for this study. Four different idealized calcification models were built starting from the patient-specific model (Figure 1). Three different elastic modules of the calcification were tested: 2.75 MPa, 50 MPa and 20 GPa. [3][4][5].

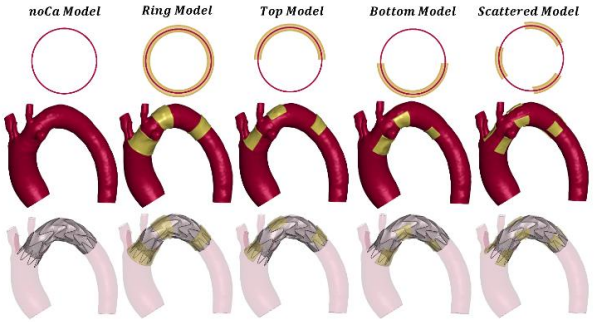


Figure 1- Model illustration and stent-graft implantation simulations in the five models. Calcifications are in yellow.

A total of thirteen simulations of the TEVAR procedure were performed, following the 'tracking method' [1]: the four calcified models times three different Young Modulus plus a reference model without calcification, included for comparative analysis.

Results

Comparing the models from a qualitative point of view, the stent-graft apposition looked the same for all the models, suggesting a good stent-graft apposition even in the presence of calcifications (Figure 1). Relevant results were also achieved with the analysis of the von Mises stresses calculated on aorta and calcification, which presented an opposite trend. Figure 2 highlighted that as the Young modulus of the calcification was reduced from 20 GPa to 2.75 MPa, the stresses on the calcification post-TEVAR implant were highly reduced. While it was the opposite for the aorta: as the Young modulus of the calcifications decreased, the stresses on the aorta raised.

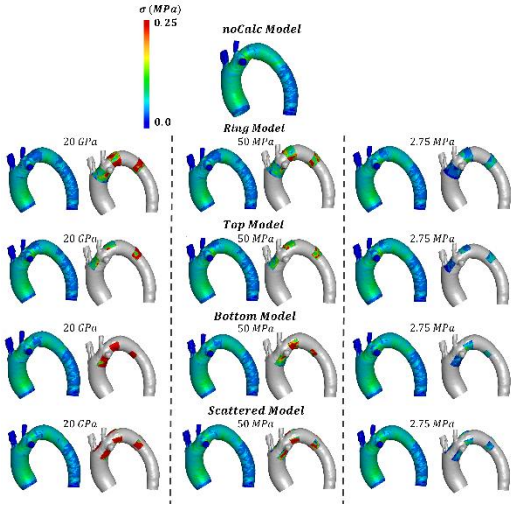


Figure 2- von Mises stresses on the aorta (left) and on the calcifications (right) in the analyzed models.

Regarding the stresses on the stent, the calcification models exhibited higher stresses compared to the non-calcified model (not shown). For what concerned the contact pressure results, instead, the ring model showed very high contact pressure (not shown).

Discussion

From this analysis the calcifications appeared to function as load-bearing structures, reducing stress on the aorta while increasing stress on the stent-graft and on the calcifications. This was a significant finding, as an increase in wall stress on the aorta was associated with a higher risk of aneurysm rupture.[4] In this case, however, calcifications helped reduce the average von Mises stresses on the aorta, potentially lowering the likelihood of aneurysm rupture. This study suggests that TEVAR could still be feasible, at least from the perspectives of stress analysis and qualitative device comparison.

References

1. Ramella et al, Ann Biomed Eng, 50:1941–53, 2022
2. Upchurch et al, J Vasc Surg.,73:55S-83S, 2021.
3. Loree et al, J Biomech., 27:195–204, 1994.
4. Maier et al, Biomech Model Mechanobiol.,9:511–21, 2010
5. Marra et al, Acta Biomater., 2:515–20, 2006

Acknowledgements

PNRR 2022 Mission 4, Component 1: 2022L3JC5T" project, funded by the European Union – NextGenerationEU, under the National Recovery and Resilience Plan (NRRP)

PANCREATIC PHANTOM FOR SURGICAL TRAINING: ANALYSIS OF THE MAIN MECHANICAL PROPERTIES OF HYDROGELS AND SYNTHETIC MATERIALS AS POSSIBLE CANDIDATES

Arianna Callera (1,2) , Giulia De Cristofaro (1), Emma Confortola (2), Federica Potere (1), Paola Nastri (1) Matteo Pagnanelli (2,3), Giovanni Capretti (2,3), Gennaro Nappo (2,3) Alessandro Zerbi (2,3), Francesco Cellesi (1), Maria Laura Costantino (1), Francesco De Gaetano (1,2)

1. Department of Chemistry, Materials and Chemical Engineering "Giulio Natta", Politecnico di Milano, Italy.
2. Department of Biomedical Sciences, Humanitas University, Pieve Emanuele, Milan, Italy;
3. IRCCS Humanitas Research Hospital, via Manzoni 56, 20089 Rozzano, Milan, Italy

Introduction

Post-operative pancreatic fistula (POPF) is one of the most severe complications of pancreatic surgery, particularly following pancreatoduodenectomy. The soft consistency of pancreatic parenchyma makes anastomosis challenging and prone to leakage of enzyme-rich fluids, leading to tissue damage and prolonged recovery. Synthetic pancreatic phantoms that replicate the organ's mechanical properties are essential for training surgeons in innovative techniques and testing new materials to reduce POPF incidence. This study aimed to identify a suitable material for developing a synthetic pancreatic phantom, focusing on mechanical properties such as elasticity, suturability, and tactile resemblance.

Materials & Methods

This project, a collaboration between Politecnico di Milano and Humanitas University, evaluated the mechanical properties of pancreatic tissue (elastic modulus: 2.361 ± 1.349 kPa) as a benchmark. Two material classes, room-temperature vulcanizing (RTV) silicones and gellan gum hydrogels, were analyzed for their potential to replicate pancreatic tissue properties. Mechanical characterization was performed using indentation, creep tests, and tensile testing. Silicone formulations were tuned with a softener (Slacker, Smooth-On Inc.) to adjust elasticity. Gellan gum samples were prepared with varying concentrations (0.5–1%), focusing on achieving elasticity comparable to the pancreas. Sutured samples underwent tensile testing to assess stress at failure. (*Figure 1*).

Results

Gellan gum hydrogels, at low concentrations (0.5–1%), demonstrated elastic moduli closely matching that of pancreatic tissue (*Figure 1*). However, they lacked mechanical integrity and failed to support sutures, which is a critical requirement. RTV silicones showed greater versatility; formulations incorporating additives achieved tunable elastic moduli. The best candidate, Ecoflex 00-20 with 33.3% Slacker, exhibited an elastic modulus of 9.120 ± 2.818 kPa and a tensile tisting at failure of 14.913 ± 2.413 kPa, closely mimicking porcine pancreatic tissue (18.510 ± 6.754 kPa). Additionally, surgeons considered the tactile response and suturability of Ecoflex 00-20 to be the most comparable to human pancreatic tissue.

Discussion

Gellan gum hydrogels, despite their biocompatibility and low cost, fell short due to their lack of suturability, a fundamental property for a training phantom. RTV silicones demonstrated a broader range of mechanical tunability and provided a better balance between elasticity and suture-holding capacity. Although the elasticity of Ecoflex 00-20 slightly exceeds that of

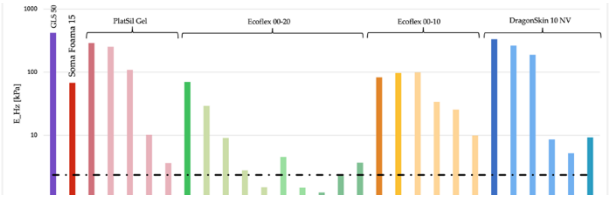


Figure 1. Mean values of the elastic moduli of the silicones analysed.

pancreatic tissue, its tactile feel and performance during suturing were deemed suitable by surgeons. Furthermore, the material's long-term stability and ease of use make it a strong candidate for phantom development (*Figure 2*).

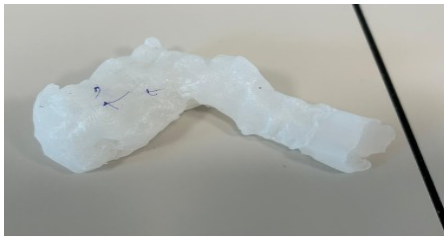


Figure 2. Pancreatic phantom sutured by surgeons

Conclusion

This study identified Ecoflex 00-20 with 33.3% Slacker as the most promising material for producing synthetic pancreatic phantoms. Its mechanical properties closely replicate those of human pancreatic tissue, and its ability to withstand suturing makes it ideal for surgical training applications. The first prototype of the pancreatic phantom has been developed, providing a reliable tool for clinicians to practice and innovate surgical techniques aimed at reducing the incidence of POPF. Future work will refine the prototype and explore additional mechanical parameters to enhance its fidelity to human tissue.

CLINICAL UTILITY OF COMPUTATIONAL HEMODYNAMIC MODELLING IN CORONARY ATHEROSCLEROSIS

Diego Gallo (1), Alessandro Candreva (1,2), Maurizio Lodi Rizzini (1), Andrea Erriquez (3), Barbara E. Stähli (2), Gianluca Campo (3), Simone Biscaglia (3), Umberto Morbiducci (1)

1. Politecnico di Torino, Italy; 2. Zurich University Hospital, Switzerland; 3. Università di Ferrara, Italy

Introduction

The current assessment of coronary atherosclerosis is limited in its ability to determine the risk of future adverse cardiovascular events. Several recent trials have demonstrated the benefits of a physiology-based assessment of patients in identifying those at higher risk of complications. However, such assessment is limited to the evaluation of the pressure drop across the greatest luminal narrowing [1]. Here, we hypothesize that the incorporation of hemodynamic analysis based on wall shear stress (WSS) may provide additional prognostic insights. Such hypothesis is tested in the largest patient cohorts to date to demonstrate the clinical utility of computational hemodynamics in coronary artery disease.

Methods

Study participants. 333 patients from the FIRE trial [1] were included. Patients had myocardial infarction (MI) in a clearly identifiable culprit lesion and at least 1 non-culprit lesion in a different coronary artery. The non-culprit lesion with the greatest percentage area stenosis (%AS) was considered for each patient. Study protocol was approved by local ethic committees.

Computational hemodynamics. Vessel geometries were reconstructed based on 3D quantitative coronary angiography. CFD simulations were carried out using a finite element-based code (CAAS Workstation WSS software, Pie Medical Imaging). The variability of the contraction/expansion action exerted by WSS on the endothelium along the cardiac cycle was quantified in terms of topological shear variation index (TSVI) [2]:

$$\mathrm{TSVI} = \left\{ \frac{1}{\mathrm{T}} \int_0^{\mathrm{T}} [\mathrm{DIV_w} - \overline{\mathrm{DIV_w}}]^2 \mathrm{dt} \right\}^{1/2}$$

where $\mathrm{DIV_w}$ is the divergence of the normalized WSS vector field [2] and T is the duration of the cardiac cycle. TSVI values were averaged over the lesion, defined as the segment containing the minimum lumen area, bounded by the nearest proximal and distal non-narrowed cross-sections.

Outcomes and statistical analysis. Outcome events were death, MI, stroke, or ischemia-driven coronary revascularization occurring within 1 year after the baseline MI. Cox proportional-hazard models were fitted to estimate hazard ratios (HR) for "conventional" risk factors (clinical and patient variables) and TSVI with respect to the outcomes. The incremental prognostic value of TSVI was assessed using the likelihood ratio test.

Causal inference. The causal chain lumen narrowing – hemodynamics – clinical outcome was analyzed using Bayesian networks, where each significant predictor at the univariate Cox analysis and the outcome of interest were represented by a node, while the probabilistic relations among them were represented by edges. The influence of %AS and TSVI on the outcomes was assessed in terms of the so-called percentage indirect causal strength, quantifying the contribution of each factor to the variance of the outcome [3].

Results

Higher lesion TSVI was associated with a higher risk of MI (HR 1.01, p=0.014), and ischemia-driven coronary revascularization (HR 1.01, p=0.013). The incremental prognostic value of TSVI was significant for both MI (p=0.031) and revascularization (p=0.030). The Bayesian networks of causal relationships for MI and revascularization are shown in Fig. 1. Among the causal factors, TSVI was the most influential for MI, with indirect causal strength equal to 6.59%. Its parent node, %AS, had an approximately seven-fold weaker influence (0.89%). For revascularization, TSVI was the most influential direct causal factor (1.04‰), with %AS having a slightly stronger influence (1.08‰) than TSVI.

Discussion

Our findings indicate that TSVI, but not %AS, is an independent predictor of MI or revascularization within 1 year. The causal inference analysis demonstrates that the influence of TSVI on both MI and revascularization is not determined from lumen narrowing, but new 'information' is added. Taken together, the findings highlight the potential clinical utility of TSVI in identifying lesions leading to MI or revascularization.

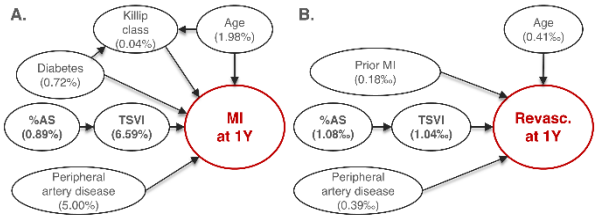


Figure 1: Bayesian networks and percentage indirect causal strengths for MI and revascularization.

References

1. Biscaglia et al., N Engl J Med, 389:889-898, 2023.
2. Morbiducci et al., Ann Biomed Eng, 48:2936-2949, 2020.
3. Janzing et al., Proc Mach Learn Res, 238:2188-2196, 2024.

Acknowledgements

D.G. acknowledges funding from PNC 0000001 D3 4 Health (CUP B83C22006120001).

COMPUTATIONAL STUDY TO ASSESS HEMODYNAMIC FORCES IN DESCENDING THORACIC AORTIC ANEURYSMS

Francesca Duca[1], Daniele Bissacco[2,3], Luca Crugnola[1], Chiara Faitini[4], Maurizio Domanin[2,3], Francesco Migliavacca[1], Santi Trimarchi[2,3], Christian Vergara[1]

1. LaBS, Department of Chemistry, Materials and Chemical Engineering 'Giulio Natta', Politecnico di Milano, Milan, Italy; 2. Clinical and Community Sciences Department, Università degli Studi di Milano, Milan, Italy; 3. Unit of Vascular Surgery, I.R.C.C.S. Fondazione Ca' Granda Policlinico Milano, Milan, Italy; 4. Mines-Paris-PSL, Paris, France

Introduction

Descending Thoracic Aortic Aneurysm (DTAA) is defined as a localized increase in the descending segment of the Thoracic Aorta (TA). Thoracic Endovascular Aortic Repair (TEVAR) is the preferred treatment option for DTAA and it is based on the aneurysm sac exclusion through the deployment of a self-expandable stent-graft. For a successful TEVAR procedure, it is important to identify the correct Landing Zones (LZs) (*Table 1* on the left) where to perform the stent-graft anchoring. LZs with a hostile biomechanical environment may cause an inadequate sealing of the endoprosthesis, leading to its migration or endoleaks [1]. In this context, we propose a Fluid-Structure Interaction computational analysis with the aim of providing quantitative information, at the pre-operative level, useful to predict successful TEVAR outcomes.

Methods

Starting from the segmentation and the virtual manipulation of a healthy TA, we develop twelve TA ideal models: three healthy cases, one for each Aortic Arch (AA) type [2] (i.e., Type I, Type II and Type III), and nine aneurysmatic cases, varying the ubication of DTAA (i.e., Proximal, Central and Distal), further divided according to the AA type. Then, we build three patient-specific configurations by segmenting pre-operative CTA scanning of patients who would undergo TEVAR procedure. In our simulations, we include a turbulence model and we imposed different Young's Moduli for the healthy and the aneurysmatic portion of the aortic wall, considering DTAA stiffer.

Results

Our numerical results, presented in [3], show that the presence of DTAA causes an increase of peak pressure within the aneurysmal sac, especially in Type I and II configurations. The aneurysm shows very low values of blood velocity and blood recirculation regions. The standard deviation distribution of the ensemble velocity proves that Type III cases present a higher likelihood of transition to turbulence. In our analysis, we propose a hemodynamic risk index useful to correlate blood forces with the risk of stent-graft migration associated to each LZ. In all the configurations, the risk index shows the greatest values in correspondence of the aneurysm and high-risk is also found in the AA region, where the proximal sealing is often performed (*Table 1*).

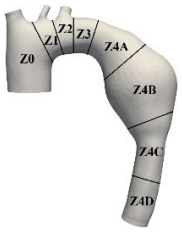
LZs map	LZ	PT-09	PT-40	PT-71
	Z0	0.2	0.1	5.3
	Z1	4.7	41.5	0.8
	Z2	0.2	0.0	51.3
	Z3	0.2	0.8	72.1
	Z4A	82.6	0.0	0.6
	Z4B	7.5	8.7	55.5
	Z4C	0.3	1.6	0.3
	Z4D	0.3	258.6	0.2

Table 1: Risk index for each LZ for the three patient-specific configurations. Red cells identify LZs involved by the pathology while green cells identify suitable LZs.

Results in the patient-specific cases show similarities with the corresponding ideal scenarios (*Figure 1*).

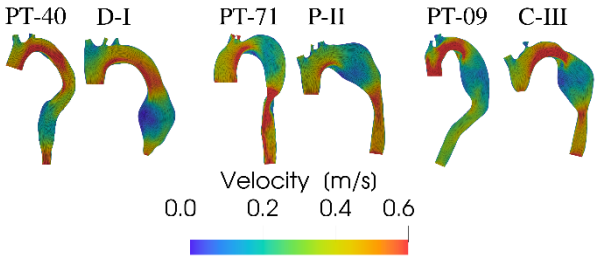


Figure 1: Systolic peak velocity for the patient-specific configurations and for their corresponding ideal cases.

Discussion

Our pre-operative analysis is a useful tool for clinicians to identify the suitable LZs to perform a correct stent-graft sealing (*Table 1*). Given the accordance between the patient-specific and ideal results, the analysis of the ideal cases supports a general *a priori* assessment of the hemodynamics of any patient-specific case.

References

1. Marrocco-Trischitta, M. M., et al, European Journal of Cardio-Thoracic Surgery, 55:990-997, 2019.
2. Madhwal, S., et al, The Journal of invasive cardiology, 20:200-204, 2008.
3. Duca, F., et al, preprint bioRxiv 2024.11.22.624794, 2024.

Acknowledgements

This work was supported by research project MIUR PRIN22 n.2022L3JC5T and by PNRR 2022 Mission 4 Component 1: 2022L3JC5T, both funded by European Union-NextGenerationEU.

COMPUTITIONAL MODELING FOR PRE-OPERATIVE PLANNING OF PATIENT-SPECIFIC VENTRICULAR ASSIST DEVICES IMPLANT

Eleonora Costagliola (1), Salvatore Pasta (1,2), Michele Pilato (3), Sergio Sciacca (3)

1. Department of Engineering, Università degli Studi di Palermo, Viale delle Scienze Ed.8, Palermo, Italy

2. Department of Research, IRCCS ISMETT via Tricomi, 5, Palermo, Italy

3. Department for the Treatment and Study of Cardiothoracic Diseases and Cardiothoracic Transplantation, IRCCS-ISMETT, Palermo, Italy, IRCCS ISMETT via Tricomi, 5, Italy

Introduction

Ventricular assist devices (VADs) are used in patients for the treatment of end-stage heart failure, helping the left ventricle pump blood to the rest of the body. When a VAD is implanted, clinical evidence suggests that the device inflow needs to be placed below the papillary muscle with the device axis being parallel to the intraventricular septum. Under these conditions, the risk of adverse hemodynamic events is greatly reduced [1]. Moreover, the Heartmate III manufactured by Abbott is a large device with the risk of pushing the ribs and then leading to patient pain.

This study aims to develop a cardiac tool based on computational simulations and extended reality to improve the implantation of VAD.

Materials and methods

Diagnostic computed tomography (CT) images were used to generate 3D models of the relevant cardiac structures (the rib cage and left ventricle) using the medical imaging software Mimics (Materialise, Belgium) as depicted in Figure 1 (A). A computed-aided-design (CAD) model was developed for the Heartmate III VAD device using photography and caliber measurement. Thus, segmented anatomies were meshed to account meshed 520,188 tetrahedral elements for the ribs, 261,984 tetrahedral elements for the left ventricle using the ICEM CFD (v21.0, ANSYS Inc., Canonsburg, PA). The VAD device and the ribs were modeled as a rigid material (Figure 1 (B)). The left ventricle was modeled using an anisotropic and hyperelastic material model as done previously [2]. The VAD was placed near the apex according to surgeon indications and the insertion was simulated using a velocity boundary conditions in ABAQUS/Explicit software (ABAQUS v2023, SIMULIA Inc., Providence, RI, USA). Specifically, the simulation was divided into two steps: 1) the device was inserted into the left ventricle using the surface at the base of the device inflow as the only surface enabled for contact conditions (penalty with friction coefficient of 0.15); 2) the velocity boundary conditions was disabled and the elastic recoil determined the springback of the device while a contact between the bottom device surface and the ribs was activated.

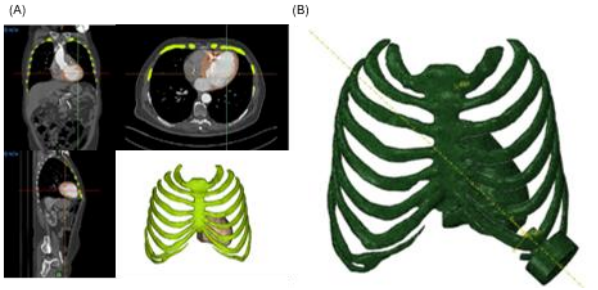


Figure 1 (A) 3D models segmentation in Mimics, (B) Models of the interest with mesh.

Results and Discussion

Realistic deformation of the left ventricle and interaction with the rib cage during the VAD insertion highlights were observed. The simulations provided data on the displacement of cardiac structures and the forces exerted during VAD insertion ensuring precise positioning of the device. Figure 2 illustrates final VAD positioning with optimal alignment with the apex of the left ventricle, ensuring stability and minimizing structural interference with surrounding tissues.

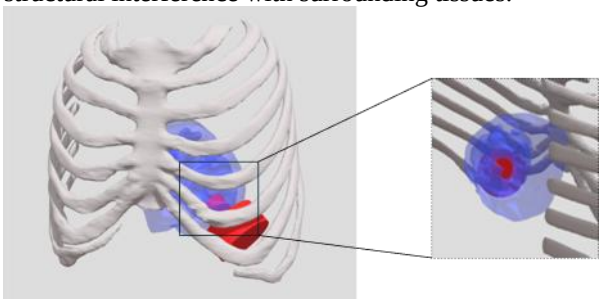


Figure 2 Final content of VAD implantation from different views.

Conclusions

The study presents a pipeline for creating cardiac simulations for pre-operative planning of VAD implant. Findings demonstrate the importance of role played by numerical simulations in procedural planning. This benefits physicians, simulation experts and enhance patient safety.

References

1. Marsden et al, WIREs Mech Dis, 6:169-188, 2014.
2. Costagliola et al, Med Eng Phys , 134:104258, 2024.

TOWARD PATIENT-SPECIFIC IN SILICO PLANNING OF TRANSARTERIAL EMBOLIZATION FOR LIVER CANCER TREATMENT

Enrico Sangiorgio[1,2], Valentina Mazzi[1], Giuseppe De Nisco[1], Selene Andreetta[3], Federica Sacco[3], Giuseppe Isu[3], Diego Gallo[1], Umberto Morbiducci[1]

1. Politecnico di Torino, Italy; 2. Università degli Studi di Palermo, Italy; 3. Medics srl, Italy.

Introduction

Transarterial embolization (TAE) is a commonly used therapeutic approach in the management of patients with intermediate-stage hepatocarcinoma (HCC) [1]. When surgical resection and liver transplantation are not viable options, TAE is employed to selectively occlude the hepatic arteries supplying the HCC through the local catheter injection of microparticles. The latter can also serve as drug-delivery systems for chemotherapeutics or radiopharmaceuticals [1]. In recent years, computational fluid dynamics (CFD) has emerged as a valuable tool for analyzing the influence of clinically variable parameters on embolizing agents' downstream distribution and, ultimately, treatment outcomes [2]. CFD simulations facilitate the modeling of particles transport in hepatic arteries, thereby enabling *in silico* replications of the TAE procedure [2]. In this context, personalized *in silico* models are essential for ensuring the reliability of the simulated embolization procedure, considering the substantial variability in hepatic arterial anatomy and cancer progression scenarios. However, the adoption of simulated TAE is still limited to a few single-patient cases, thus restricting the generalizability of findings [2]. This study aims to assess the feasibility of a unified computational framework across various TAE clinical scenarios.

Methods

Hyper Accuracy 3D® (HA3D®) technology, developed by Medics srl (Torino, Italy), is employed to generate patient-specific 3D anatomical reconstructions of the liver parenchyma, vasculature, and tumor lesions from computed tomography images. Then, the geometry of the hepatic arterial tree is extracted and discretized in Ansys Fluent (Ansys Inc., Canonsburg, United States). On the discretized domain, the equations governing the fluid motion and particles transport are solved using the Finite Volume method. In doing that, blood is modeled as an incompressible fluid, and the simplified Quemada model is adopted to account for blood shear-thinning behavior [3]. Personalized outflow boundary conditions (BCs) are prescribed by assigning a flow rate value, which is given by the sum of a healthy and a tumor flow contribution, to each outlet [3,4]. The estimation of the two flow terms is based on the evaluation of (i) hepatic segment volumes and intra-segment branching fractions (i.e., healthy flow), and (ii) tumor volume and tumor perfusion percentages, which are calculated from the reconstructed 3D geometries using a region-growing model (i.e., tumor flow) [3,4]. The inlet BC is prescribed in terms of a spatially uniform velocity profile adopting a generalized flow waveform, which is scaled to ensure that the average inflow equals the sum of the estimated outflows [3].

Results

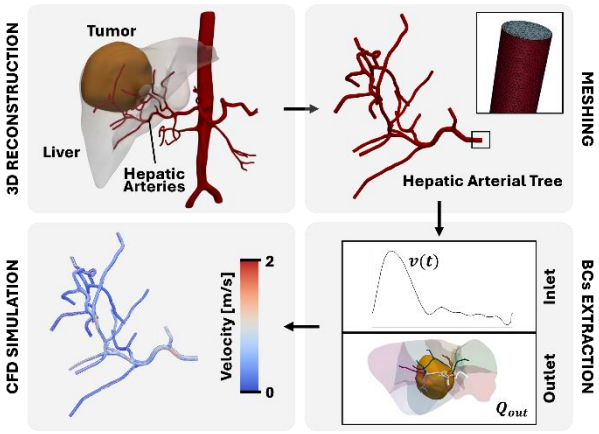


Figure 1: Patient-specific computational workflow for TAE replication, comprising the following steps: (i) 3D model reconstruction, (ii) meshing, (iii) BCs extraction, and (iv) CFD simulation.

Using the workflow of the *in silico* platform presented in Figure 1, clinically relevant aspects, such as the drug dose delivered to the tumor, can be assessed simulating various TAE settings – including catheter type, catheter position, particle properties, or drug injection strategy – and evaluating the impact of such critical variables in order to tailor the procedure to the patient case.

Discussion

By tailoring CFD simulations to individual anatomical and hemodynamic characteristics, the framework herein presented shows significant potential for pre-treatment planning of TAE. In the future, it can be enriched by (i) adopting truncation strategies to enhance computational efficiency, and (ii) including patient-derived inflow BC.

References

1. Pérez-López et al, Acta Biomaterialia, 149:1-15, 2022
2. Aramburu et al, Cardiovasc Interv Radiol, 45:12-20, 2022
3. Aramburu et al, Int J Num Meth Biomed Eng, 32(11), 2016
4. Bomberna et al, Front Bioeng Biotech, 10(914979), 2022

Acknowledgements

This work was carried out within the project TEPSIM – MUR – M4C2 1.5 of PNRR-NGEU (GA No. ECS00000036). ES scholarship is part of the project PNRR-NGEU, which has received funding from the MUR – DM 630/2024.

HIGH-PERFORMANCE COMPUTING FOR HIP REPLACEMENT IN SILICO TRIALS

Enrico Toccaceli (1), Antonino Amedeo La Mattina (2), Massimiliano Mercuri (1), Cristina Curreli (2)

1. Department of Industrial Engineering, Alma Mater Studiorum - University of Bologna, Italy
2. Medical Technology Lab, IRCCS Istituto Ortopedico Rizzoli, Bologna, Italy

Introduction

Total hip replacement (THR) is the standard treatment for degenerative hip conditions, including osteoarthritis and rheumatoid arthritis, and it demonstrates a high success rate (90% at 10-year follow up). Nevertheless, THR procedures are not without failure, and aseptic loosening, primarily caused by the loss of primary stability, is the most common cause for revision, accounting for 36% of all failures [1]. New THR designs are continuously being developed to overcome the issues related to current solutions. The use of in silico models is increasingly recognized as a promising approach to investigate device safety and/or effectiveness. However, many simulation workflows are computationally expensive, and running a large cohort of simulated patients that represents the population of interest is often too demanding. The aim of this study is to investigate the use of high-performance computing (HPC) infrastructures to run in silico trials to assess the primary stability of total hip replacements.

Methods

The computational pipeline began with the output from computer-aided surgical plannings. These included femoral head resection and accurate prosthesis placement. CT data of five patients were taken from the HFValid dataset [2] and the implant geometry was provided by Adler (Milan, Italy). The surgical planning was performed using an in-house developed interactive software based on Hip-Op [3]. Then, an automatic Boolean subtraction technique, implemented using SpaceClaim (Ansys Inc., PA, USA) and Python, was employed to remove intersecting regions between the femur and the hip implant. An in-house developed Python clone of Bonemat [4] was then used to map CT densitometric data into a heterogeneous material mesh for the bone tissue, ensuring an accurate representation of patient-specific material properties [5]. A subject-specific finite element (FE) model was generated using Ansys Mechanical APDL (Ansys Inc., PA, USA) to simulate contact mechanics. The loading conditions applied replicate the maximum forces on the hip joint during walking and stair climbing. All the modeling steps after the planning were ported to a HPC cluster (Leonardo, CINECA, Bologna, Italy), and submission scripts for SLURM scheduler were developed, thereby facilitating efficient resource management. Special attention was given to configuring virtual environments and managing software dependencies, using tools for dependency control and precompiled modules. The integrity and stability of the pipeline were also evaluated.

Results

The adaptation of the pipeline to the HPC infrastructure resulted in a 30% reduction of single simulation wallclock time compared to local servers, while preserving stable and reproducible results. Moreover, the concurrent simulation of multiple virtual patients allowed for massive parallel processing, thus dramatically decreasing the time-to-solution of the model cohort. The results of the test performed demonstrated scalability and robustness of the workflow.

Discussion

The integration of the in silico trial simulation workflow with HPC infrastructure represents a transformative step in the evaluation of new THR designs. By leveraging the scalability of HPC, the workflow enables simulations to be performed on a larger and more diverse cohort of virtual patients, thereby improving the statistical robustness of primary stability assessments. These advancements not only enhance efficiency and reduce the time-to-solution of simulations but also support the inclusion of more detailed and complex models. Ultimately, the ability to simulate and analyze multiple scenarios in parallel speeds up the research and development cycle, enabling quicker implementation of innovative designs. The combination of in silico simulations and HPC resources underscores a new era of innovation in orthopedic device development.

References

1. Hauer et al., Arch Orthop Trauma Surg, 144:5199–5204, 2024.
2. Aldieri et al., Hip-Fracture validation collection, University of Bologna, 2022, DOI: 10.6092/unibo/amsacta/7126.
3. Lattanzi et al., Med Infrom Internet, 27:71–83, 2002.
4. Taddei et al., Med Eng Phys, 29(9):973-9, 2007.
5. Aldieri et al., Comput Methods Programs Biomed, 240:107727, 2023.

Acknowledgements

This study was funded by the Italian Ministry of University and Research (MUR) – Project “IST4HR – In Silico Trials for Hip Replacements” – CUP J53D23002330006 – Grant Assignment Decree No. 742.
We acknowledge CINECA for the availability of HPC resources and support.

A FE-DRIVEN TOPOLOGY OPTIMIZATION APPROACH FOR ADVANCED 3D PRINTING OF TRANSTIBIAL PROSTHETIC SOCKET

Cristina Falcinelli (1), Iacopo Bianchi (2), Alessia Carugno (1), Archimede Forcellese (2)

1. Department of Engineering and Geology, University G d'Annunzio Chieti-Pescara, Italy; 2. Department of Industrial Engineering and Mathematical Science, Università Politecnica delle Marche, Italy

Introduction

Conventional manufacturing of transtibial prosthetic sockets (TPS) is a labor-intensive process [1], resulting in material waste, long processing times, and high costs. Furthermore, the quality of the final product is highly dependent on the expertise of the technician. To overcome these limitations and ensure a more sustainable and optimized production pipeline, combining the 3D printing and Topology Optimization (TO) may represent a promising approach. The 3D printing, which creates objects from three-dimensional data using digitally controlled material deposition techniques, reduces material waste, shortens the fabrication time, and eliminates the need for most skill-based manual operations. It also allows the production of complex geometries and highly customized parts. TO, a computational technique used to determine the optimal material distribution in a given space [2], enables the design of lighter, more material-efficient, and comfortable wearable devices, offering cost-efficiency in both materials and processing. As such, the aim of this study is to: 1) develop a finite element (FE)-based TO algorithm to identify the optimal material configuration within a TPS, 2) perform a validation analysis to confirm the structural performance of the optimized shape, and 3) fabricate the optimized TPS using 3D printing technology to evaluate the manufacturing time and cost and compare the innovative solution costs with the traditional alternative.

Methods

A TPS of a male patient with a left-side amputation was scanned using the Occipital System SA38 to reconstruct the 3D geometry. The residual limb geometry was created through CAD modeling to account for soft tissues. Both the TPS and residual limb geometries were imported into COMSOL, discretized using 10-node tetrahedral elements, and modeled as homogeneous isotropic linearly elastic materials. The TPS was assumed to be made of Polyamide (PA12) with a Young's modulus of 1029 MPa and a Poisson's coefficient of 0.4, and the residual limb was modeled with a Young's modulus of 200 kPa and a Poisson's coefficient of 0.49 [3]. The TPS and residual limb were considered bonded. A FE-based TO algorithm was implemented, starting with a static analysis to compute stress/strain patterns, followed by iterative TO analyses to determine the optimal material distribution. A FE analysis was carried out to validate the structural performance of the optimized shape by comparing the original prosthetic socket and the optimized design in terms of displacement field and Von Mises stress distribution. Finally, the optimized TPS was 3D printed using a FDM 3D printing machine and a cost comparison was made between the optimized and traditional manufacturing methods.

Results

FE-based TO determined the optimal material distribution for the TPS (Figure 1a). Validation analysis confirmed the structural performance of the optimized shape, showing that the displacement distribution remained nearly unchanged compared to the non-optimized TPS except for the superior part of the medial region of the TPS. The Von mises stress distribution resulted more distributed across the optimized design, although the new design exhibits higher peak Von Mises stress values compared to the non-optimized design. Figure 1b shows the 3D-printed TPS. The proposed approach resulted in a 50% reduction in production time and an 80% reduction in manufacturing costs compared to traditional processes. Additionally, optimizing material distribution led to a 38% reduction in material usage.

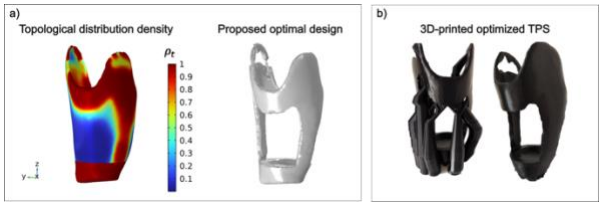


Figure 1: a) *Topological density distribution (ρ_t) and the proposed optimal design of TPS. b) The 3D-printed optimized TPS*

Discussion

The proposed approach highlights the feasibility and advantages of using 3D printing and TO for TPS design offering significant improvements in both material efficiency and cost-effectiveness. Moreover, this approach allows for the creation of highly customized TPS, ensuring better comfort for the patient. Future work will involve investigating additional loading conditions, exploring different materials and SLS technology for 3D printing, and conducting experimental tests on the optimized TPS.

References

1. Wang et al, Engineering, 6:1258-1266, 2020.
2. Sigmund et al, Struct Multidisc Optim, 48:1031-1055, 2013.
3. Jia et al, J Biomech, 37:1371-1377, 2004.

VALIDATION OF A COMPREHENSIVE METHODOLOGY FOR SIMULATING PATIENT-SPECIFIC LASER REFRACTIVE SURGERIES

Benedetta Fantaci (1), Elena Redaelli (2), Monica Martí (3), Anton Barraquer (3), Rafael Barraquer (3), Jorge Grasa (1), Begoña Calvo (1,2)

1. I3A, Universidad de Zaragoza, Spain.; 2. Centro de Investigación Biomédica En Red CIBERN-BBN),Spain; 3. Centro de Oftalmología Barraquer, Barcelona, Spain

Introduction

Laser refractive surgeries have become the preferred treatment for correcting low-to-medium refractive errors by reshaping the cornea with a laser to eliminate the refractive defect. In this work, we present a comprehensive methodology to simulate three refractive procedures—Photorefractive Keratectomy (PRK), Laser In-Situ Keratomileusis (LASIK), and Small Incision Lenticule Extraction (SMILE)—using patient-specific finite element models (FEM), which account for the corneal geometry, intraocular pressure (IOP), and material behavior.

Methods

The patient's corneal topography serves as the input to our methodology [1]. Corneal surfaces are obtained using a clinical topographer and reconstructed through polynomial fitting to generate the FE model. Patient-specific material properties are then computed using an artificial neural network (ANN) [2], trained on simulated non-contact tonometry data, a clinical exam that measures corneal deformation in response to an air puff. A non-linear anisotropic HGO constitutive model is employed to represent the behavior of corneal tissue, accounting for two families of collagen fibers [3]. The model incorporates the patient's IOP calculated using the equation proposed by Redaelli et al [4]. Sliding boundary conditions are applied to the corneal base. The surgical treatment plan is retrieved to define the dioptric target to be corrected. Before running the simulation, the stress-free configuration is recovered by means of a zero-pressure algorithm. Then, the model is pressurized with patient's IOP and the three surgical procedures (PRK, LASIK and SMILE) are simulated on the same patient. PRK consists of a surface ablation; in LASIK, a hinged flap is created and lifted to ablate the corneal stroma; in SMILE a lenticule is created and extracted through a small incision. 24 eyes of 12 patients, who previously underwent the three treatments, were selected to validate the methodology and an optomechanical analysis was conducted.

Results

Three patients with similar characteristics were compared from a mechanical perspective (Figure 1.b): PRK was found to be the least invasive treatment in terms of the stress and strain induced by the surgery. SMILE resulted in the highest stress increase at the posterior cornea, with a 12.6% increment compared to 4.3% for PRK and 7.4% for LASIK. From an optical perspective (Figure 1.a), the refractive outcomes were assessed by calculating the mean anterior curvature and comparing it with the clinical data of the 12 patients. A mean error of 0.5 D with respect to clinics was observed.

Discussion

The methodology enables the analysis of the impact of various refractive treatments on patients' corneas by incorporating patient-specific mechanical properties and intraocular pressure (IOP). It can be applied in presurgical evaluations to test multiple treatment setups and assess the optomechanical effects of different procedures on the same patient. A preliminary validation of the methodology is presented, demonstrating good optical accuracy when compared with clinical data. The same methodology will be applied to a larger dataset of patients who have undergone all the three treatments.

References

1. Fantaci B. et al., TVST. Vol.13, 11, 2024.
2. Redaelli E. et al., Comp in Bio and Med (under review).
3. Wang S. et al., J Bio Eng, 143(3), 2021.
4. Redaelli E. et al., Frontiers in Biotech. And Eng., 2024.

Acknowledgments

This project has received funding from the European Union's Horizon 2020 research and innovation programme under grant agreement No 956720.

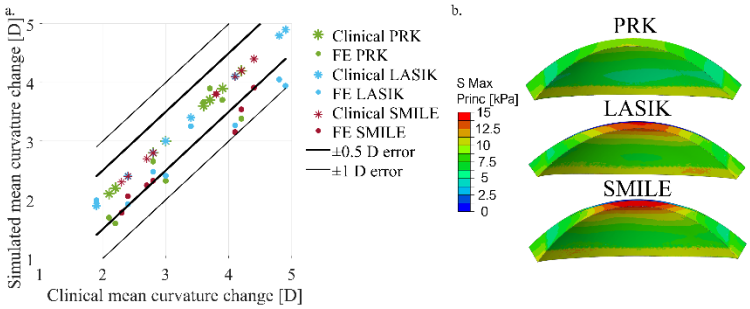


Figure 1: a. Clinical vs. simulated mean curvature change; b. Maximum principal stress distribution caused by the three treatments.

DYNAMIC MODULATION OF CELL MORPHOLOGY USING A PHOTOSWITCHABLE PDR1M–BASED PLATFORM

Francesca Mauro (1,2), Carlo F. Natale (2), Valeria Panzetta (1,2,3), Paolo A. Netti (1,2,3)

1. Interdisciplinary Research Centre on Biomaterials (CRIB), University of Naples Federico II, 80125 Naples, Italy;
2. Istituto Italiano di Tecnologia, IIT@CABHC, 80126 Naples, Italy;
3. Department of Chemical, Materials and Production Engineering, University of Naples Federico II, 80125 Naples, Italy;

Introduction

The cellular microenvironment is critical in regulating cellular functions, influencing a wide range of biological processes [1]. Bidirectional communication between cells and the extracellular matrix (ECM) occurs through the transmission of biochemical and biophysical signals at the sub-micrometric level [2]. This interaction involves various sub-cellular components, including focal adhesions, cytoskeletal structures, and the nucleus. In this context, over the years, multiple surfaces exhibiting topographical, mechanical, and chemical cues have been developed, driven by advancements in fabrication technologies, to enhance our understanding of cell-material interactions [3,4]. However, most of these are static and do not reliably recapitulate the dynamic nature of the ECM. For this reason, we developed a pDR1m-based photo-switchable platform that enables precise control of surface topographic features in both space and time, providing a powerful tool to study mechanotransduction-driven processes.

Methods

Poly(disperse red 1 methacrylate) (pDR1m) was spin-coated onto glass-bottom Petri dishes to create a thin film, and a sub-micrometre grating was inscribed using a scanning confocal microscope with a 514 nm laser. The removal of the patterned grating was achieved using a mercury lamp. MCF10A cells were cultured in DMEM/F12 supplemented with 5% horse serum and seeded onto pDR1m substrates at a density of 10^3 cells/cm², 24 hours before pattern inscription. Then, cells were fixed in paraformaldehyde 4% and immuno-stained for actin (Phalloidin). Cell orientation was analysed using Fiji.

Results

To evaluate the ability of the pDR1m platform to induce dynamic variations in subcellular structures, specifically cell morphology, confocal z-stack images of phalloidin-stained cells were analysed to assess changes in cell orientation upon topography photo-switching. In particular, confocal images were captured on flat surfaces, 3 hours post Flat–Pattern switching and 3 hours post Pattern–Erased switching (Figure 1A). The results revealed that photopatterning caused cells to align more prominently along the pattern direction ($\theta \sim 20°$), while photoerasure led to a return to a more random orientation ($\theta \sim 45°$), as for cells on the flat surfaces (Figure 1B).

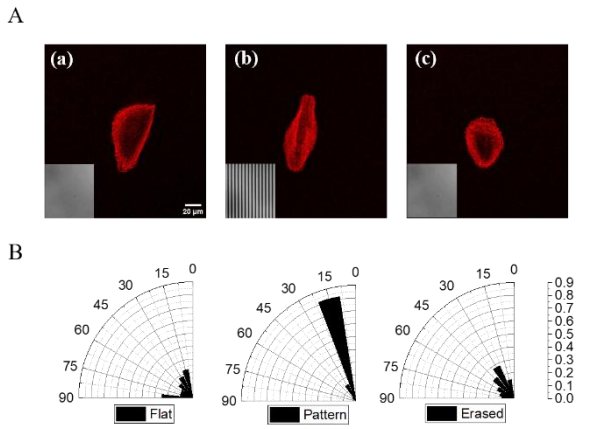


Figure 1: A) Confocal images of phalloidin-stained MCF10A cells on the flat (a), on photopatterned (b) and on erased (c) surfaces. B) Angular plots of cell orientation on the different surfaces.

Discussion

Topographical cues play a crucial role in regulating cell behaviour, influencing various processes at multiple levels, including adhesion, migration, proliferation, and differentiation. These cues provide spatial and mechanical signals that cells interpret and respond to within their microenvironment. In this study, we developed an innovative photo-switchable platform designed to deliver cyclic topographical stimuli, enabling precise control and guidance of cellular behaviour in both space and time. By leveraging the unique properties of this platform, we were able to observe dynamic changes in cell orientation in response to the cyclic modulation of surface features. Our findings demonstrated that the platform effectively induces reversible and cyclic alterations in cell orientation, underscoring its potential to dynamically regulate cellular responses. This ability to provide controlled, spatiotemporal guidance offers a powerful tool for studying mechanotransduction and guiding cell decisions in tissue engineering applications.

References

1. Ventre M et al, J R Soc Interface. 2012;9: 2017–2032.
2. Frantz C et al, J Cell Sci. 2010;123: 4195–4200.
3. Mirbagheri M et al, Mater Horiz. 2019;6: 45–71.
4. Cai S et al, Nanotechnol Rev. 2020;9: 971–989.

PREDICTING SPRINGBACK IN NITI ANNULOPLASTY RINGS WITH PHASE-SPECIFIC STRESS SCALING

Francesca Rossi (1), Dario Carbonaro (1), Carlo Guala (2), Giovanni Giordano (2), Claudio Chiastra (1), Cristian Faggian (2), Alberto Audenino (1)

1. Polito^{BIO}Med Lab, Politecnico di Torino, Italy; 2. Corcym s.r.l., Italy

Introduction

Functional tricuspid insufficiency, commonly associated with mitral valve disease, is generally treated using prosthetic annuloplasty rings (ARs). These devices are manufactured from nickel-titanium (NiTi) tubes through a shape-setting process, which involves heat treatment of the tube while it is inserted into a circular mold, to define the final shape of the AR. However, residual stresses left in the NiTi after the heat treatment cause springback of the AR upon removal from the mold, resulting in deviations from the intended geometry. In this context, the present study proposes a computational procedure based on finite element (FE) analysis for the prediction of springback of NiTi ARs.

Methods

Four NiTi tubes, two laser-cut and two non-laser-cut, each available in two different sizes (i.e., sizes 1 and 2), underwent a shape-setting process to achieve a circular shape. The process consisted of two main steps: (1) insertion of the NiTi tube into a circular mold and (2) heat treatment in a high-temperature salt bath, followed by removal from the mold. This procedure was repeated three times for each of the four NiTi tubes. After shape-setting, their geometries were reconstructed using the optical measurement machine Smart-Scope ZIP250 (OGP Hommel srl). FE models of the NiTi tubes were developed using hexahedral elements and a super-elastic constitutive material model for NiTi. The FE analysis replicating the experimental procedure was performed in Abaqus Standard (Dassault Systemes Simulia Corp.) and comprised two main steps: (1) insertion of the NiTi tube into the mold, modelled with rigid surfaces (Fig. 1a); (2) heat treatment and extraction of the NiTi tube from the mold (Fig. 1b). The heat treatment process was modelled by scaling the stresses with constant relaxation coefficients. Specifically, relaxation coefficients r_p and r_a were applied to stresses exceeding the upper plateau stress of NiTi (i.e., when the material is in the transition phase between austenite and martensite) and to stresses below the upper plateau stress (i.e., when the material is in the austenitic phase), respectively. First, the relaxation coefficients were calibrated by fitting the FE model to the experimental data of the laser-cut tube with size 1, minimizing the difference at four points along the NiTi tube (Fig. 1c). Thereafter, the procedure was validated by comparing the geometries predicted by the calibrated FE model with those obtained experimentally for the laser-cut tube with size 2 and the non-laser-cut tubes with sizes 1 and 2 (Fig. 1d).

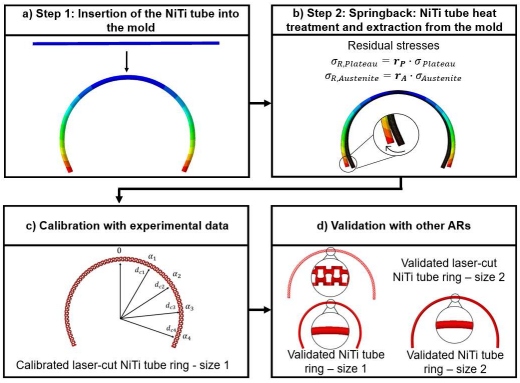


Fig. 1: Main steps of the computational procedure for the springback prediction in NiTi annuloplasty rings.

Results

Relaxation coefficients r_p = 2% and r_a = 27% were determined by the calibration procedure for the laser-cut NiTi tube with size 1. This resulted in a maximum percentage error of 0.84% (at point α_4) in the distance between the geometry predicted by the FE analysis and that measured experimentally (Fig. 2a). Moreover, the computational procedure was successfully validated for the other NiTi tubes, as illustrated in Fig. 2b.

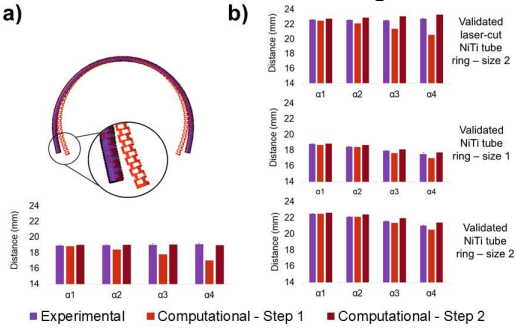


Fig. 2: a) Calibration and b) validation of the computational procedure for the springback prediction.

Discussion

The computational procedure enabled the springback prediction across various NiTi tubes, highlighting the role of phase-dependent residual stresses in springback. To conclude, the computational procedure provides a valuable tool for improving the design and manufacturing of NiTi ARs, reducing the need for trial-and-error adjustments during the design phase.

Acknowledgements

This work is part of PNRR MUR - M4C2 1.5 – NODES, funded by European Union - NGEU (GA No. ECS00000036)

MULTISCALE AND MULTIMODAL CHARACTERIZATION OF THYMUS VISCOELASTICITY AND MICROSTRUCTURE FOR BIOMIMETIC DESIGN APPROACHES

Francesco Fontana (1), Ludovica Cacopardo (1), Giulia Paties Montagner (1), Nicole Guazzelli (1), Arti Ahluwalia (1)

1. University of Pisa, Italy

Introduction

The thymus has a pivotal function in the generation of immunocompetent T cells. Despite this function strictly relies on its complex extracellular matrix, to date, the organization of its 3D mesh structure, as well as its mechanical properties have been poorly investigated [1]. This missing gap hampers any attempt to model and engineer this organ.

Methods

Fresh thymuses were provided by a local slaughterhouse (Macelli di San Miniato s.r.l., Pisa, Italy). After cutting, samples (20x20x10 mm) were fixed on a petri dish and partially submerged with water. Indentation (tip radius = 2.5 mm) and compression tests were performed with a Mach-1 v500css (Biomomentum Inc., Montreal, Canada) equipped with a 17 N multiaxial load cell (Figure 1). For indentation mapping, stress relaxation tests (iSR) were performed, while in the case of bulk compression different stimuli were applied (step, ramp and sinusoid) performing bulk stress relaxation (bSR), epsilon-dot (bε̇) and cyclic testing.

The constitutive equation of a Generalized Maxwell model (n=2) was fitted to experimental curves to derive the viscoelastic descriptors: relaxation time (τ), instantaneous and equilibrium moduli (Einst and Eeq) as well as storage and loss moduli (E' and E'') [2].

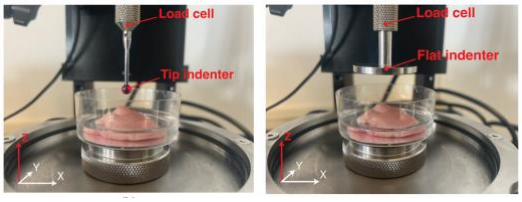


Figure 1: Indentation and compression setup

Histological (hematoxylin and eosin) and scanning electron microscopy (SEM) images were also acquired and analyzed with ImageJ to derive microstructural features: pores (P) and fibers (F) dimensions as well as medulla thickness (MT) and area (MA), cortex thickness (CT) and area (CA) and parenchymal (PT%) and adipose (AT%) tissue percentage.

Results

Figures 2, 3 and 4 respectively report the results for thymus characterization.

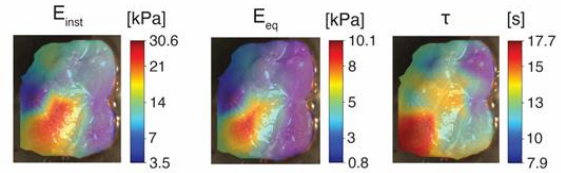


Figure 2: Indentation mapping

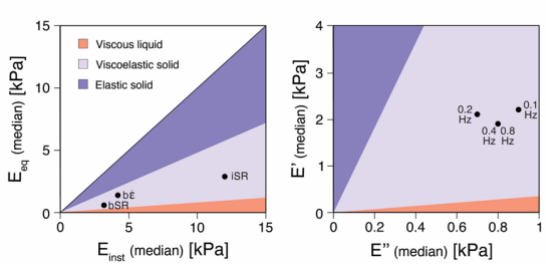
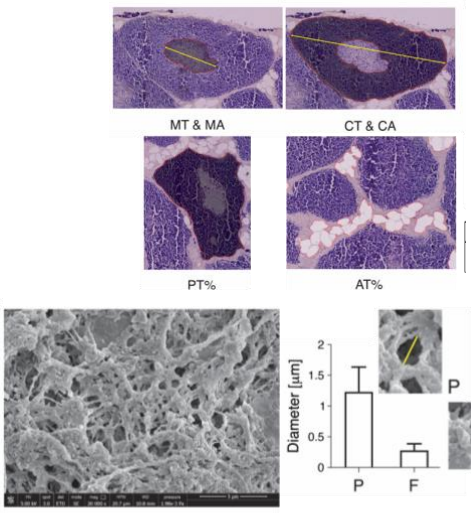


Figure 3: Mechanical characterization



	MT [μm]	CT [μm]	PT% [%]	AT% [%]	C/M [-]
Mean ± SD	2075 ± 699	3342 ± 1310	83 ± 4	7 ± 3	7 ± 1

Figure 4: Microstructural characterization

Discussion

Despite intrinsic differences among the type of tests, the mechanical results in Figure 2 demonstrate that the thymic tissue presents a high viscoelastic nature. Moreover, the quantification of microstructural features shown in Figure 3 can be useful for engineering biomimetic scaffolds providing immune cells with optimal culture conditions.

In the future, this biomimetic approach may have a crucial role in the advancement of therapeutic approaches for the treatment of hematological disorders.

References

1. C. S. Silva et al, Adv. Healthc. Mater., 10:20, 2021.
2. Cacopardo et al, TEB, 28: 912–925, 2022.

Acknowledgements

The work was partially supported by the Italian Ministry of Education and Research (MUR) in the framework of the FoReLab project (Departments of Excellence).

CHALLENGES AND REQUIREMENTS FOR THE DEVELOPMENT OF BIOREACTORS FOR BONE TISSUE ENGINEERING IN SPACE

Stefano Gabetti (1,2), Liyana I. Popova (3), Umberto Morbiducci (1,2), Michele Balsamo (3), Diana Massai (1,2)

1. Dept. of Mechanical and Aerospace Engineering and PolitoBIOMed Lab, Politecnico di Torino, Italy;
2. Interuniversity Center for the Promotion of the 3Rs Principles in Teaching and Research, Italy;
3. Kayser Italia Srl unipersonale, Italy

Introduction

International space agencies are focusing on long duration crewed missions to the Moon and Mars. Thus, space biomedicine is emerging as a critical field to ensure the health, safety, and performance of astronauts. Among others, reduced gravity represents a major risk factor, as it strongly affects the astronauts' musculoskeletal system, altering bone remodelling mechanisms and increasing the likelihood of fractures [1]. Health monitoring of astronauts and *in vitro* studies carried out on the International Space Station (ISS) have demonstrated that microgravity significantly affects bone cell viability, morphology, and matrix [2]. However, cell-only experiments fail to replicate the three-dimensional (3D) features of bone tissue overlooking the interactions among bone cells and their dynamic environment, thus the processes underlying bone loss remain unclear. In this scenario, *in vitro* modelling inspired by bone tissue engineering (BTE) holds great promise. The development of *in vitro* 3D bone tissue models—featuring bone cells seeded in scaffolds and cultured under bone-like physico-chemical conditions in bioreactors—is crucial for investigating the impact of the space conditions on human bones and for proposing and testing new countermeasures and therapeutic strategies [3]. Here, we analyzed the main challenges concerning the design and use of BTE bioreactors in space, outlining key design requirements.

Methods

To define the basic architecture of the bioreactor for BTE in space, we reviewed the main solutions developed for Earth-based investigations, with a focus on the delivery of bone-like physical stimulations (e.g., fluid-induced shear stress, compression, and electric fields). From a complementary perspective, bioreactors designed for biological research in space were analysed. Lastly, to identify safety and regulatory challenges for in-orbit biological experiments, technical documents and guidelines, including information from NASA and ESA websites, were examined.

Results

A primary requirement for space bioreactors is ensuring compatibility with available on-board facilities and environment constraints. This specification translates into the minimization of bioreactor volume, mass, and power consumption. Moreover, mechanical and electrical interfaces must be compatible with the module intended to accommodate the bioreactor. For its operability, the bioreactor must adopt a gravity-independent circuit for fluid handling and debubbling. To comply with safety requirements, the bioreactor must be equipped with at least one leak-proof level of containment. Furthermore, to enable bone biology investigations, the bioreactor must ensure continuous medium flow through the 3D cultured constructs (Fig. 1). This would both guarantee efficient mass transport during cell seeding / tissue culture and provide fluid-induced shear stress, known to be essential for promoting bone cell proliferation, differentiation, and matrix mineralization [4]. To mimic the native bone environment, additional physical stimulation units could be implemented for providing intermittent compression and/or electromagnetic fields known to promote osteogenic differentiation and bone tissue maturation [5]. To support parallelization for high-throughput studies, the bioreactor units must operate with low power consumption. Finally, to guarantee automation, a feedback-loop monitoring and control unit equipped with in-line sensors must be included. This will enable real-time measurement of the culture conditions and consequently to adapt them, minimizing human intervention while enhancing reliability and safety.

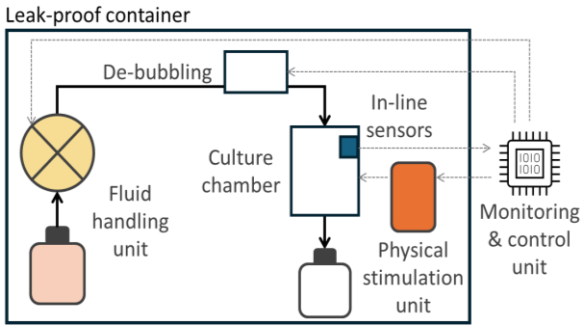


Figure 1: Proposed space bioreactor architecture.

Discussion

Bioreactors that meet the defined requirements could be used as powerful platforms for investigating the effects of space altered gravity on bone cells and tissue. This biomimetic, data-driven approach holds the potential to yield valuable insights for possible countermeasures and therapies in space biomedicine, while advancing BTE and regenerative medicine strategies on Earth. However, developing BTE bioreactors for space demands a robust collaborative effort among experts in stem cell biology, biotechnology, and engineering and between academia and aerospace companies. Thus, we believe it is time to unite efforts and work collectively toward this innovative and transformative goal.

References

1. Stavnichuk et al, Npj Microgravity, 6:1, 2020
2. Gambacurta et al., Sci. Rep., 9: 8343, 2019
3. Scatena et al., IAC Proceedings, 2023.
4. Hoffmann et al., Front. Bioeng. Biotech., 3:10, 2015.
5. Gabetti et al., Sci. Rep. 12:13859, 2022.

PERSONALIZED PROSTHESIS FOR TRANSFEMORAL AMPUTEES: IMPLANT STABILITY OF THE OsteoCustom STEM

Giulia Galteri [(1)], Valentina Betti [(1)], Domenico Alesi [(2)], Stefano Zaffagnini [(2)], Marco Palanca [(1)], Emanuele Gruppioni [(3)], Luca Cristofolini [(1)]

1. Dept of Industrial Engineering, Alma Mater Studiorum - University of Bologna, IT

2. Centro Protesi INAIL, Vigorso di Budrio, IT; 3. IRCCS Istituto Ortopedico Rizzoli, Bologna, IT

Background

The use of osseointegrated prostheses in the treatment of transfemoral amputation offers several advantages as an alternative solution to socket prostheses [1]. Transfemoral osseointegrated prostheses, like other uncemented prostheses, experience the risk of aseptic loosening and post-operative periprosthetic fractures, with an incidence between 3% and 30% [2]. Osseointegrated off-the-shelf prostheses are manufactured in a limited number of sizes, and the anatomical parameters of the medullary canals are not considered [3]. For these reasons, (i) optimal fit-and-fill is not always achieved, (ii) a number of patients are not eligible for implantation with commercial devices. A new concept of customized osseointegrated prosthesis (OsteoCustom) was developed. While improved fit-and-fill is generally expected from customized prosthesis, the improved implant stability and better load transfer must be proven.

Material and Methods

Six pairs of human femurs were obtained through an ethically approved donation program. CT scans (slice thickness=0.6mm, in plane resolution=0.5mm) were performed to assess the dimension of the femoral canal and choose the correct size of the implant. Six specimens were implanted with commercial stem (replicas of Badal X, OTN implants), while the six contralateral ones were implanted with OsteoCustom stem. The specimens were CT scanned again (fig.1). The proximal femur was embedded into a metal pot. A speckle pattern was prepared on the surface of the femur, while to track stem-bone micromotions, set of markers was placed on the distal end of the prosthesis.
Mechanical tests were performed using a uniaxial testing machine (Instron 8500, 10kN load cell). Two loading scenarios (compression-flexion, simulating the heel strike during gait, and torsion) were simulated to measure the primary implant stability and load transfer [4]. A 4-cameras 3D-DIC system (Aramis Adjustable 12M, GOM) was used to measure the displacement and strain fields on the femur and prosthesis. For both loading scenarios, the full-field strain distributions were measured in two regions of interest: close to the osteotomy (ROI1) and close to the stem tip (ROI2, fig.1) during the peak load of each cycle. The elastic micromotions and permanent migrations of the stem with respect to the bone were measured. A non-parametric Wilcoxon paired test was used (Prism 9.5.1, $p<0.05$).

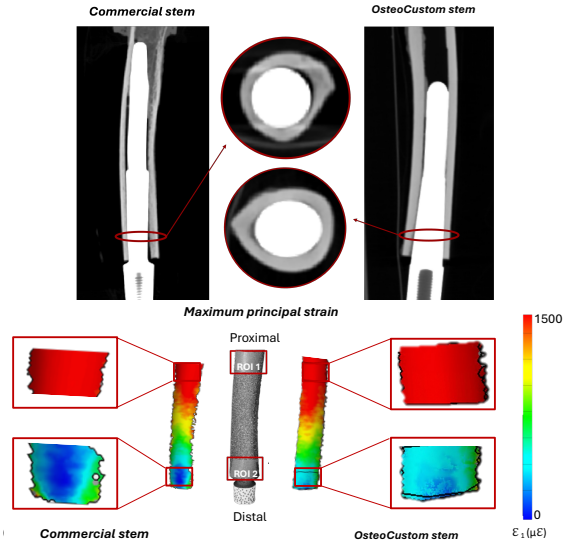


Figure 1: top) CT scan of a typical implantation of the commercial stem (left) and CT scan of the contralateral implantation with the customized stem (right) with a zoom on a distal cross-section. Bottom) Full-field distribution of the max. principal strains (eps1) of typical specimen with commercial (left) and the contralateral with the customized stem (right)

Results

The translational inducible micromotions during the compression-flexion test for the OsteoCustom stem were more than 4 times smaller than for the commercial one ($p<0.05$). The rotational inducible micromotions of the OsteoCustom stem were more than 3 times smaller than the commercial one ($p<0.05$). Similar results were found from the torsional test. The full-field strain distribution of the commercial stem showed a slightly higher strain concentration near the stem tip (max principal strain, $\varepsilon 1 = 1928 \pm 127$ microstrain) than the OsteoCustom ($\varepsilon 1 = 1758 \pm 130$ microstrain).

Discussion and Conclusion

These results support the hypothesis that the OsteoCustom stem can offer better primary stability and load distribution compared to commercial implants, highlighting the potential benefits of the OsteoCustom prosthesis, which is capable of including a wider range of femoral anatomies than the current standard.

References

1. Gerzina C. et al. 2019, J.Clin. Orthop. Trauma
2. Galteri et al. 2023, Fronties
3. Betti, Galteri et al. 2024, JOSR
4. Galteri et al. 2024, Frontiers

Acknowledgements

Work funded by INAIL (PR19-CR-P5-OsteoCustom, PR23-CR-P5-OsteoAMI).

CFD-BASED INVESTIGATION OF HEMODYNAMICS IN CORONARY ARTERIES

Gianluca Diana, Silvia Puleo, Francesco Scardulla, Leonardo D'Acquisto, Salvatore Pasta

1. Department of Engineering, University of Palermo, Viale delle Scienze, Ed. 8, 90128 Palermo, Italy

Introduction

Coronary arteries are blood vessels that surround the surface of the heart and have the important role of supplying oxygenated blood to the cardiac muscle. However, over time and due to certain risk factors, these vessels become susceptible to coronary artery disease (CAD), a condition often caused by atherosclerosis, or the accumulation of fatty plaques on the arterial walls. This phenomenon leads to a narrowing of the vascular lumen and can potentially lead to serious complications such as angina, myocardial infarction or even sudden cardiac death [1]. Computational models based on finite element analysis and computational fluid dynamics (CFD) have been used to investigate the hemodynamic alterations associated with CAD. These techniques allow detailed simulations of blood flow and provide valuable insights into the biomechanics of the blood vessels [2]. The primary objective of this study is to analyze a model of a healthy coronary artery and a pathological one affected by CAD, to examine and compare the hemodynamic differences and, therefore, to emphasize the importance of treating coronary plaques and mitigating their potentially lethal consequences. In clinical practice, one of the most common approaches to managing coronary artery narrowing involves the implantation of stents. These devices are designed to restore the arterial lumen, ensuring adequate blood flow and preventing further hemodynamic complications [3].

Methods

The specific anatomies of the coronary arteries, both for the healthy and pathological cases, were reconstructed from computed tomography (CT) images of the patient. Segmentation of the coronary sections was performed using dedicated techniques implemented in the Mimics Medical software (Materialise, Leuven, Belgium). The reconstructed models were then imported into ANSYS ICEM CFD (Ansys Inc., PA, USA) for the creation of a finite element mesh. The mesh was developed using a combination of tetrahedral elements and a smaller portion of triangular elements. This configuration ensures greater versatility and better adaptability even in areas characterized by high geometric complexity, while maintaining low calculation times. CFD analysis was conducted on the LS-Dyna software (Ansys Inc., PA, USA). Physical properties of blood, including density and viscosity, were implemented and patient-specific boundary conditions were prescribed for each outlet of the analysed coronary segment. Boundary conditions modelling was performed using the three-element Windkessel model, which physiologically represents the arterial network downstream of the outlets.

Results

The results obtained show significant differences in the pressure and velocity fields, determined by the presence of the atherosclerotic plaque in the pathological model. In the healthy case, the blood flow presents a uniform distribution of velocity and pressure along the entire coronary tract. The velocity field shows averagely constant values, with minimal variations at the bifurcation points. Similarly, the pressure field does not show anomalous concentrations, indicating a stable and physiological flow condition. In the pathological case, the presence of the atherosclerotic plaque causes a significant narrowing of the vessel lumen, which leads to an acceleration of the flow and an increase in velocity at the points proximal to the bifurcation. Instead, the pressure field shows higher and concentrated pressure gradients near the stenosis, representing an additional biomechanical load on the arterial walls.

Discussion

The results highlight the biomechanical impact of the atherosclerotic plaque on coronary flow. In the pathological model, the increase in velocity in the stenosis region leads to local flow accelerations that can induce the formation of turbulence, which not only increases the mechanical stress on the vessel wall, but can also promote inflammatory processes and rapid plaque progression. Increased pressure gradients could accelerate plaque degeneration, increasing the likelihood of thrombus formation, which is the main cause of acute cardiovascular events such as myocardial infarction. Furthermore, bifurcation points, already subject to higher hemodynamic stress due to their geometry, are particularly vulnerable in the presence of plaques. In this context, coronary stent implantation represents a key therapeutic solution and a future development of this study involves the implementation of a coronary stent in a CFD simulation to analyze the improvement of pressure and velocity fields in the diseased coronary artery. From a methodological point of view, the use of CFD models has proven to be extremely effective in providing a detailed view of blood flow dynamics and in simulating pathological conditions that are difficult to observe in vivo.

References

1. Virmani et al. *Journal of Interventional Cardiology*, 15: 439–446, 2002. doi:10.1111/j.1540-8183.2002.tb01087.x
2. Catalano et al. *Perfusion*, 2676591241239277, 2024. doi:10.1177/02676591241239277
3. Collet et al. *European Heart Journal*, 42:1289-1367, 2021. doi:10.1093/eurheartj/ehaa575

DEEP-LEARNING AND POD-BASED MODELLING FRAMEWORK FOR REAL-TIME SIMULATIONS OF CORONARY PRESSURE PROFILES

Girolamo Mastronuzzi (1), Diego Gallo (1), Umberto Michelucci (2,3), Bianca Griffo (1), Maurizio Lodi Rizzini (1), Valentina Mazzi (1), Umberto Morbiducci (1)

1. Politecnico di Torino, Italy; 2. Lucerne University of Applied Sciences and Arts, Switzerland; 3. TOELT LLC, Research and Development, Switzerland

Introduction

The gold-standard assessment of the significance of coronary artery stenoses is based on the estimation of pressure [1]. The simulation of coronary pressure profiles with high-fidelity computational fluid dynamics (CFD) is computationally expensive for clinical settings. To face this limitation, the use of reduced-order methods like Proper Orthogonal Decomposition (POD) has been proposed, which in turn are markedly affected e.g. by intersubject anatomical variability [2]. This study proposes a surrogate model that integrates POD with multi-channel 1D convolutional neural networks (CNNs) to address these challenges. By using vessel geometry as the sole input, the model predicts blood pressure profiles along the coronary centerline.

Methods

The 3D model geometry of 184 mildly stenosed coronary arteries was reconstructed from coronary angiography and used for hyperemic CFD simulations, carried out using a finite volume-based solver (ANSYS Fluent®, ANSYS Inc., Canonsburg, PA) [3]. A centerline-based geometric parameterization strategy was applied to extract vessel length, cross-sectional area (CSA), and centerline curvature along the vessel. The extracted geometric features were provided as input to a 1D-CNN model trained to predict POD weights, which were then used to reconstruct pressure profiles through a linear combination of POD modes derived from CFD data, used as ground-truth (Fig. 1). Models have been validated with a Monte Carlo (MC) cross-validation approach. In detail, 20 models were (i) trained with randomly resampled training and validation sets, and (ii) tested on a hold-out test set. In addition, a nested cross-validation (NCV) was performed to complement the MC analysis with an unbiased estimate of the model performance [4]. Predictive capability was measured using normalized root mean squared error (NRMSE).

Results

Training a single surrogate model averaged 90 seconds on a system featuring a 12th Gen Intel Core i7-12700H CPU and an NVIDIA GeForce RTX 4050 Laptop GPU, with predictions for new geometries taking ~1 second. Table 1 shows NMRSE distributions across the MC test set and NCV outer folds (mean±SD of the 5th percentile, median, and 95th percentile) indicating good overall performance, albeit susceptible to the particular split used in the training data. The MC test set's pressure drop across the vessels (ground-truth average 11.6±8.4 mmHg) is predicted with an average error of 2.6±3.4 mmHg. The pressure prediction ranges are generally consistent with CFD pressure profiles, with discrepancies at sudden pressure variations (e.g., pressure recovery, Fig. 2).

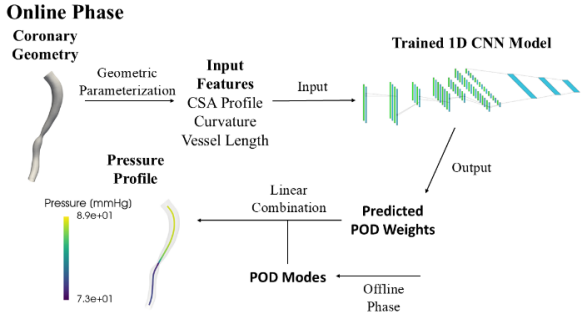


Figure 1: Online phase of the proposed framework.

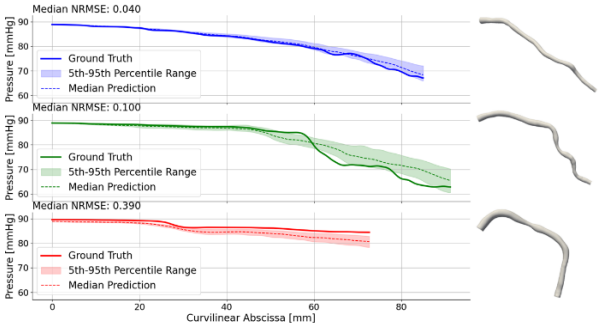


Figure 2: Predicted pressure profiles for the best, average and worst performing cases in the MC test set.

	5th Percentile	Median	95th Percentile
MC	0.067±0.059	0.120±0.095	0.223±0.138
NCV	0.043±0.021	0.193±0.040	0.480±0.118

Table 1: NRMSE results for MC and NCV experiments.

Discussion

Given the relatively small sample size and the simplicity of the input data, consisting of easily available geometric features, the performances of the proposed approach are very promising. Generalization ability could be enhanced by increasing dataset size. To improve prediction accuracy, the framework can be easily expanded by incorporating additional input features, including hemodynamic factors.

References

1. De Bruyne, N Engl J Med, 367:991-1001, 2012.
2. Ye et al, J Computation Physics, 469, 2024.
3. Candreva et al, Atherosclerosis, 342:28-35, 2022.
4. Berrar, Encyc Bioinform Comput Bio, 1:542-545, 2019.

Acknowledgements

BG scholarship is part of the project NNR-NGEU, which has received funding from the MUR – DM 352/2022.

IN SILICO MODELS OF POST-DILATATION IN TAVI PATIENTS

Letizia Maria Perri (1), Benedetta Grossi (1,2), Francesco Migliavacca (1), Gianluigi Condorelli (2), Giulio Stefanini (2), Giulia Luraghi (1)

1. Department of Chemistry, Materials and Chemical Engineering, Politecnico di Milano, Milan, Italy
2. Department of Biomedical Sciences, Humanitas University, Pieve Emanuele, Milan, Italy

Introduction

Transcatheter Aortic Valve Implantation (TAVI) is a minimally invasive procedure that is emerging as a promising solution for treating aortic stenosis. As part of the procedure, balloon post-dilatation aims to reduce the paravalvular leakage (PVL) by optimizing the adhesion between the prosthesis and patient's aortic root [1]. This study focuses on developing a computational model to simulate post-dilatation in patient-specific anatomies, aiming to predict potential complications and improve clinical outcomes. This work involves (i) creating a balloon model for post-dilatation, (ii) conducting patient-specific simulations, and (iii) validating the model against clinical data. Furthermore, in this study, the simulation results achieved are compared with those from previous simulations without post-dilatation [2] in order to assess any improvements in predicting procedural outcomes.

Methods

A post-dilatation balloon model is reconstructed, and three different simulations are carried out to reproduce deflation, crimping and inflation. The balloon is then integrated into patient-specific anatomical models reconstructed from preoperative CT images. In this study, two patients undergoing balloon post-dilatation with implanted self-expandable valves are analyzed. Subsequently, finite-element simulations of the post-dilatation are performed. Model validation is first based on qualitative and quantitative comparisons with post-operative clinical data, such as angiographies and CT images. In addition, CFD simulations are conducted to evaluate and predict the PVL both in the case of post-dilation and in the absence of this phase.

Results

The results of the post-dilatation simulation on patient A are depicted in Fig. 1. A qualitative match between simulated and in vivo implanted stent configurations is evident from the superimposition of simulation results and angiographic images, as observed in Fig. 2A. Among all post-dilation simulations executed, the maximum and the minimum orifice area (OA) percentage differences between the final configuration of the simulated stent and segmented one are 2.33 ± 1.32 % and 1.14 ± 0.92 %; in terms of eccentricity, the maximum and minimum percentage error are 1.7301 % and 0.1112 %.

Comparing these results with the simulations without post-dilatation [2], we obtain maximum improvements of 70 % and 75 % for OA and eccentricity respectively

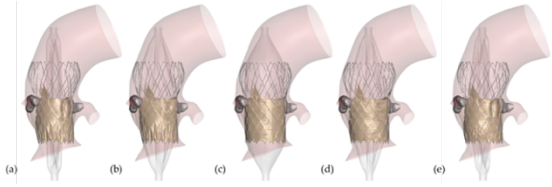


Figure 1: Steps of post-dilatation procedure in patient A. (a) Balloon integration in patient anatomy; (b) inflation; (c) balloon at nominal diameter post-inflation; (d) deflation; (e) deflated balloon at the end.

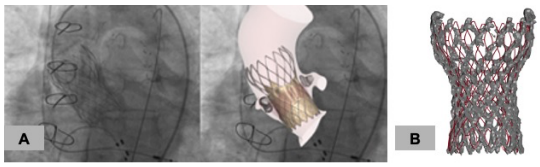


Figure 2: Patient A. (A) Qualitative comparison of post-dilatation configuration of the prosthesis implanted in the aortic root (right) with post-operative angiographies (left). (B) Model validation with CT scans segmentations.

Discussion

The results obtained show that the reproduction of post-dilatation in simulations cannot be ignored. In fact, this phase can significantly modify the stent configuration, as demonstrated by the strong reduction in the error of the parameters considered.
Finally, the addition of this procedure to the simulations represents a further step in the field of computational modelling of TAVI, providing a tool capable of supporting clinical decision-making and predicting possible post-implantation complications. CFD simulations are still ongoing, preliminary results are showing improvements in the prediction and evaluation of PVL.

References

1. Li et al, Front Bioeng Biotechnol, 11:1333138, 2023.
2. Grossi et al, Comput Biol Med, 182: 109159, 2024.

Acknowledgements

L.P., F.M. and G.L. are supported by the European Research Council (ERC, project PROTEGO, G.A. 101162753).

NUMERICAL SIMULATIONS FOR THE DESIGN OF AORTIC ENDOGRAFT RINGS: AN AUTOMATED APPROACH

Luca Romizi (1), Ferdinando Auricchio (1), Michele Conti (1), Alessandro Caimi (1)

1. Department of Civil Engineering and Architecture, Università degli Studi di Pavia, Via Ferrata 3, Pavia, Italy

Introduction

The aorta is the main artery of the human body, its functionality can be hindered by serious pathologies such as aneurysm which consists in an abnormal enlargement of the vessel [1]. The minimally invasive procedure, called Endovascular Aneurysm Repair (EVAR), is becoming a valid alternative to the gold-standard open-heart surgery, thanks to the positive clinical outcome achieved with a less invasive strategy [1]. Nevertheless, stent-grafts can be characterized by multiple different shapes that can influence their mechanical performance and may impact negatively to the vessel [2]. Since the components can be numerous, their manual design can be affected by errors introduced by the designer and can be very time consuming.

The proposed work aims at design and developing a Python based automatic pipeline, which retraces all the manual action required to the design and simulation of different devices from an R&D perspective obtaining a fast and standardized process basing the activity on V&V 40 workflow [3].

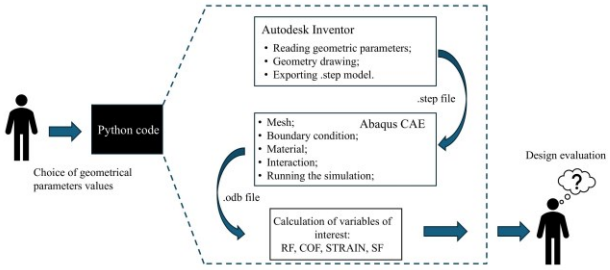


Figure 1: automatic steps executed by the Python code.

Methods

To assess the mechanical response of these different devices before their actual production, numerical simulations have been used [4]. The simulations were run in Abaqus 2022 (Simulia, Dassault Systems) while the 3D model of the rings was created in Autodesk Inventor professional 2023.

Different variables were calculated to compare the impact of different device geometry: the maximum strain (maximum deformation of the ring), the Chronic Outward Force (COF) force exerted by the ring on the vessel and the safety factor (SF) the ratio between fatigue strain limit and alternating strain, have been questioned.

The two main analyses can be summarized as the following Contexts of Use (COU):

COU.1) The device is reduced (crimped) to the diameter of the catheter of the delivery system, using a cylindrical rigid surface (crimper) and then freely released to obtain the maximum strain reached and the complete curve of radial-force.

COU.2) Once the device has been crimped onto the catheter it is released within a cylindrical tube simulating vessel and finally subjected to cyclic loading by changing the diameter of the crimper to obtain the factor of safety.

The rings were modelled with Nitinol to give a super elastic behaviour and were meshed using hexahedral elements C3D8R with reduced integration while the crimper was meshed with surface elements. The boundary conditions were set to obtain a uniform radial crimping. The steps of the automated approach can be seen in Figure 1.

Results

From the results obtained is noted how these are closely related to the geometric parameters of the stent. Is noted how the height (longitudinal distance between two opposite peaks) of the stent influences the variables of interest as reported in Figure 2.

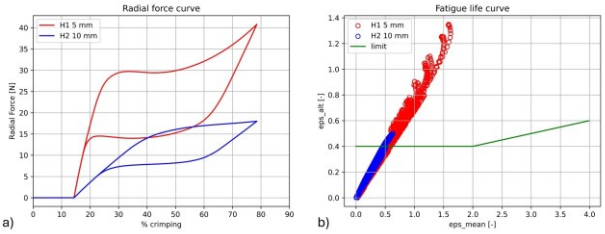


Figure 2: results obtained for one ring design with two different heights. a) Radial Force curve, b) Fatigue life curve.

Discussion

From the set of rings analysed as a whole, appropriate observations and choices can be made on how to structure a complete model. The *home-made* Python software has proven to be a powerful tool that allowed to automatize and standardize the entire operator-dependent process, reducing the execution of the design and setting procedure to a few seconds.

References

1. Jaunoo, S. (2008). Int J Surg **6**(3): 266-2694.
2. Kapoor, et al. Materials & Design **237**: 112556.
3. Kuemmel, et al. CPT Pharmacometrics Syst Pharmacol 9(1): 21-28.
4. Zhou, et al. Journal of Materials Science & Technology **35**(11): 2682-2692.

FROM BENCH TESTING TO IMPLANTATION: AN *IN SILICO* COMPARATIVE STUDY BETWEEN PLLA AND NITI BRAIDED VASCULAR STENTS

Agnese Lucchetti (1), Levi G. Juhl (1), Anna Corti (2), Claudio Chiastra (3), Ted J. Vaughan (4), Dario Carbonaro (3)

1.RWTH Aachen University, Germany; 2. Politecnico di Milano, Italy; 3. Politecnico di Torino, Italy; 4. University of Galway, Ireland

Introduction

Bioresorbable braided stents (BSs) represent a promising solution for treating peripheral artery disease (PAD), providing temporary mechanical support before gradually degrading into biocompatible byproducts. Previous studies highlighted the low mechanical characteristics of bioresorbable BSs, compared to permanent metallic BSs. However, the implantation procedure of bioresorbable BSs in femoral arteries has not been yet investigated, leaving uncertainty on whether their mechanical characteristics are adequate for effective treatment of PAD. Thus, the aim of this study is to investigate the mechanical characteristics and treatment performance of a PLLA BS and compare them to those of a metallic BS with the same geometry.

Methods

Finite element (FE) models of a bioresorbable BS, made of poly-L-lactic acid (PLLA), and of a permanent metallic BS, made of nickel-titanium (NiTi), with the same geometry, were developed for comparison (Fig. 1a) [1]. Parallel-plate compression and crimping bench tests were simulated using Abaqus/Explicit (Fig. 1c). The forces generated by the PLLA BS in the two bench tests were compared with experimental data from a previous study [2]. Finally, FE analyses of the BS implantation procedure in a diseased femoral artery, including angioplasty followed by stent implantation, were conducted to assess the treatment performance of the BSs. The arterial model was reconstructed from computed tomography, assuming a constant wall thickness, and was modeled as homogeneous and isotropic, considering three different sets of material parameters to represent various arterial conditions [3].

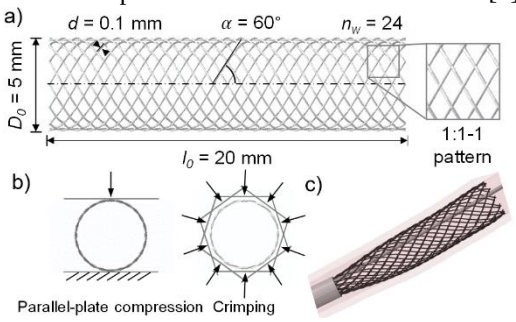


Fig. 1. a) FE model of the BSs, b) bench tests, c) implantation procedure.

The following quantities were measured to assess the treatment performance of the BSs: *i)* the maximum principal stress in the BSs during catheter insertion, *ii)* the lumen gain (LG) achieved through stent implantation, and *iii)* the contact pressure on the arterial wall after stent deployment.

Results

The FE model of the PLLA BS was successfully validated against experimental data. The forces generated by the PLLA BS were markedly lower than those by the NiTi BS in both virtual bench tests. No permanent deformations were observed for both BSs during insertion into the catheter. However, the PLLA BS exhibited a small safety margin relative to the material's yield limit (peak maximum principal stress of 87 MPa with a yield stress of 110 MPa). Fig. 2a presents the LGs for one arterial condition (i.e., medium stiffness), following both angioplasty and stent implantation at five locations. The PLLA BS induced markedly lower LGs compared to the NiTi BS. Fig. 2b illustrates the contact pressure on the artery considering one arterial condition. The PLLA BS generated lower contact pressures compared to the NiTi BS. Additionally, unlike the NiTi BS, the PLLA BS exhibited a non-uniform contact pressure distribution, indicating low conformability to the arterial wall and the presence of regions with malapposition.

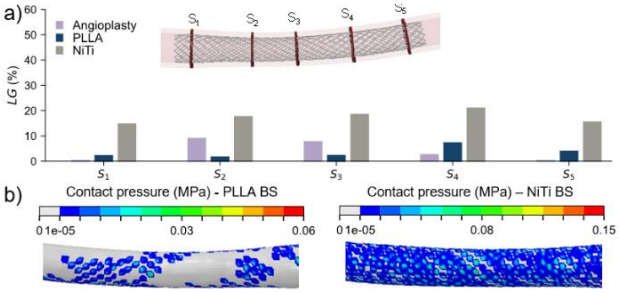


Fig. 2. FE analysis of the BSs implantation: a) LG, b) Contact pressure, for one of the arterial conditions.

Discussion

The PLLA BS exhibited markedly lower forces in both bench tests compared to the NiTi BS, ascribable to the low mechanical characteristics of PLLA. The FE simulation of BS implantation highlighted the low treatment performance of the PLLA BS across all three arterial conditions, in terms of risk for permanent deformations, low LGs, and poor conformability. In conclusion, the computational procedure proved to be effective to investigate the mechanical properties and treatment performances of the BSs and could be extended to other vascular stents.

References

[1] Carbonaro et al, Comput Methods Programs Biomed, 242:107781, 2023.
[2] Lucchetti et al, J Mech Behav, 138:105568, 2023.
[3] Noble et al, J Mech Behav, 101:103453, 2020.

INVESTIGATING THE PRINCIPLES BEHIND CELL COORDINATED MIGRATION AS A FUNCTION OF MICROENVIRONMENT SPACE-TIME WARPING

Nicole Guazzelli (1), Francesco Fontana (1), Paolo Signorello (1), Giulia Paties Montagner (1), Arti Ahluwalia (1), Ludovica Cacopardo (1)

1. University of Pisa, Italy

Introduction

Living organisms rely on cellular coordination, generating intricate motion patterns to fulfil physiological functions such as growth, development and regeneration. Although these patterns are often associated with physical or biochemical signalling, cell motion has never been investigated considering microenvironment space-time warping in the case of soft tissues and substrates (Figure 1). Considering micro-relativity effects, cell time perception may thus vary as a function of this warping affecting cell motility and coordination.

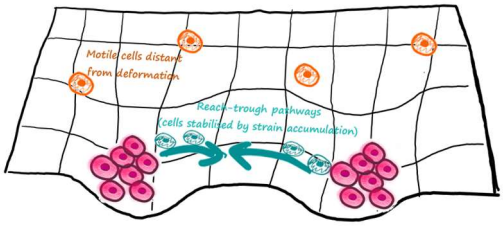


Figure 1: Cell motion in space-time warped microenvironments

Methods

Adipose-derived mesenchymal stem cells (ADSCs) were seeded on dextran-permeated agarose substrates [1]. Polymer concentrations were optimised a priori to match the mechanical properties of the adipose niche using an in-silico model which describe the interaction between gel solid and liquid phase. The gel solid phase was described as a homogeneous porous system (agarose concentration = 5 mg/mL), while dextran (varying in the range 0-40 mg/mL) in the liquid phase was modelled as spherical agglomerate linked to the water molecules. After deriving matrix permeability on the base of Carman-Kozeny formulations, reaction-diffusion equations were used to model the fluid flow through the solid network considering an apparent diffusion coefficient which accounts for hindered diffusion in porous media according to Brinkmann's theory. Flory's theory and the Amsden obstructing scaling model will be finally used to correlate transport and the mechanical properties of the agarose hydrogels trough the average mesh size (ξ) [2]. Lumped parameter representation was used to derive gel viscoelastic descriptors: relaxation time (τ), instantaneous (E_{inst}) and equilibrium (E_{eq}) elastic moduli. Model predictions were finally validated with compression tests at different constant strain rates using universal testing machines [1]. After 7 days of culture, cells were fixed and stained with DAPI and phalloidin as preliminary assessment of cell migration patterns.

Results

Figure 2 shows the viscoelastic descriptors derived for the agarose gels and the reach-out motion observed on dextran (20 mg/mL)-permeated agarose (5 mg/mL) substrates.

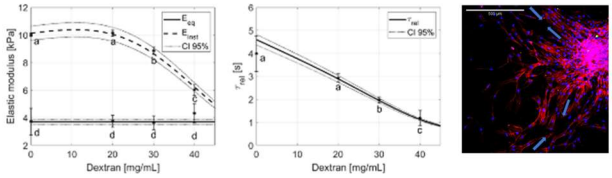


Figure 2: Computational and experimental E_{inst}, E_{eq} (left) and τ (center). Confocal image (right) outlining ADSC reach out motion on dextran (20 mg/mL)-permeated agarose (5 mg/mL) substrates

Discussion

The preliminary results suggest that the presence of cell clusters and the resultant substrate warping in space and time may modulate cell migration. Further studies will focus on the integration of the computational setup in an in-silico model describing cell-substrate interaction based on motor clutch theories to predict the formation of cell focal adhesions in space and time. Relative cell time will be considered by tuning focal adhesion unbinding rates and lifetimes as a function of substrate. On the base of the in-silico results, culture chamber will be designed to systematically investigate cell migration as a function of: i) different distances between clusters, which may affect the combination of the generated strain fields; ii) different cell numbers in the clusters, resulting in different cluster size/weights; iii) substrate with different viscoelastic properties which affect substrate deformation over time. Substrate deformation and cell migration will be characterized combining atomic force microscopy and advanced imaging techniques.

In the future, this study will pave the way for engineering substrates able to guide cell motion in regenerative medicine and in-vitro applications as well for defining algorithms capable of predicting pathological outcomes.

References

1. Cacopardo et al, JMBBM, 89:163-167, 2019.
2. Lee et al, Science, 6452:482–487, 2019.

Acknowledgements

The work was supported by the Italian Ministry of Education and Research (MUR) in the framework of the FIS2 grant INTERCELLAR (CUP: I53C24003110001)

MECHANICAL EVALUATION OF HUMAN TENDONS: SUITABILITY OF ALLOGRAFTS FROM DONORS AGED OVER 65

Andrea Tancredi Lugas (1), Gianpaolo Serino (1,2), Antonia Barbazza (3), Diletta Trojan (3), Cristina Bignardi (1,2), Mara Terzini (1,2)

1. Polito^{BIO}Med Lab, Politecnico di Torino, Turin, Italy;
2. Department of Mechanical and Aerospace Engineering, Politecnico di Torino, Turin, Italy;
3. Fondazione Banca Dei Tessuti del Veneto Onlus, Treviso, Italy

Introduction

Allograft tendons are commonly used in surgical ligament reconstruction. The advantages of using allografts include the lack of donor-site morbidity, a reduction in surgery time and hospitalization, and a better cosmetic result [1], as well as the avoidance of injury to the extensor or flexor apparatus. Since allografts are widely used, it becomes crucial to identify any potential factor that could adversely affect their mechanical properties, aiming to minimize the risk of failure. In this context, the role of the donor's age is still unclear [2]. The purpose of the study is to determine if donor age of allografts used for ligament reconstruction could affect the biomechanical tissue properties. This analysis aims to contribute to the ongoing debates on this topic and potentially enhance the availability of allografts, which nowadays are the preferred choice in ligament revisions. The hypothesis was that the donor age does not affect the quality of cadaveric tendons used for the ligament reconstruction [3].

Methods

Anterior tibial, posterior tibial, extensor, gracilis, semitendinosus, peroneal, flexor, and semi-Achilles tendons from different donors were tested. For the purpose of this study, the donors were divided into two groups: aged over 65 and aged under 65. The samples were cut into 2 or 3 specimens with a 65 mm gauge length. Pictures were taken from two directions to optically measure the cross-sectional area, and the specimens were gripped in pneumatic jaws of a tensile test machine for uniaxial tensile testing (Figure 1), where they were loaded at a constant rate of 0.1 mm/s in displacement control until failure.

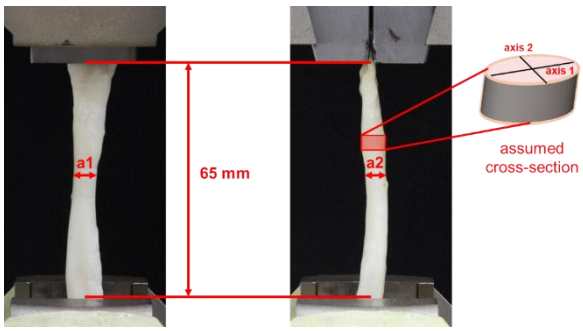


Figure 1: Test setup and specimen dimensions.

The ultimate tensile strength (UTS), elongation at break (EAB), toe (Etoe) and linear elastic moduli (Elin) were computed from the stress-strain curve of each test. For each sample, the parameters computed for each specimen were averaged and used as descriptors of the tendon mechanical properties in order to compare the two age groups. A two-way nested analysis on variance was conducted to investigate the influence of the donors and the age on the mechanical parameters.

Results

Statistically significant differences associated with the "donor" factor were observed for the Etoe parameter in the semi-Achilles and peroneal tendons, as well as for the Elin parameter in the posterior tibial tendons. Additionally, statistical differences related to the "Under 65/Over 65" age grouping of donors were found for the EAB parameter in the semitendinosus tendons and for the Elin parameter in the posterior tibial tendons. The statistical differences observed between donors within the same age group are expected and are not the primary focus of this investigation. However, when examining the statistical differences related to the "Under 65/Over 65" factor, it is noted that semitendinosus tendons from donors over 65 show greater elongation to failure compared to tendons from donors under 65, as well as a higher elastic modulus in the linear region for posterior tibial tendons from over 65 donors compared to those from under 65 donors.

Conclusion

The mechanical tests performed indicate that, within the analyzed variation ranges, age does not have a statistically significant impact on the mechanical properties of tendons. Age proved to be a less determining factor compared to the intrinsic variability, both inter- and intra-sample, of human tissues. The only statistically significant differences were observed in the semitendinosus (EAB) and anterior tibial tendons (Elin). However, these differences do not discourage the use of tendons from donors over 65, which exhibit greater elongation to failure and a higher elastic modulus in the linear region of the stress-strain curve.

References

1. Giannini et al, Int Ortop, 32(2):145-51, 2008
2. Swank et al, Am J Sports Med, 43(2):453-9, 2015
3. Grassi et al, Knee Surg Sports Traumatol Arthrosc, 32(5):1123-1142, 2024.

OPTIMIZATION OF NON-INVASIVE VENTILATION INTERFACES: EXPERIMENTAL INSIGHTS INTO REDUCING CO_2 REBREATHING

Margherita De Luca[1,2], Andrea Formaggio[1,2], Mara Terzini[1,2], Giovanni Putame[1,2], Carlo Olivieri[3], Simone Borrelli[1,2] and Alberto L. Audenino[1,2]

1. *Department of Mechanical and Aerospace Engineering, Politecnico di Torino, Torino (Italy)*
2. *Polito[BIO]Med Lab, Politecnico di Torino, Torino (Italy)*
3. *Sant' Andrea Hospital, ASL VC, Vercelli (Italy)*

Introduction

Non-Invasive Ventilation (NIV) is an effective treatment for various respiratory conditions, including acute respiratory distress syndrome (ARDS) [1]. A key challenge in this context is the rebreathing phenomenon, defined as the re-inhalation of CO_2 that accumulates within the patient interface, potentially compromising the therapy's effectiveness. Closed circuit continuous positive airway pressure (CPAP) systems [2] have recently shown several advantages over traditional open systems, but concerns regarding rebreathing persist. This study experimentally investigates whether inhaled CO_2 levels during CPAP therapy remain within safe limits in closed circuit, focusing on the influence of inlet and outlet port positioning on the patient interface and the addition of recirculation airflow to enhance CO_2 washout and reduce inhaled CO_2 levels.

Methods

Closed circuit CPAP system was assembled using commercial components, including a primary turbine to maintain a pressure level of 5 cmH_2O, a secondary turbine for recirculation flowrate, antiviral filters, one-way valves, a CO_2 absorber, and a lung simulator mimicking ARDS patient parameters. The upper part of Figure 1 illustrates the patient tested interfaces under three airflow conditions (0, 60, 80 l/min): one commercial helmet (A, Lateral Inlet/Lateral Outlet), three custom-made helmets (B, Lateral Inlet/Front Outlet; C, Up Inlet/Front Outlet; D, Up Inlet/Up Outlet), and two commercial full-face masks (E, One-port mask; F, Two-ports mask). CO_2 was introduced at a 4-5% concentration to replicate exhaled mixture of individuals [3]. Data were collected over 60 seconds for 34 breathing cycles. Inspired CO_2 percentage was calculated by integrating CO_2 concentration over the inspiratory phase and normalizing it by tidal volume.

Results

The commercial helmet A exhibited the highest inhaled CO_2 values (2% at 0 l/min, reduced to 1.3% at 80 l/min). Repositioning the inlet port over the patient's head (C) significantly reduced inhaled CO_2, achieving the lowest levels (0.6% at 80 l/min) for helmets. Increasing airflow rates consistently reduced CO_2 levels, with the largest decrease occurring between 0 and 60 l/min (average 0.6%). For masks, the Two-ports consistently showed the lowest CO_2 levels (from 0.4% at 0 l/min to0.1% at 80 l/min) and was the only configuration that achieved values below the 1% safety threshold even without additional airflow.

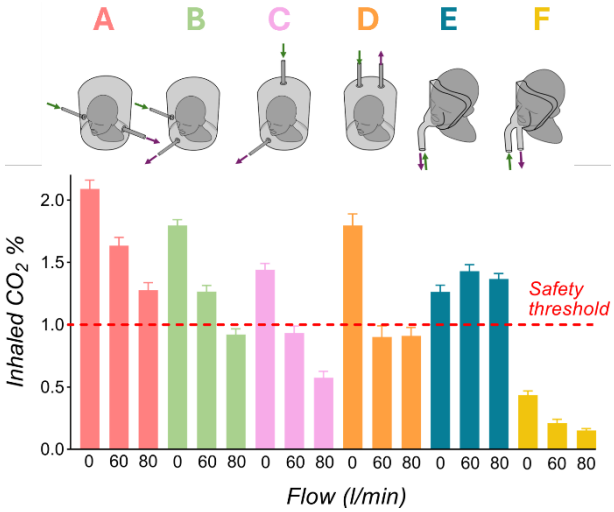


Figure 1: Tested interfaces: A. Lateral Inlet/Lateral Outlet helmet, B. Lateral Inlet/Front Outlet helmet, C. Up Inlet /Front Outlet helmet, D. Up Inlet /Up Outlet helmet, E. One-port mask, F. Two-ports masks. Green and violet arrows indicate the inlet and outlet ports, respectively. Bar chart: mean and standard deviation of inhaled CO_2 percentage. The X-axis shows the recirculation airflow (0, 60, 80 l/min); the red dashed line is the safety threshold for acceptable inspired CO_2 values [4].

Discussion

The findings of this study emphasize the importance of the outlet position on the patient interface in reducing CO_2 rebreathing during NIV. Among the tested configurations, the Up Inlet/Front Outlet helmet and the Two-ports mask proved to be the most effective. The custom Up Inlet/Front Outlet helmet achieved inhaled CO_2 levels below the 1% safety threshold with an additional flow rate of 60 l/min, while the Two-ports full-face mask maintained the safety levels even without additional flow. Although the tests were conducted on a closed circuit, the measured CO_2 originates solely from accumulation within the interface thanks to the CO_2 absorber placed within the circuit, making the results generalizable to traditional CPAP systems. Optimizing the design of inlets and outlets, along with managing additional flows, represents a key strategy to minimize CO_2 rebreathing and enhance patient safety during the delivery of NIV therapy.

References

1. David-João et al. Journal of Critical Care, 49: 84-91, 2019.
2. Cavaglià et al. Artif. Organs, 45(7):754-761, 2021
3. Al Hussain et al. Can J Respir Ther. 58: 111-114, 2022
4. NIOSH. "Occupational exposure to carbon dioxide." 1976

Acknowledgements

This work is part of the NODES project (MUR – M4C2 1.5 of PNRR, grant agreement no. ECS00000036)

AGEING AND DEGENERATIVE CHANGES AFFECT SURFACE STRAINS IN HUMAN INTERVERTEBRAL DISCS

M. Pasini[1], G. Cavazzoni[1], L. Cristofolini[1], M. Palanca[1]

1. *Dept of Industrial Engineering, Alma Mater Studiorum – University of Bologna, Bologna, IT*

Introduction

Low back pain (LBP) is the major leading cause of musculoskeletal disability, affecting more than 600 million people worldwide, due to increasing aging and sedentary lifestyles in high-income countries (1). Intervertebral disc (IVD) degeneration is one of the main underlying causes of LBP (2). Indeed, IVDs are exposed to pathological, genetic, traumatic and environmental factors that may trigger degenerative changes [1]: the nucleus generally becomes more fibrotic and less gel-like, while the annulus fibrosus fibres become irregular, bifurcating and interdigitating (3). These changes in composition and organization affect the load sharing, leading to alterations in the biomechanical behaviour of the spine.

This study aims to mechanically characterize young, adult and elderly human IVDs, investigating the effect of age-related changes in stiffness and maximum and minimum principal strains.

Methods

Ten spines from human donors of different ages were collected (Prot.n.113043). Three groups were defined: "young" (34±3 years old), "adult" (57±2 years old) and "elderly" (78±9 years old) donors. 15 thoracolumbar spine segments consisting of two vertebrae and an IVD in the middle, and cranial and caudal vertebrae for fixation in the testing rig, were dissected by removing fat, muscles and the anterior longitudinal ligaments, without damaging the vertebrae and the IVDs. So far, results are reported only for adults and old specimens. MRI (Ingenia 1.5T, Philips, Sagittal T2-weighted Spin-Echo sequence) scans were acquired for each specimen to assess the degeneration level of IVDs. Degeneration was evaluated using the clinically used Pfirrmann scoring system: young and adults IVDs exhibited mild level of degeneration, while elderly severe level (4).

Specimens were biomechanically tested in the elastic regime under pure axial compression using a state-of-the-art spine simulator (MIB4.0-MAS2-S). The loading protocol consisted in applying ten preconditioning cycles between 50N and 300N, at 0.5 Hz, then loading the specimen to reach a compressive strain on the surface of the vertebrae (6) similar to the strains associated to physiological loads (approximately -3000με), in 10s. Stiffness was evaluated as the linear interpolation slope of the load-displacement points between 20% and 80% of the maximum load. Images in zero-strain condition were acquired to evaluate the DIC measurement uncertainties as the median of the strains in the sagittal plane. Maximum and minimum principal strains were measured with a four-camera 3D-DIC system (Aramis Adjustable 12M, GOM), on the IVDs surface, with a measurement spatial resolution of ≈ 2 mm.

Results

DIC random errors did not exceed 80με. No differences were observed in stiffness between adult (1205±738 N/mm) and elderly (944±1197 N/mm) donors.

Maximum principal strains were not different between adults (15226±6500με) and elderly (15803±12531με). Minimum principal strains were larger for elderly specimens (-5754±9657με) than adults' ones (-3630±3961με) (*Figure 1*). In elderly IVDs, principal strain concentrations were observed, localized in the central region of the IVDs.

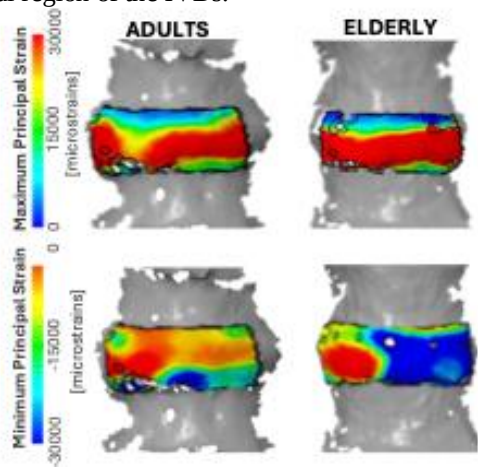


Figure 1: Examples of 3D maximum and minimum strain maps for adults (left) and elderly (right).

Discussions

Elderly IVDs concentrate larger strains in the anterior portion of the anulus fibrosus with respect to adults' ones, suggesting that a redistribution of loads occurs with ageing. Indeed, with degeneration, the NP becomes stiffer, leading to a shift of the compressive load from the NP to the AF and creating regions with higher stress and strain gradient in the AF (3,5).

Further analyses and mechanical tests are still ongoing to expand this evidence and include young IVDs' characterization. Once completed, these results may improve the current knowledge and be used to define clear and rigorous constitutive laws as well as to develop, train and validate computational models.

References

1. Ferreira *et al.*, Lancet Rheumatol (2023)
2. Luoma *et al.*, Spine (2000)
3. Urban *et al.*, Arthritis Res and Ther (2003)
4. Pfirrmann *et al.*, Spine (2001)
5. Cavazzoni *et al.*, Acta Biomaterialia (2025)
6. Palanca *et al.*, Bone (2021)

Acknowledgements

The study was funded by the MULTIDISC project thanks to the fundamental contribution of Fondazione del Monte of Bologna and Ravenna.

EVALUATION OF PEEK AND PLA COMPOSITE FEMORAL IMPLANTS USING FINITE ELEMENT ANALYSIS

Marta Spataro (1), Dario Milone (1)

1. Department of Engineering, University of Messina, Contrada di Dio, 98166 Messina, Italy

Introduction

Total hip arthroplasty cementless implants rely on bone growth and minimizing micromotions to prevent aseptic loosening and stress shielding. Advances in porous and biomimetic implant designs, as well as materials like PLA and PEEK, aim to improve load distribution and reduce stress shielding [1], [2]. This study uses finite element simulations to evaluate stress shielding reduction in uncemented THA models with composite material implants.

Materials and Methods

The standardized femur model was used as the base geometry of the Finite Element model. A generic prosthesis was designed and adjusted for optimal cortical bone contact, enhancing primary stability without bone removal. The femoral head was removed via a neck cut, aligning the implant to prevent misalignment between the shaft axes. A Boolean operation simulated a cementless press-fit. A 4-noded tetrahedral mesh with a maximum element size of 3 mm was applied. Materials were modelled as linear elastic, homogeneous, and isotropic, with a bonded contact approach for osseointegration.

Material	E [MPa]	ν
Cortical bone	18600	0,3
Trabecular bone	179	0,3
Titanium	118000	0,33
PLA + HA	1900	0,3
PEEK	3000	0,38

Table 1: Material properties

The model's distal portion was fixed. Physiological loading during walking, calculated with Adams software, was applied to the implant head using a 10-second cycle. Strain energy density (SED) serves as an indicator of the bone remodelling stimulus [3], thus it was measured in Gruen zones to evaluate stress shielding (SS), quantified as:

SS(%) = ΔSED (Intact-Implanted) / SED(Intact) (1)

Negative SS indicates increased stress, promoting a more physiological load distribution. Ideally, SS values near zero suggest minimal stress shielding and optimal load transfer.

Results

Figure 3 shows stress shielding (SS) variations across the 7 Gruen zones.

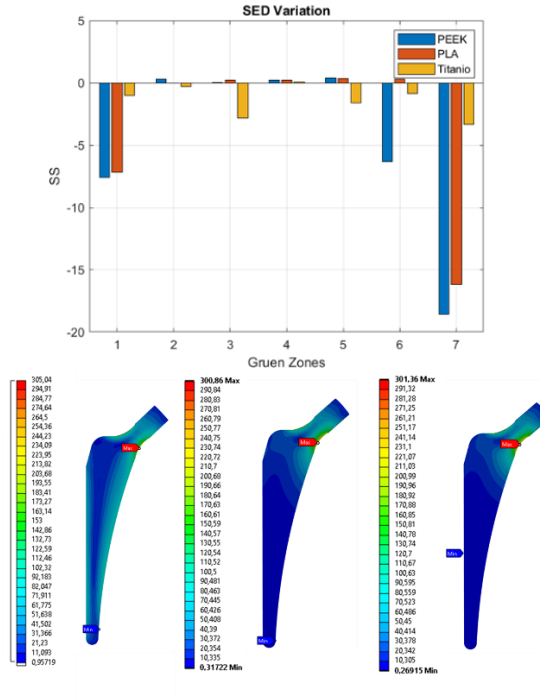


Figure 1: Top: Stress shielding increase among the 7 Gruen Zones. PEEK and PLA may offer a more physiological stress distribution, particularly in Gruen zones 1 and 7 where stress shielding (SS) reaches its most negative values. Bottom: Comparison between a) Titanium, b) PEEK and c) PLA implants stress distribution.

In GZ1, PEEK and PLA promote physiological load distribution with negative SS, while titanium shows less effect. From GZ2 to GZ5, all materials exhibit minimal SS, indicating balanced load transfer. In GZ6, PEEK and PLA increase stress, while titanium maintains near-zero SS. In GZ7, PEEK and PLA enhance distal femur loading, reducing stress shielding.

Discussion

Stress shielding is a key challenge in total hip arthroplasty, where conventional titanium implants can limit load transfer to surrounding bone, causing bone resorption and implant loosening. Findings suggest these PEEK and PLA composites offer improved load distribution, particularly in Gruen zones 1 and 7, potentially reducing bone resorption and enhancing implant longevity.

References

1. H. Bougherara et al., *J Biomed Mater Res A*, 82A:27–40, 2007.
2. S. Arabnejad et al., *J Orthop Res*, 35:1774–1783, 2017.
3. R. Huiskes et al., *J Biomech*, 20:1135–1150, 1987.

PERFUSION DRIVEN SHEAR STRESS REGULATES PERIODONTAL LIGAMENT STEM CELL BEHAVIOR IN 3D PRINTED SCAFFOLDS

Beatrice Masante (1,2), Mafalda Santos (3), Stefano Gabetti (1,2), Federico Mussano (4), Alberto Audenino (1,2), Joao C. Silva (1,2), Diana Massai (1,2)

1.Dept. of Mechanical and Aerospace Engineering and Polito^{BIO}Med Lab, Politecnico di Torino, Italy; 2. Interuniversity Center for the Promotion of the 3Rs Principles in Teaching and Research, Italy; 3. Dept. of Bioengineering and iBB -Institute for Bioengineering and Biosciences, Instituto Superior Técnico, Universidade de Lisboa, Portugal; 4. Bone and Dental Bioengineering Lab, CIR-Dental School, Dept. of Surgical Sciences, University of Torino, Italy.

Introduction

In vivo, the periodontal ligament (PDL) is exposed to mechanical forces such as compression, tension, and shear stress, which are known to play a crucial role in regulating cell growth, cell differentiation, and tissue development [1]. *In vitro*, the effect of shear stress on PDL cells remains to be elucidated. In this study, we investigated the impact of fluid-induced shear stress on human PDL stem cells (hPDLSCs) seeded into three-dimensional (3D) thermoplastic polyurethane (TPU) scaffolds and cultured within a direct perfusion bioreactor.

Materials and Methods

TPU scaffolds (diameter = 10 mm; height = 5 mm) with varying pore sizes (100, 200, and 300 µm) were designed and fabricated using a 3D printer (i3 mk3s+, Prusa Research). Computational fluid dynamics (CFD) simulations (COMSOL Multiphysics 6.0, Comsol Inc.) were conducted for each scaffold geometry, imposing a flow rate of 0.3 mL/min, to estimate the fluid-induced shear stress developing on the scaffold structure. To assess the optimal scaffold design, preliminary biological experiments were performed. The scaffolds were seeded with hPDLSCs (1.5×10^6 cells per scaffold) and the constructs were cultured under static conditions for 10 days, with Alamar Blue assays conducted on days 1, 4, 7, and 10. Once defined the optimal scaffold geometry (pore size = 200 µm), the hPDLSCs-seeded constructs were pre-cultured under static conditions for 7 days, followed by additional 7 days of direct perfusion culture in a bioreactor (Fig. 1A) [2] at a flow rate of 0.3 mL/min (n = 3). Control constructs were maintained under static conditions for the entire duration. Alamar Blue assays were performed on days 1, 7, and 14. Confocal microscopy and quantitative real-time PCR (qRT-PCR) analyses were conducted at day 14.

Results

CFD simulations revealed fluid-induced shear stress values of 5.42, 2.40, and 1.43 mPa for scaffolds with pore sizes of 100 µm, 200 µm (Fig. 1B), and 300 µm, respectively. From the cellular viability tests at day 10 (8000 a.u, 12000 a.u., 11000 a.u. for 100 µm, 200 µm, and 300 µm pore-size scaffolds, respectively), the 200 µm pore-size scaffold was selected as the optimal geometry. The Alamar Blue assays showed that perfusion did not affect cellular metabolic activity, although confocal analysis revealed a reduced number of cells in perfused constructs (Fig. 1C). Furthermore, in constructs cultured under perfusion, the qRT-PCR analysis showed increased expression of collagen type I and osteopontin, typical of tooth root development [3], and PDL-related gene collagen type XII, responsible for inhibiting the tissue mineralization [4].

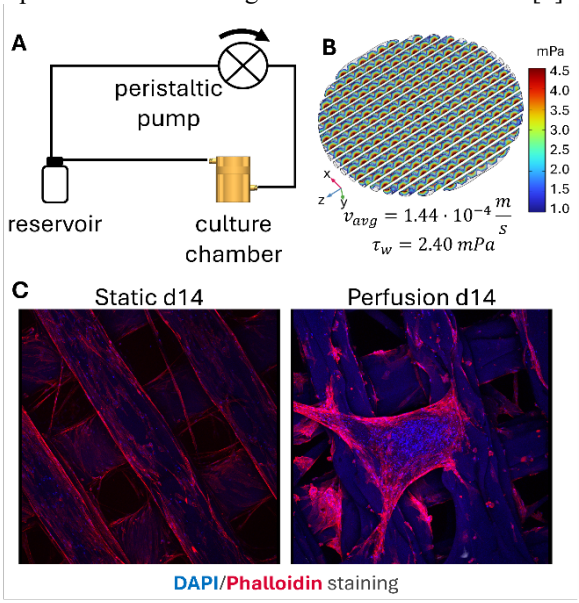


Figure 1. (A) Perfusion bioreactor scheme; (B) CFD results for the 200 µm pore-size scaffold, only a layer is represented; (C) Dapi/Phalloidin staining performed at day 14 on static (left) and perfused (right) scaffold (cell nuclei in blue, actin filament in red).

Conclusions

In this study, we demonstrated that fluid-induced shear stress influences the mechano-biological behavior of hPDLSCs cultured on TPU scaffolds. Notably, direct perfusion promoted the upregulation of markers associated with extracellular matrix synthesis and PDL-specific genes, suggesting the potential multilineage differentiation of hPDLSCs. These results offer important insights for the development of novel PDL tissue engineering strategies and regenerative medicine applications. Further biological experiments are ongoing to investigate the signaling pathways triggered by fluid-induced shear stress in hPDLSCs.

References

1.Roato et al., *Nanomaterials,* 12(21):3878, 2022
2.Gabetti et al., *Scientific Reports*, 12:13859, 2022
3.Foster et al, *Bone*, 107:196-207, 2018
4.MacNeil et al., *Arch Oral Biol*, 43(10):779-87, 1998

IN SILICO MODELING OF DECELLULARIZED EXTRACELLULAR MATRIX HYDROGEL MECHANICALLY STIMULATED IN A BIOREACTOR

Matteo Nifosì (1), Elena Merotto (1), Sara Manzoli (1), Martina Piccoli (2) Silvia Todros (1), Piero G. Pavan (1,2)

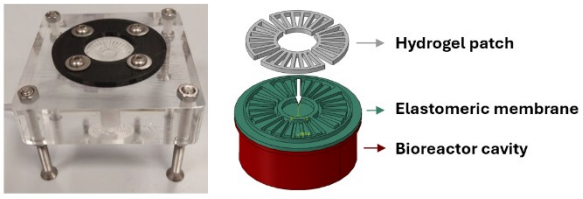
1. Department of Industrial Engineering, University of Padova, Italy; 2. Fondazione Istituto di Ricerca Pediatrica Città della Speranza, Padova, Italy

Introduction

Congenital diaphragmatic hernia is a severe condition in which the diaphragm fails to form properly, resulting in defects that, in many cases, must be solved surgically. For this purpose, tissue-engineered patches made of decellularized extracellular matrix hydrogel (dECM-hydrogel) from skeletal muscle hold great promise [1]. The patches are seeded with cells and mechanically stimulated in vitro in a custom-made bioreactor to radially orient the collagen fibers within the dECM-hydrogel patch [2], aiming at replicating the complex aligned cellular architecture of healthy muscle. Finite element analyses (FEA) are developed to study the stress and strain fields to which cells are subjected inside the hydrogel, with the aim to assess the optimal mechanical stimulation protocol prompting cell viability and differentiation into skeletal muscle.

Methods

The dECM-hydrogel is prepared following the protocol described in a previous study [3] and casted on an elastomeric membrane in a bioreactor (Figure 1). A hydraulic circuit deforms the membrane inducing its curvature [2] and deforming the hydrogel patch. FEA are performed (ABAQUS Standard, Simulia, Dassault Systèmes, France) to assess the deformation of the patch. The model includes the elastomeric membrane, the bioreactor cavity and the dECM-hydrogel patch.



(a) (b)

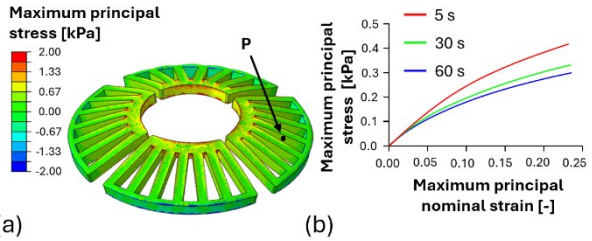
Figure 1: (a) Physical and (b) geometric solid model of the main elements of the bioreactor.

The instantaneous behavior of the dECM-hydrogel was described as linear elastic, and the time-dependent behavior with a generalized Maxwell model. The elastic modulus was measured by nanoindentation using atomic force microscopy, assuming the hydrogel as almost-uncompressible. The constitutive parameters related to the time-dependent response were obtained starting from rheometric data by using a non-linear optimization algorithm implemented in MATLAB (MathWorks®), to deduce and define the viscoelastic model in the time domain starting from data in the frequency domain [4].

As a preliminary study, different FEA were performed, in which the maximum curvature of the elastomeric membrane, corresponding to the physiological strain level of the diaphragm, was reached by applying to the bioreactor cavity a linear ramp of pressure in 5, 30 and 60 s.

Results and discussion

The viscoelastic constitutive parameters in the time domain were estimated with a suitable fitting quality, verified by comparing experimental data and numerical results in terms of storage (G′) and loss (G″) moduli with R^2 equal to 0.95 and 0.97, respectively. The contour of the maximum principal stress in the hydrogel patch deformed in 5 s (Figure 2a) shows the stress distribution within the hydrogel channels. The stress-strain behavior within one of the hydrogel channels (Figure 2b) highlights an increasing hydrogel stiffness when a higher deformation rate is applied.



(a) (b)

Figure 2: (a) Contour of maximum principal stress of the hydrogel patch stimulated in 5 s, at the maximum deformation; (b) Stress-strain behavior of the hydrogel in the node P, shown in part (a), deformed in different time intervals (5 s, 30 s, 60 s).

References

1. Boso et al, Materials, 13(11):2483, 2020.
2. Maghin et al, npj Regen Med, 7(1):25, 2022.
3. Boso et al, Biomedicines, 9(7):709, 2021.
4. Tapia-Romero et al, Ing Invest Tec, 21(2):1, 2020.

Acknowledgements

This work was supported by the National Recovery and Resilience Plan, Mission 4, Component 2, Investment 1.1, by the Italian Ministry of University and Research, funded by the European Union Next Generation EU – Project Title “Novel visible light-degradable hydrogels embedded with cell-laden proteinosomes for the 3D bioprinting of diaphragm-like muscle tissues (3D-L-INKED)” (CUP C53D23008360001). The activity has been carried out in collaboration with Tissue Engineering Laboratory, Istituto di Ricerca Pediatrica Città della Speranza, Padova.

COMPUTATIONAL ANALYSIS OF DRUG DELIVERY IN OBSTRUCTED AND STENTED TRACHEA

Mauro Malvè (1), Carmen Sánchez-Matás (2), José Luis López-Villalobos (3), Rocío Fernández-Parra (4)

1. Public University of Navarra, Spain; 2. University Hospital 'Virgen de la Arrixaca', Spain; 3. University Hospital 'Virgen del Rocío', Spain; 4. Catholic University of Valencia San Vicente Mártir, Spain

Introduction

Computational analysis of how drugs are delivered, deposited and transported in the human upper airway is a very important area of research in respiratory medicine, particularly in cases of narrowed or stenosed trachea. Tracheal stenosis, whether present from birth or developed later in life, poses significant obstacles to traditional drug delivery techniques due to altered airflow patterns and limited access to the intended sites. Furthermore, the use of stents to relieve tracheal stenosis poses additional challenges by affecting how drugs are deposited and transported. In this scenario, computational modelling serves to clarify the complex interactions between anatomical features, airflow behavior and pharmaceutical factors that influence drug movement in the upper airways [1]. Despite the extensive work dedicated to healthy patients, only a few works have focused on bronchial obstructions [2,3]. In this work, using simplified upper airway shapes and varying degrees of stenosis and stent dimensions, we performed an extensive parametric computational fluid dynamics (CFD) analysis with the aim of evaluating drug delivery situations in both scenarios with and without the presence of stenosis or stent.

Methods

The parametric models were generated using Rhinoceros (McNeel & Associates) and include the metered dose inhaler (MDI) and the 'path lung model' [3] with three tracheal stenoses (30, 50 and 70%) at different stenosis locations (posterior, central, right and left, Fig 1a) and two stented models (tubular and Y stent) with thicknesses of 1 and 1.5 mm (Figure 1b and 1c).

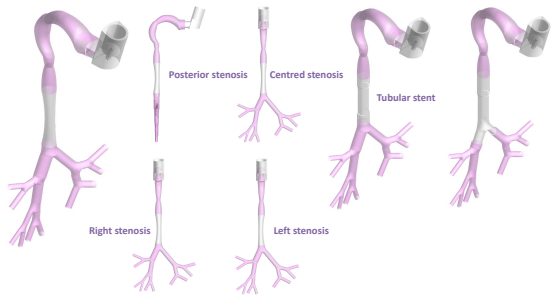


Figure 1: Diseased trachea with 30% stenosis in the posterior, middle, right and left trachea; b) Stented models with tubular and Y stents (thickness 1 mm).

Patient-specific inspiratory flows were obtained by spirometry before and after prosthesis implantation. The airflow was modelled as unsteady and turbulent. The aerosol flow considered particle sizes of 1, 5, 10 and 15μm. CFD simulations of the two-phase flow were performed using Ansys CFX (Ansys Inc.).

Results

In the stenosed models, only small particles (1μm) tended to reach the lower airways in all disease states. However, the stented configuration improved delivery (see Figure 2). Larger particles tended to be deposited entirely in the upper airways. For the stented geometries, delivery was significantly improved compared to that obtained with stenoses of 30, 50 and 70% and particles of 5, 10 and 15μm, but controversial deposition was found for all particle sizes. In addition, significant deposition was observed in the oral cavity and in the stented regions.

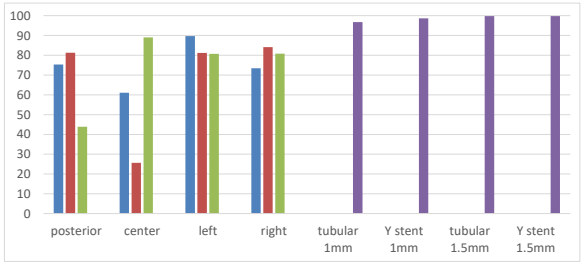


Figure 2: Comparison of 1μm particles reaching the lung for stenosed and stented airways.

Discussion

Stented airways show improved drug deposition compared to stenosed airways. However, significant deposition was found in the regions where the device is located as the tracheal lumen is reduced. Given that tracheal endoprostheses promote contraindications such as inflammation, tissue reaction and granulation, further studies are needed to elucidate the role of local overdosing around the stent regions.

References

1. Kleinstreuer et al, Respir Physiol & Neurobiol, 163:128-138, 2008.
2. P. Singh et al, Int J Env Res Pub Health, 17(3):1119, 2020.
3. Yan et al, Powd Tech, 356:148-161, 2019.
4. Yeh et al, Bull of Math Biol, 42:461-480, 1980.

Acknowledgements

This study is supported by grants PID2021-125731OB-C31 and PID2021-125731OB-C33 from MCIN/ AEI/10.13039/501100011033/ and FEDER ('A way to build Europe`).

MORPHOLOGICAL CHARACTERISATION OF THE HUMAN TIBIAL CANAL THROUGH STATISTICAL SHAPE MODELLING

Francesca Montigiani[1], Giulia Galteri[1], Valentina Betti[1], Luca Cristofolini[1]

1. *Dept of Industrial Engineering, Alma Mater Studiorum-University of Bologna, Italy*

Introduction

Morphological analysis of the medullary canal of the tibial bone is becoming increasingly important with the development of devices requiring osteointegration. Indeed, transtibial amputations account for approximately 41.8% of all amputations globally [1].
In recent years, osseointegrated devices have demonstrated significant advantages over traditional solutions. These benefits include enhanced stability, improved load transfer, and more effective proprioception [2]. However, to fully leverage these advantages, such devices must be designed to fit optimally with the anatomy of the host bone. To optimize the design of these devices, morphological studies have primarily focused on the tibial bone using statistical shape modelling (SSM) to represent an average bone shape and its variations [3]. Nevertheless, detailed analyses of the medullary canal have often been overlooked. This study aims to investigate the morphology of the tibial medullary canal using SSM, with the objective of assessing inter-subject variability and determining whether the development of patient-specific osseointegrated devices is necessary.

Materials and Methods

So far, 40 computed tomography tibia images were analysed (the convergence tests are going) [4][5]. Each tibia was segmented (Mimics) to isolate the region of interest, corresponding specifically to the medullary canal between 20% and 80% of the total tibial length. To overcome the problems related to the different pose during image acquisition, registration, was performed to align the medullary canals (with a dedicated script in Matlab). Twelve different segment lengths were simulated. The first cut was performed at 25% of the total tibial length, with subsequent levels evaluated in 5% increments, extending up to 80% of the total length (Fig. 1). A Statistical Shape Model (SSM) was developed for each segment length to statistically analyse the morphological variations and describe their variation across a population. The SSM relies on Principal Component Analysis (PCA) to identify the principal modes of geometric variation relative to the mean shape [6]. The resulting shapes, represented as the mean ±2σ, accounted for approximately 95% of the total shape variation. Finally, geometric parameters of interest were calculated by reconstructing the medullary canal at 5 mm intervals for each segment lengths. These parameters included segment length, radius of curvature, mean diameter, variations in maximum diameter respect to the distal and proximal regions, and the degree of non-axial symmetry of the canal.

Results

The PCA results for each segment length of the tibial medullary canal showed that the five levels appear sufficient, as the modes of shape variation accounted for over 85% of the total variance. These variations were strongly associated with geometric parameters such as length, mean diameter, and maximum diameter variation in the distal and proximal regions. For instance, at length of 45% the mean diameter and the maximum diameter variation respect to the proximal regions showed great relevance. Conversely, the radius of curvature and the length did not appear to have a major influence. At segment of 80% the length and mean diameter showed greater relevance, while and the maximum diameter variation respect to the proximal regions and the radius of curvature did not show relevance.

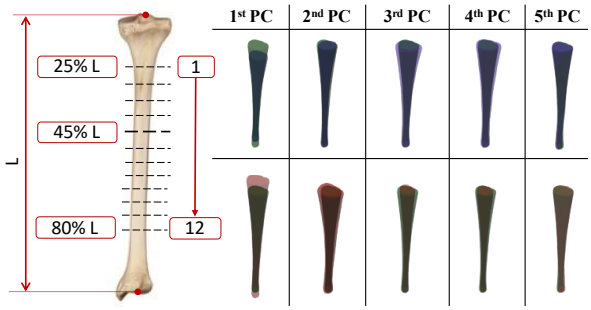


Figure 1: LEFT: simulated segment length. RIGHT: the mean canal shape (green), +2σ (red), -2σ (blue) for the 80% level.

Discussion

The application of the SSM enabled a quantitative assessment of the morphological variations in the tibial medullary canal. Preliminary results demonstrated the feasibility of parametrising these variations based on segment length. Consequently, the analysis provides insights into the importance of these parameters relative to the segment lengths. Additional CT image analyses are currently underway to reach convergence and further validate and generalise these findings.

References

1. Krueger et al. (2012), *J. Trauma Acute Care Surg.*
2. Galteri et al. (2023), *Frontiers*
3. Keast et al. (2023), *PeerJ*
4. Edgar, HJH et al (2020). NMDID. Office of the Medical Investigator, University of New Mexico.
5. Kistler, M. (2013). VSDFullBody CT Collection [Data set]. In Journal of Medical Internet Research. Zenodo.
6. Zhang et al. (2014), *CMBBE: Imaging & Visualization*

Acknowledgements

Work funded by INAIL (PR23-CR-P5-OsteoAMI).

DESIGN AND VERIFICATION OF A NOVEL CERAMIC INTERBODY FUSION CAGE: A NUMERICAL MODELLING APPROACH

Davide Ninarello, Giorgia Brambilla, Camilla Crivellaro, Luigi La Barbera
LaBS, Department of Chemistry, Materials and Chemical Engineering "G.Natta", Politecnico di Milano

Introduction

Lumbar interbody fusion (LIF) is the gold standard to treat severe lumbar interbody disk pathologies. Standard cages in titanium and peek exhibit certain limitations, including the potential for subsidence and pseudoarthrosis [1]. This points to a need for novel implants that make use of cutting-edge materials like b.Bone™ (GreenBone Ortho, Italy), a biphasic ceramic made from rattan wood subjected to a biomorphic transformation. A ceramic biodegradable interbody cage could both induce bone formation and be completely resorbed over time. However, the mechanical resistance of such brittle material becomes a critical aspect to be considered during the design process [2]. *In silico* models allow to save both time and costs compared to standard experimental try-and-error approach, directly obtaining the optimized geometry to be manufactured and tested.

This work presents an *in silico*-driven cage geometry optimization exploiting a validated fully-parametric lumbar spine model [3] and LIF surgery simulations. The final goal of the design process is the optimized cage design manufacturing and testing, according to standard ISO 23089-2:2021 [4].

Methods

The mechanical response of b.Bone™ cage was experimentally characterized and modelled through a transversely isotropic material constitutive model. A lateral approach (LLIF) was selected and simulated through a detailed finite element model, considering 3 steps: (i) removal of the structure for the cage insertion and distraction of the vertebrae, (ii) insertion of the cage and fixation of the district through titanium rod bars (5.5 mm) and (iii) application of complex loading conditions combining follower load with a bending movement in flexion, extension, axial rotation and lateral bending (Figure 1b). The cage design (G_i) was iteratively optimized to minimize failed volume (Figure 1c) and bone-cage interface strains (parameter indicating risk of subsidence). This involved adjusting cage medio-lateral width and incorporating variable holes for instrumentation accommodation and graft placement. The optimized designs were then virtually tested against standard ISO 23089-2 in axial compression, torsion, shear and subsidence, before manufacturing.

Results

The evaluation of load sharing between the anterior and posterior columns following surgery demonstrated a significant increase in load carried by the posterior column compared to the intact model. This finding aligns with established literature and supports the validity of the numerical model.

All cage designs led to a reduction up to 98% in the range of motion, ensuring an effective fixation. In terms of cage mechanical resistance, flexion was the most critical loading condition, and the simulations demonstrated that the longitudinal holes created in the cage have a major effect on the mechanical resistance, compared to transversal holes. Nevertheless, the optimized cage design presented an acceptable failed volume below 10% for every simulated task.

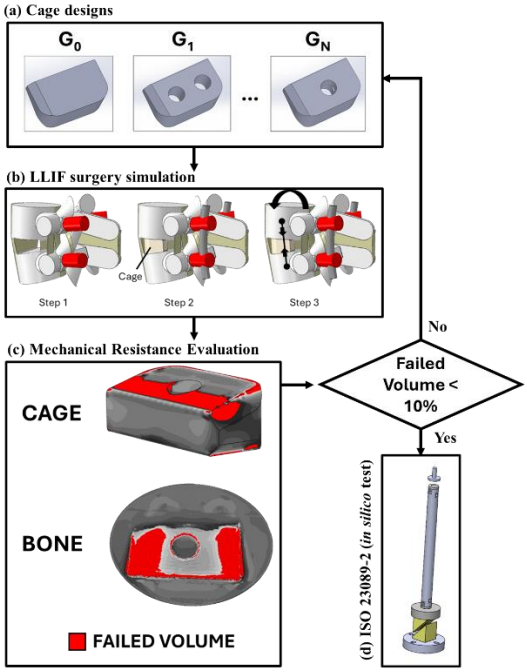


Figure 1: Workflow presenting the steps for the cage geometry optimization

Discussion

An *in silico* iterative approach allowed cage design optimization leading to rapid prototypes manufacturing, reducing material waste. The surrounding vertebral bone was subjected to similar or lower strains level compared to standard commercial cages with proved clinical effectiveness. Furthermore, the biodegradability of the implant material would allow gradual bone ingrowth and replacement, mitigating the long-term risk of subsidence.

References

1. Mobbs et al, J Spine Surg. 1(1): 2-18, 2015
2. Ninarello et al, J Mech Behav Biomed Mater. 2024
3. Bellina et al, J. Biomech. 111951, 2024
4. ISO 23089-2 (2021)

Acknowledgements

This research work was partially funded by NextGenerationEU program, MUR, Italia domani - P.N.R.R. and GreenBone Ortho S.p.A, Italy

CHITOSAN-COATED MAGNETIC NANOPARTICLES FOR THE TREATMENT OF INTESTINAL MOTILITY DISFUNCTIONS

Paolo Signorello (1), Ludovica Cacopardo (1), Cláudia Martins (2), Bruno Sarmento (2), Arti Ahluwalia (1)

1. Research Centre "E. Piaggio" and Department of Information Engineering, University of Pisa, Italy.
2. Instituto de Investigação e Inovação em Saúde – i3S, University of Porto, Portugal.

Introduction

Intestinal dysmotility represents a significant health burden, often leading to severe and life-threatening complications. Current therapeutic options remain limited, underscoring the urgent need for innovative treatment strategies [1]. This study introduces a novel, minimally invasive approach based on the oral delivery of magneto-responsive nanoparticles (Fe_3O_4) functionalized with chitosan to enhance mucoadhesion and cytocompatibility. To ensure gastric protection and facilitate controlled release in the intestinal tract, these nanoparticles were encapsulated within a pH-responsive alginate hydrogel. Figure 1 shows a schematic description of the strategy.

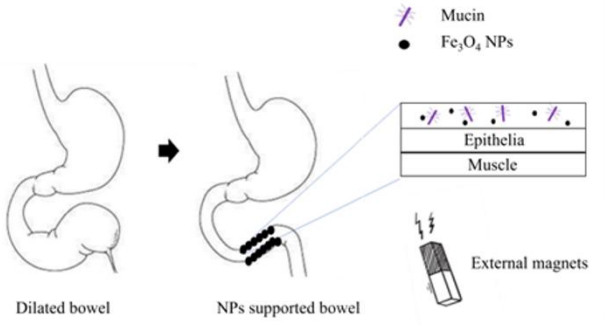


Figure 1. Schematic description of the proposed minimally invasive strategy.

Methods

Fe_3O_4 nanoparticles (200 nm in diameter) were coated with chitosan via an adsorption method. Chitosan-coated magnetic nanoparticles (CS-NPs, Fig. 2A) were characterized for size, zeta potential, stability under varying pH conditions, and mucoadhesive properties (ZetaSizer Nano ZS). Cytotoxicity was assessed on intestinal cell lines (Caco-2, HT29-MTX, HIF, and HPMEC), and an advanced 3D intestinal in vitro model [2] was used to evaluate NP translocation and their effects on nutrient absorption. An alginate-based hydrogel encapsulated the NPs, protecting them from the stomach's acidic environment (Fig. 2B). NP release studies were conducted in simulated gastric and small intestinal conditions.

Results

CS-NPs showed enhanced stability and mucoadhesion compared to uncoated NPs, with increased size and zeta potential. Stability tests demonstrated resilience in gastrointestinal pH conditions. The mucoadhesion tests revealed stronger binding to mucins. Cytotoxicity assays indicated high cell viability. The advanced 3D model (Fig. 2C) confirmed that CS-NPs did not cross the intestinal barrier, and nutrient absorption was unaffected. Release studies showed that the hydrogel protected the NPs and enabled controlled release in the small intestine.

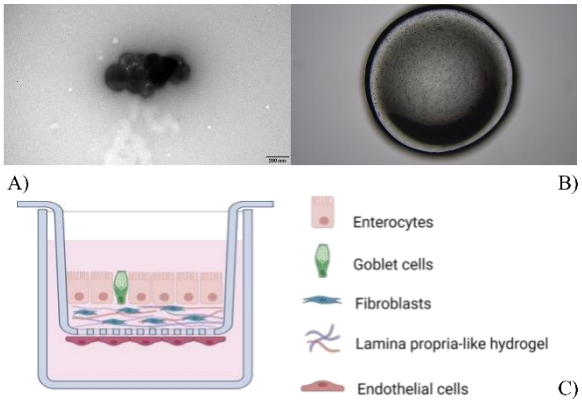


Figure 2. A) TEM image showing the morphology and size of CS-NPs (Jeol JEM 1400); B) CS-NPs encapsulated within a pH-responsive alginate hydrogel for gastric protection and controlled intestinal release; C) Schematic representation of the advanced 3D in vitro model [2].

Conclusions

In conclusion, this study demonstrates the feasibility of using chitosan-coated magnetic nanoparticles encapsulated in a pH-responsive hydrogel as a minimally invasive approach to address intestinal motility disorders. These findings pave the way for future smart therapeutic strategies, combining safety, targeted delivery, and efficacy in treating gastrointestinal conditions.

References

1. Hashmi S. et al, A. Jour. of Ph. Liv. Physio, (2021).
2. Ferreira B. et al, Jour. of Con. Rel. (2025).

EX-VIVO ASCENDING AORTA MODEL

Ariel F. Pascaner (1), Martina Schembri (2), Michele Conti (2,3), Jasper F. De Kort (4,5), Jessica Bassi (6), Mauro Di Giancamillo (6), Santi Trimarchi (4,7), Ferdinando Auricchio (2), Alessandro Caimi (2)

1. Section of Vascular Surgery, Cardio Thoracic Vascular Department, Fondazione IRCCS Cà Granda Ospedale Maggiore Policlinico, Milan, Italy

2. Civil Engineering and Architecture Department, Pavia University, Pavia, Italy

3. 3D and Computer Simulation Laboratory, IRCCS Policlinico San Donato, San Donato Milanese, Italy

4. Section of Vascular Surgery, Cardio Thoracic Vascular Department, Fondazione IRCCS Cà Granda Ospedale Maggiore Policlinico, Milan, Italy

5. Department of Vascular Surgery, University Medical Centre Utrecht, Utrecht, The Netherlands

6. Department of Veterinary Medicine and Animal Sciences, Università degli Studi di Milano, Milan, Italy

7. Department of Clinical Sciences and Community Health, Università degli Studi di Milano, Milan, Italy

Introduction

Ex-vivo animal models are widely used to study physiological and pathological aortic biomechanics and the arterial interaction with cardiovascular devices such as stent grafts [1][2]. Among the different animal models, the porcine aorta mimics the best human aortic behavior [3]. However, it would be clinically relevant to study the aortic root and ascending aorta (AA) [4], for which the porcine AA is shorter than that of humans one. For this reason, this work aimed to create an ex-vivo animal model that allows a proper study of the AA.

Methods

To overcome the shortness of the porcine AA, the proposed model was extended by suturing together an AA of another porcine aorta (*Fig 1a*). Geometrical and functional aspects were evaluated to assess the goodness of the model. All samples were tested within 24h since the harvesting. The samples were connected to a mock circulatory loop (MCL) and pressurized at different pressure levels: 80, 100, 120 mmHg with continuous flow of 4-5 L/min. Axial and longitudinal 2D ultrasound images of the vessel's lumen (*Fig 1b*) were acquired to measure diameter at various anatomical landmarks manually. CT scans of 3 samples were acquired using an ad-hoc, in-house developed, portable MCL to validate manual measurements. Afterward, the samples were pressurized with the pulsatile flow to achieve human physiological working conditions, i.e., heart rate of 75 bpm, cardiac output of 4-5 L/min, systolic (SBP) and diastolic blood pressure (DBP) of 120-125 mmHg, 75-80 mmHg (*Fig 1d*). Ultrasound videos, synchronized with pressure signals, were automatically segmented (*Fig 1c*) and were used to compute distensibility. Pulse Wave Velocity (PWV) was calculated from input and output flow signals.

Results

Ten models were tested. All the values obtained were compared to the same values, taken from the literature, of the human aorta [5]. Preliminary results show a geometric similarity (diameters) and functional similarity (distensibility and PWV) of our model, especially for the ascending part, with a young human aorta. Table 1 reports the preliminary results of one sample (over the ten tested) compared with humans. The elaboration of CT scans demonstrates the goodness of the manual measurement of the diameters. The mean error between the echo and CT of one sample (over the three acquisitions done) was 0.82 ± 0.71 mm.

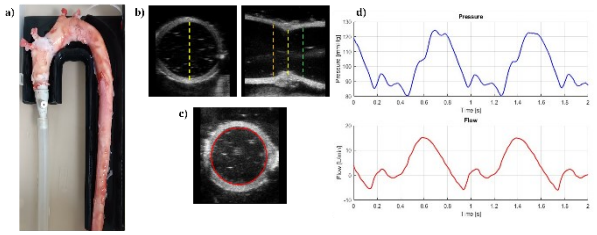


Figure 1: a) AA model; b) Axial and Longitudinal eco images with measure of diameter; c) Processed echo-video: inner diameter over eco-video synchronized with pressure signals; d) Pressure and Flow waveform of the model.

AA Parameters	Young Human	AA Model
Diameter [mm]	29	24,1
Distensibility[10^{-3}*mmHg^{-1}]	6,83	2,43
PWV	4,56	4,48

Table 1: Comparison of AA diameter, AA distensibility and PWV of one sample (sample 4) with literature values of human aorta.

Discussion

Given the importance of the studies on the endovascular management of AA pathologies, the proposed model provides an optimal tool to perform in-vitro studies, with clinical impact, on the evaluation of the performances of cardiac devices such as stent graft or to perform simulation of surgical procedures.

References

1. Peelukhana, Srikara V., et al., *Annals of biomedical engineering* 45 (2017): 592-603.
2. de Kort, Jasper F., et al., *Annals of Vascular Surgery* 112 (2025): 129-138.
3. de Beaufort, Hector WL, et al., *European Journal of Vascular and Endovascular Surgery* 55.4 (2018): 560-566.
4. Atkins, Aidan D., et al., *Methodist DeBakey Cardiovascular Journal* 19.2 (2023): 29.
5. Redheuil, Alban, et al., *Hypertension* 55.2 (2010): 319-326.

BIOPOINT: A PARTICLE-BASED MODEL FOR NUCLEAR MECHANICS AND CELL-ECM INTERACTIONS

Sandipan Chattaraj (1), Julius Zimmermann (1), Francesco Silvio Pasqualini (1)

1. Synthetic Physiology Lab, University of Pavia, Pavia, Italy

Introduction

Morphogenesis, the process of shape formation in tissues and organs, is governed by complex biochemical and mechanical interactions occurring across multiple scales. Both intracellular (e.g., nuclear deformation) and extracellular (e.g., cell-extracellular matrix or ECM interactions) mechanical properties play crucial roles in these processes. While experimental studies provide valuable insights, computational models are essential to complement these findings and offer predictions that guide further research. In this work, we present BIOPOINT, an enhanced particle-based computational framework built on the Subcellular Element Modeling (SEM) approach. This framework enables the investigation of nuclear mechanics and cell-ECM interactions by incorporating experimentally derived parameters and validating predictions against relevant biological experiments.

Methods

BIOPOINT extends SEM by introducing two key innovations: (1) a deformable nucleus represented by multiple interacting particles, and (2) explicit modeling of ECM using a lattice of particles that interact with cytoplasmic particles via calibrated potentials. These enhancements allow the model to better capture the mechanical complexity of cells and their environment. Model parameters, including nuclear and cytoplasmic stiffness and viscosity, were calibrated using single-cell indentation experiments conducted with atomic force microscopy (AFM). Validation was performed using simulations of cell spreading on ECM patterns of varying geometries and cell migration through narrow constrictions, with results compared to experiments.

Results

The BIOPOINT framework successfully reproduced experimentally observed behaviors, including nuclear deformability, cell spreading dynamics, and cell migration through confined environments. During single-cell indentation simulations, the force-time profiles closely matched experimental data[1], allowing for the derivation of elastic and viscous properties of the nucleus and cytoplasm. Simulations of cell spreading on ECM patterns recapitulated experimental evidences[2] that ECM geometry significantly influences cell and nuclear shape, with circular ECM patterns leading to near-symmetric spreading and elongated patterns inducing anisotropic deformation.

Finally, simulations of cell migration through constrictions revealed that nuclear deformation is highly dependent on nuclear stiffness and cytoplasm-nucleus interactions, as seen in recent experiments[3]. These findings underscore the importance of incorporating deformable nuclei and explicit ECM modeling in computational studies of cell mechanics so that they can be incorporated in the study of tissue morphogenesis.

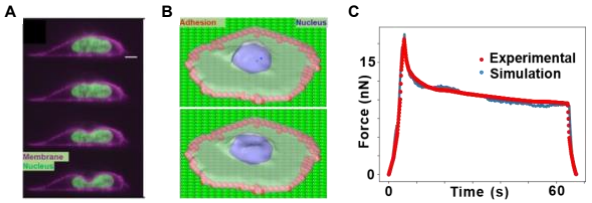


Figure 1: Nuclear indentation experiments from Hobson et al.1 (A) simulated with BIO-POINT (B) to calibrate model parameters (C).

Discussion

BIOPOINT represents a significant advancement in SEM-based modeling by bridging experimental and computational approaches to study morphogenesis. The explicit treatment of the nucleus and ECM enables a more accurate representation of the mechanics underlying cell behavior. However, some discrepancies between simulated and experimental nuclear shapes highlight the need for further enhancements, such as incorporating actin filaments and microtubules, which play critical roles in nuclear mechanics. Future work will focus on these additions, as well as on optimizing the computational framework for faster calibration of parameters using advanced techniques like Bayesian optimization. By providing a flexible and biologically grounded framework, BIOPOINT can serve as a valuable tool for researchers studying nuclear mechanics, cell-ECM interactions, and related phenomena in morphogenesis.

References

1. Hobson CM et al., MBoC, 31:1788-1801, 2020.
2. Versaevel M et al., Nat Commun, 3, 2012
3. Keys J et al., J Cell Sci, 137, 2024.

Acknowledgements

This work was supported by the European Research Council (ERC) starting grant (#852560) to FSP.

NONINVASIVE ASSESSMENT OF LEFT VENTRICULAR PERFORMANCE USING 3D ECHOCARDIOGRAPHY

Gianni Pedrizzetti (1)

1. Department of Engineering and Architecture, University of Trieste, Italy

Introduction

The pressure-volume (PV) loop description for the left ventricle (LV) as a volumetric pump (*i*), the time course of the intraventricular pressure gradients (IVPG) inside the LV (*ii*), in conjunction with the properties of the strain tensors for the surrounding muscular tissue (*iii*), represents three physics-based evaluations that offer deep insights into the physiological function of the heart. However, the invasive nature of acquiring PV loops and IVPG limits their widespread use in clinical and research settings. This highlights the need for the development of noninvasive techniques. This presentation aims to demonstrate the feasibility of utilizing three-dimensional echocardiography (3DEcho) as a noninvasive tool to describe LV PV loop, hemodynamic performance through IVPG, and spatial-temporal pattern of the LV strain tensors. This analysis is performed on a large cohort of healthy individuals (1403 subjects) recorded in 19 centers from 15 countries across 6 continents; therefore, it also aims to report reference values for these parameters across a broad spectrum of age groups, ethnic backgrounds, and sex.

Methods

This study utilizes 3DEcho data collected from the World Alliance of Societies of Echocardiography Study [1]. It employs physics-based methodologies to analyze the dynamic behavior of the endocardial border, enabling the construction of noninvasive LV PV loops (Figure 1), the evaluation of blood propulsion via IVPG [2], and the assessment of LV performance through strain tensor analysis [3].

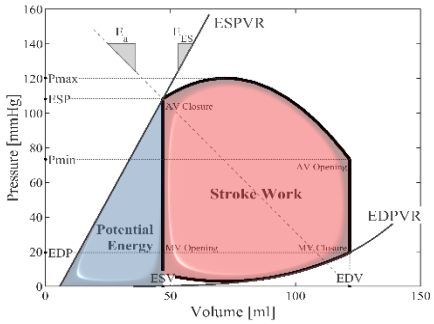


Figure 1: Schematic representation of the parameters of the pressure-volume (PV) loop.

Results

The analysis reveals that sex and age significantly influence certain parameters: women exhibit smaller LV volumes and higher ejection fraction (EF) generally growing with aging. In contrast, PV loop parameters and strain patterns display a common behavior (Figure 2) with limited differences with sex and age, while no significant variation is found in hemodynamic performance (IVPG) between sexes, though performance diminishes with aging. When comparing ethnic groups, Asian populations are found to have smaller heart sizes, higher EF, more pronounced strain, and better PV loop scores compared to White populations. In turn, White populations show similar LV size to Black populations but demonstrate higher EF, strain, and PV loop scores. IVPG values across these populations were relatively consistent.

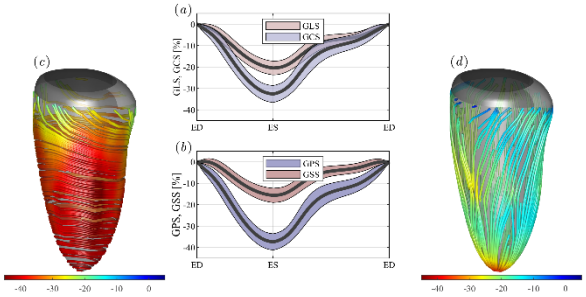


Figure 2: Deformation time-space pattern for the entire population. (a)(b) Time course of global deformation parameters (mean ± st. dev.). (c)(d) Spatial pattern for (c) 1st principal strain and (d) 2nd principal strain.

Conclusions

This study shows the feasibility of applying advanced physics-based methods to 3DEcho to provide an in-depth analysis of LV function. It provides reference values for advanced parameters and their dependence on sex, age, and ethnic differences.

References

1. Addetia K, Miyoshi T, Amuthan V, Citro R, Daimon M, Gutierrez Fajardo P, et al. Normal Values of Left Ventricular Size and Function on Three-Dimensional Echocardiography: Results of the World Alliance Societies of Echocardiography Study. J Am Soc Echocardiogr 2022;35(5):449.
2. Vallelonga F, Airale L, Tonti G, Argulian E, Milan A, Narula J, Pedrizzetti G. An Introduction to Hemodynamic Force Analysis: Analysis: moving into the new frontier of cardiac deformation analysis. J Am Heart Assoc 2021;10:e023417.
3. Pedrizzetti G, Sengupta S, Caracciolo G, Park CS, Amaki M, Goliasch G, Narula J, Sengupta PP. Three-dimensional Principal Strain Analysis for Characterizing Subclinical Changes in Left Ventricular Function. J Am Soc Echocardiogr 2014;27;1041-50.

Acknowledgements

This study was partially funded by the Italian Ministry of Education and Research with grant: PRIN 2022AJT27Y.

COMPUTATIONAL MODELING OF THE AORTA SUBJECTED TO RADIAL TENSION

Laura Pellerito (1), Massimiliano Zingales (2), Stéphane Avril (3)

1. *Department of ME.PREC.C., University of Palermo, Palermo, Italy;*
2. *Department of Engineering, University of Palermo, Palermo, Italy;*
3. *Mines Saint-Étienne, Sainbiose INSERM 1059, France*

Introduction

Aortic Dissection is one of the most prevalent catastrophic cardiovascular events, affecting 35 out of 100 000 patients for people aged 65-751 [1]. This lethal condition is characterized by delamination and separation of adjacent lamellae within the medial layer of the aorta [2]. The internal damage propagates radially, and characterizing the arterial wall through radial tensile testing provides insights into the underlying damage mechanisms [3]. The biphasic nature of aortic tissue is crucial in the evaluation of tissue response, as it is necessary to consider the volume change induced by this very specific loading condition. The aim of this study is to develop a Computational Model, implemented in FEBIO software, to simulate radial tensile test and study the propagation of damage in aortic dissection, starting from experimental data.

Methods

Radial tensile tests with controlled displacement were conducted on 10 samples of bovine aortic tissue. Using the experimental data obtained, a biphasic model for aortic tissue was designed in FEBio software [4]. A reactive viscoelastic damage material was chosen to simultaneously capture the viscoelastic properties of aortic tissue and its damage mechanisms during radial tension testing [5]. Additionally, a constitutive model was developed in Wolfram Mathematica, ensuring consistency with the mechanical properties of the aortic tissue.

Results

A biphasic model with a reactive viscoelastic damage material as a solid matrix successfully developed in FEBio to simulate the behavior of aortic tissue under radial tensile testing. Sensitivity analysis, combined with experimental data, allowed for the identification of all parameters of the damaged viscoelastic reactive material. The model accurately fit the experimental data and demonstrated theoretical consistency.
Further development in Wolfram Mathematica provided a constitutive relationship that aligned with the observed mechanical behavior, producing stress-stretch curves closely matching those obtained from FEBio simulations.

Discussion

Despite the simplified geometry of the computational model, the identified approach effectively captures microstructural damage mechanisms and the biphasic nature of aortic tissue, enabling realistic simulation of fluid-structure interactions. The results demonstrate that the reactive viscoelastic damage model reproduces the experimental response of aortic tissue under radial tension, including stress relaxation. The viscoelasticity of the solid matrix facilitated simulation of relaxation effects, linking these to swelling phenomena in the arterial wall. From a histological perspective, the Neo-Hookean and Holtzapfel-Gasser-Ogden models were used to represent the elastin and collagen fibers of aortic tissue, respectively. The constitutive relationship developed provided a stress-stretch curve consistent with FEBio simulations, reinforcing the theoretical coherence of the model. Analysis of relaxation factors identified the fluid component as the primary driver of tissue relaxation. This model offers potential for studying the development of arterial dissection in vivo. Future research could adapt and extend these findings to investigate damage mechanisms in actual aortic dissections, contributing to improved prevention strategies.

References

[1] C. A. Nienaber *et al.*, “Aortic dissection,” *Nat Rev Dis Primers*, vol. 2, no. 1, p. 16053, Jul. 2016, doi: 10.1038/nrdp.2016.53.

[2] M. Mikich, “Dissection of the aorta: a new approach,” *Heart*, vol. 89, no. 1, pp. 6–8, Jan. 2003, doi: 10.1136/heart.89.1.6.

[3] G. Sommer, T. C. Gasser, P. Regitnig, M. Auer, and G. A. Holzapfel, “Dissection Properties of the Human Aortic Media: An Experimental Study,” *J Biomech Eng*, vol. 130, no. 2, Apr. 2008, doi: 10.1115/1.2898733.

[4] J. J. Shim and G. A. Ateshian, “A hybrid biphasic mixture formulation for modeling dynamics in porous deformable biological tissues,” *Archive of Applied Mechanics*, vol. 92, no. 2, pp. 491–511, Feb. 2022, doi: 10.1007/s00419-020-01851-8.

[5] G. A. Ateshian, “Viscoelasticity using reactive constrained solid mixtures,” *J Biomech*, vol. 48, no. 6, pp. 941–947, Apr. 2015, doi: 10.1016/j.jbiomech.2015.02.019.

BAYESIAN HIERARCHICAL IDENTIFICATION OF POPULATION-WIDE BIOMECHANICAL CONSTITUTIVE PARAMETER DISTRIBUTIONS

Marco Pensalfini (1), Adrián Buganza-Tepole (2)

1. School of Engineering and Materials Science, Queen Mary University of London, UK;
2. School of Mechanical Engineering, Purdue University, West Lafayette, Indian, United States of America.

Introduction

Owing to widespread availability of significant computational power, *in silico* approaches are progressively revolutionizing how we design and evaluate surgical procedures [1] and implants [2]. In this context, accurate description of tissue biomechanics is a prerequisite for reliable predictions and, once an adequate constitutive model has been selected, it is crucial to identify suitable parameters based on experimental data.

However, biological variability results in a wide range of behaviors across subjects, even for tissues from the same body region. Subject-specific approaches account for this by determining constitutive model parameters that capture the tissue behavior for one single subject. On the other hand, designing procedures or products intended for mass use specifically requires knowledge of how such parameters vary across the entire cohort of interest.

To address this need, we resort to Bayesian inference [3], which allows supplementing the available data with prior knowledge about the parameters. We reason that the constitutive model parameters should follow a hierarchical structure, whereby the sample-specific distributions originate from common, population-wide distributions (Fig. 1a). To demonstrate our method, we showcase its application to both computer-generated and experimentally measured skin stress-strain responses.

Methods

We generated N_s synthetic stress-strain curves by considering uniaxial extension of hyperelastic, isotropic tissue specimens described by a Holzapfel-Gasser-Ogden potential. Sample-specific constitutive parameters, $\theta = (C_{10}, k_1, k_2)$, were independently obtained from known log-normal distributions. Experimental curves were from previously reported uniaxial stress-strain data on skin [3].

The parameter identification problem was formulated using the probabilistic programming framework PyMC [4]. The posterior probability distribution of θ given the observed data ($\mathfrak{D} = \{\mathfrak{D}_1, \dots, \mathfrak{D}_{N_s}\}$) was expressed as

$$p(\theta, \mathcal{H}|\mathfrak{D}) \propto \prod_{j=1}^{N_s} p(\mathfrak{D}_j|\theta_j)\, p(\theta_j|\,\mathcal{H})\, p(\mathcal{H}), \quad (1)$$

where $p(\mathcal{H})$ encodes our prior beliefs about the population-wide parameters, $p(\theta_j|\mathcal{H})$ links population- and sample-level parameters, and $p(\mathfrak{D}_j|\theta_j)$ is the likelihood of the j-th observed curve given θ_j. For comparison, we also implemented a non-hierarchical model (Fig. 1b) with posterior probability distribution

$$p(\theta_j|\mathfrak{D}_j) \propto p(\mathfrak{D}_j|\theta_j)\, p(\theta_j) \quad \forall j \in [1, N_s]. \quad (2)$$

To sample the posterior probability distributions, we took advantage of PyMC's implementation of the No U-Turn Sampler (NUTS) Markov chain Monte Carlo algorithm.

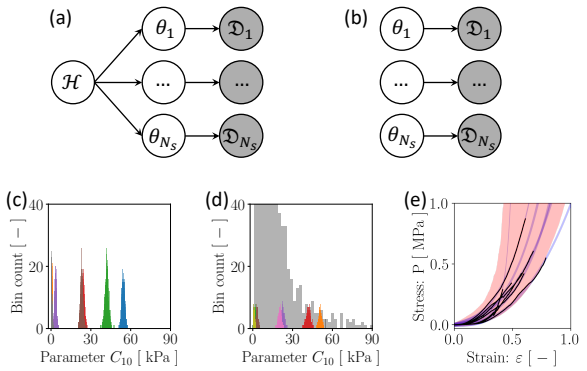


Figure 1: Bayesian parameter identification and new sample response prediction. Schemes of hierarchical (a) and non-hierarchical (b) model structures. Parameter identification results for N_s = 8 experimentally measured stress-strain curves using either approach (c: non-hierarchical; d: hierarchical), with the colored histograms corresponding to sample-level parameters and the grey histogram in indicating the population-level distribution. The curves in (e) indicate the possible new sample predictions (red: hierarchical model; blue: non-hierarchical model) vs. the observed data (black curves).

Results

Conducting parameter identification on the same dataset using both a non-hierarchical and a hierarchical approach demonstrates how the latter allows estimating both sample- and population-level parameters from just one set of available observations (Fig. 1c, d). Moreover, attempting to predict the response of a new sample using either calibrated model shows that this is only possible when parameters have been identified using a hierarchical approach (Fig. 1e), while the non-hierarchical model can only predict the responses of already observed samples.

Discussion

We have demonstrated use of a hierarchical Bayesian approach to infer population-wide parameter distributions and reasonably predict new sample responses. We expect this approach to be broadly applicable to *in silico* medicine problems that require accounting for tissue biomechanical variability across a population of interest.

References

1. Chabanas et al, Med Image Anal, 7(2):131-151, 2003.
2. Favre et al, Ann Biomed Eng, 49(12): 3213-3226, 2021.
3. Pensalfini et al, PLoS Comput Biol, 19(3): e1010902, 2023.
4. Abril-Pla et al, PeerJ Comput Sci, 9: e1516, 2023.

A COUPLED EXPERIMENTAL-COMPUTATIONAL APPROACH TO INVESTIGATE DIABETIC FOOT TISSUES

Sofia Pettenuzzo (1), Alice Berardo (1), Martina Valcelli (2), Elisa Belluzzi (3), Assunta Pozzuoli (3), Pietro Ruggieri (3), Emanuele Luigi Carniel (2), Chiara Giulia Fontanella (2)

1. Department of Civil, Environmental and Architectural Engineering, University of Padova, Italy; 2. Department of Industrial Engineering, University of Padova, Italy; 3. Department of Orthopedics and Orthopedic Oncology, DiSCOG, University-Hospital of Padova, Italy

Introduction

Diabetes is a chronic metabolic disorder affecting over 0.5 billion people globally (IDF Diabetes Atlas 2021). This pathology can lead to severe complications, such as diabetic foot, which not only impairs people's quality of life but also frequently leads to foot amputations [1]. Studying diabetic foot behaviour is crucial to understand the mechanisms behind foot ulcer development and improve wound healing preventing foot amputation. In light of this, this study aims to characterise the mechanical properties of diabetic plantar foot tissue using a coupled experimental and computational methodology.

Materials and Methods

A diabetic foot was collected from a patient (M, 76 years) who underwent amputation due to diabetic gangrene at the University-Hospital of Padova (CESC Code: AOP2649). Skin-adipose tissue and skin samples were obtained from the fingertips. For skin-adipose tissue samples, indentation tests (Fig. 1a) were performed using a loading-unloading (LU) procedure (40% strain, 1%/s strain rate) with flat and spherical indenters (Model Match-1, ©Biomomentum). For skin samples, stress relaxation (SR) tensile (5 ramps of 7% strain; 10%/s strain rate; 600s of resting) and compression tests (5 ramps of 10% strain; 100%/s strain rate; 600s of resting) were carried out. A 3D Finite Element Model (FEM) of the fingertips, composed of plantar skin-adipose tissue (Fig. 1b), was developed through a multi-step procedure (Fig. c) requiring various tools, *e.g.*, photogrammetry (Colmap). An almost-incompressible visco-hyperelastic constitutive model was used to describe all the tissues' behaviours, with the hyperelastic component defined by the Ogden formulation [2] and the parameters identified through inverse analysis of experimental tests. FE analyses simulated the experimental loading phase and SR behaviour. Comparison between mechanical parameters was evaluated using a 2-sample t-test (Minitab 2020).

Results

Mechanical parameters from LU curves, obtained with spherical and flat indenters (Fig. 2a, Table 1), showed different behaviours in terms of peak forces and stiffness (Fig. 2b). The FEM of the fingertip successfully interpreted the mechanical response of the structure (Fig. 2c) and evaluated the stress reduction during SR simulations (20% strain imposed) (Fig. 2d).

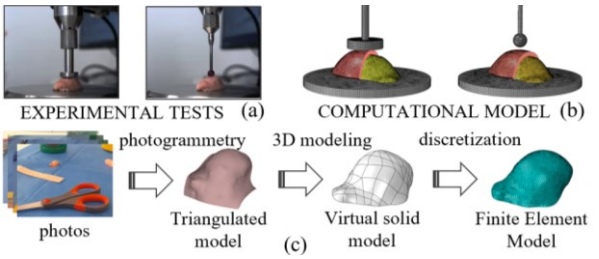


Figure 1: Indentation test setup (a); 3D FEM of fingerprints (b), multi-step procedure to achieve it(c).

Discussion

The experimental results assessed diabetic foot tissue mechanics and identified parameters for the FEM. Stress distribution analysis in the metatarsal head (one of the most stressed areas of the foot), showed compressive stresses concentrated at the skin-indenter contact, while compressive strains were mainly in the adipose tissue (Fig. 2c,d). These insights could help in the design of specific insoles for preventing plantar ulcer onset.

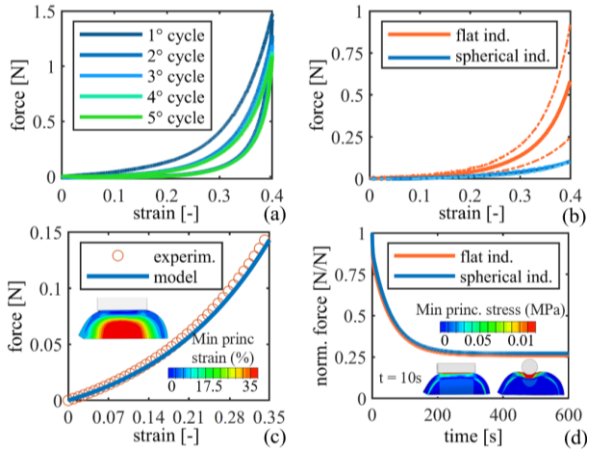


Figure 2: Example of LU force-strain curves (a); force-strain curves for flat vs spherical indenters (b). Experimental vs model results (c) and computational simulation of SR tests with contours (d).

	hysteresis area [N·mm]	peak force [N]	stiffness [N/mm]
flat I	0.15±0.10	0.57±0.31	1.14±0.58
spherical I	0.03±0.01	0.10±0.01	0.18±0.10
p-value	0.10	0.05	0.04

Table 1: LU parameters. I=Indenter. Values: mean±SD.

References

1. Cole et al, Nat Rev Nephrol, 16: 377–390, 2020.
2. Pettenuzzo et al, Bioengineering 11: 42, 2024.

VERIFICATION OF A FINITE ELEMENT MODEL TO STUDY THE RISK OF FAILURE OF A PATIENT-MATCHED OSSEOINTEGRATED IMPLANT

Ettore Pomeranzi (1), Giulia Galteri (2), Luca Cristofolini (2) and Cristina Curreli (1)

1. Medical Technology Lab, IRCCS Istituto Ortopedico Rizzoli, Bologna, Italy;
2. Department of Industrial Engineering, Alma Mater Studiorum - Università di Bologna, Bologna, Italy

Introduction

Osseointegrated implants for patients with a transfemoral amputation offer a viable alternative to *gold standard* represented by sockets prostheses [1]. The osseointegrated prostheses provide a direct connection between the prostheses and the host bone, solving the limitations shown by the sockets, such as skin lesions, reduced stability and mobility. Finite element (FE) models are useful tools, which allow to perform different biomedical studies and can generate information to support the device safety. They can be used to replicate mechanical testing *in silico* on different prostheses, simulating a wide range of boundary conditions and exploring loading scenarios that cannot be replicated experimentally [2]. However, the credibility of those models needs to be assessed following a rigorous regulatory process [2]. One of the key credibility activities required to identify and quantify potential numerical errors in FE models is known as model verification [3]. The aim of this work is to define a series of verification activities for an FE model of a patient-matched osseointegrated implant (OsteoCustom) [1] designed to assess fatigue-failure risk, as part of the device's preclinical validation phase.

Methods

A FE model was developed based on a simplified geometry of a recently designed patient-matched osseointegrated stem (OsteoCustom) and its material properties. A tetrahedral mesh was created using a patch-independent method, and the boundary conditions were defined to replicate the experimental conditions used for mechanically testing the implant [4].
To assess the credibility of our model, we followed the reference technical standard called ASME V&V-40 [3]. To perform the model verification, this standard specifies different steps to be followed: code verification, which consists of software quality assurance (SQA) and numerical code verification (NCV); calculation verification, which evaluates the discretization error, the numerical solver error and the use error. The code verification can be ensured referencing the software vendor's ISO 9001 certificate and solving standard benchmark problems with a known exact solution. To obtain the calculation verification, firstly we performed a convergence analysis on global mesh refinements to evaluate the discretization error, followed by a similar test on the local mesh (local refinements relative to the critical areas of the geometry). Both linear and quadratic elements were considered in the analysis. Secondly, a sensitivity analysis on the solver parameters, was defined to quantify the numerical solver error. For this, a list of critical solver parameters (e.g., solver type, contact penetration tolerance and contact detection method), along with their possible states or values was created.

Results

Some of the results obtained, related to the model convergence behavior for two different quantities of interest, are reported in Figure 1. The graph indicates the relative percentage difference in deformation and displacements values obtained along the direction of load application between subsequent refinements of the global mesh. The relative difference starts from higher values and progressively decreases, reaching an asymptotic behavior with variations smaller than 1%.

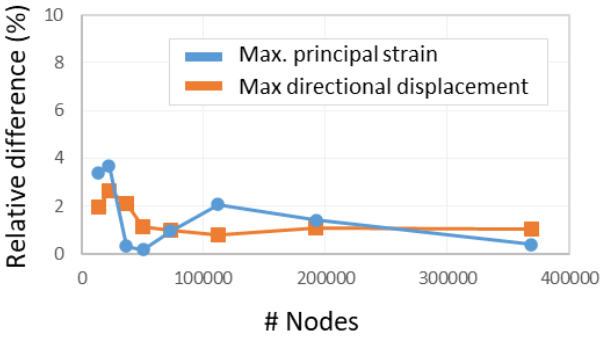


Figure 1: Mesh convergence results obtained considering peak values of maximum principal strain and directional displacements.

Discussion

Preliminary results provided valuable insight into the credibility of the FE model. Model verification is the initial step that will enable us to proceed to the validation phase, where simulation results will be compared with experimental data.

References

1. Betti et al, JOSR, 19:520, 2024.
2. Viceconti et al, Methods, 185:120-127, 2021
3. ASME, V&V 40—2018
4. Galteri et al, Frontiers 2024.

Acknowledgements

This research was funded by INAIL (Istituto Nazionale per l'assicurazione contro gli Infortuni sul Lavoro), "OsteoAMI" project grant number PR23-CR-P5.

THEORETICAL AND EXPERIMENTAL SET-UP FOR ADVANCING CONSTITUTIVE MODELLING OF MENISCAL TISSUE

Gaia Prezioso (1), Gregorio Marchiori (2), Massimiliano Zingales (3)

1. Dipartimento Me.Pre.C.C., Università degli Studi di Palermo, Palermo, Italy;
2. SC Scienze e Tecnologie Chirurgiche, IRCCS Istituto Ortopedico Rizzoli, Bologna, Italy;
3. Dipartimento di Ingegneria, Università degli Studi di Palermo, Palermo, Italy;

Introduction

The knee is one of the biggest and most important joints in the human body. It consists of highly varied components, among which meniscus plays a key role in the stabilization of the whole joint.
From a constitutive point of view, meniscus can be described as a biphasic and extremely inhomogeneous material.
In particular, this inhomogeneity affects the meniscus mechanical behavior; in fact, while anterior and posterior horns can be described as isotropic structures, the pars intermedia display a transversally isotropic behavior [1].
It is also worth to notice how meniscus, like the majority of human fibrous tissues, display a viscoelastic behavior [2], since it has memory of its past stress-strain history, and, therefore, this affects the fluid phase diffusion process.
The aforementioned characteristic would constitute an advancement in meniscus constitutive modelling. It would have an impact on knee biomechanical modelling. [3]. Consequently, the aim of this study is to develop a material model that integrate those characteristics and to design an experimental set-up to apply that model on meniscal tissue.

Methods

A new biphasic mechanical model is considered for development: the solid phase is modelled as a transversally isotropic perfectly elastic material; the fluid phase diffusion process, in order to consider the time-memory effects, are described by using a fractional-order Darcy Law [4], generalized to the anisotropic case.
Conventional unconfined and confined compression tests are reviewed for designing an unconventional experimental set-up able to reveal the constitutive parameters of the developed constitutive model.
The meniscal tissue will be characterized in the various anatomical directions, i.e. vertical, circumferential and radial, mainly because of the transversal isotropy of the meniscus pars intermedia.

Results

For what concerns the theoretical modelling, the constitutive equations for a transversally isotropic elastic material and the proposed fractional-order anisotropic Darcy Law are used to formulate a new biphasic model which correctly describe the behavior of meniscus pars intermedia.
As regards the experimental set-up, able to reveal the introduced constitutive parameters, a compression test, unconfined only for the solid phase, is designed to apply a strain ramp followed by stress-relaxation on cubic samples of meniscal tissue, thus to test a same sample along the different directions, in a random order to avoid any possible bias [1].

Discussion

The choice of this unconventional experimental setup is related to the fact that it is necessary to investigate filtration process of meniscus fluid phase, along the three different directions. Additive manufacturing will be employed to manufacture the accessories that are specifically needed, in particular for confining the solid phase only.
Once implemented, the experimental set-up, the developed constitutive model will be tested in its ability of describing meniscus mechanical anisotropy by the novel fluid flow expression.
Indeed, the described approach potentially offers a robust experimental and theoretical framework, which allow us to better understand and analyse the inhomogeneous structure of meniscus.

References

1. Berni, M., Marchiori, G., Cassiolas, G., Grassi, A., Zaffagnini, S., Fini, M., Lopomo, N.F., Maglio, M., “Anisotropy and inhomogeneity of permeability and fibrous network response in the pars intermedia of the human lateral meniscus.", Acta biomaterialia , 135: 393-402, 2021.
2. Amiri, F., Bologna, E., Nuzzo, G., Moroni, L., Zingales, M., "Fractional-order poromechanics for a fully saturated biological tissue: Biomechanics of meniscus.", International Journal for Numerical Methods in Biomedical Engineering, 39.11: e3732, 2023.
3. Alaimo, G., Piccolo, V., Cutolo, A., Deseri, L., Fraldi, M., Zingales, M., "A fractional order theory of poroelasticity.", Mechanics Research Communications, 100: 103395, 2019.
4. 4. Elmukashfi, E., Marchiori, G., Bermi, M., Cassiolas, G., Lopomo, N.F., Rappel, H., Girolami, M., Barrera, O., “Model selection and sensitivity analysis in the biomechanics of soft tissues: A case study on the human knee meniscus.”, Advances in Applied Mechanics, 55:425-511, 2022.

VERIFICATION, VALIDATION AND UNCERTAINTY QUANTIFICATION IN PATIENT-SPECIFIC TAVR MODELS

Roberta Scuoppo (1), Stefano Cannata (2), Caterina Gandolfo (2) and Salvatore Pasta (1,3)

1. Department of Engineering, Università degli Studi di Palermo, Palermo, Italy
2. Interventional Cardiology Unit, IRCCS ISMETT, Palermo, Italy
3. Department of Research, IRCCS ISMETT, Palermo, Italy

Introduction

In transcatheter aortic valve replacement (TAVR), computational models have shown potential to predict transcatheter heart valve (THV) deployment and improve patient outcomes. However, their predictive accuracy is influenced by uncertainties from imaging modalities, model assumptions, and patient variability. Systematic uncertainty analyses are essential for characterizing these uncertainties and quantifying their impact on predictions.

Model credibility assessment relies on verification, validation, and uncertainty quantification (VVUQ), as outlined by the FDA and the ASME V&V40 standard, "Verification and Validation in Computational Modeling of Medical Devices" [1].

This study applies the ASME V&V40 framework to establish the credibility of computational models simulating balloon-expandable SAPIEN 3 (S3) TAVR, employing techniques like surrogate modeling, Monte Carlo simulations (MCS), and cumulative distribution functions (CDFs) to compare simulations with clinical data.

Materials and methods

The TAVR simulations combined structural and fluid dynamics modeling. The structural simulation, performed in Abaqus/Explicit, includes crimping the S3 stent and deploying it with a balloon into the aortic root anatomy. Fluid dynamics simulations used smoothed particle hydrodynamics to model blood flow with patient-specific boundary conditions.

Verification ensures the TAVR model accurately represents the mathematical framework, minimizing discretization errors with mesh refinement and element formulation studies (keeping errors below 1%) and addressing solver errors by optimizing parameters like damping and penalty factors [2].

Uncertainty quantification entails characterizing the uncertainty inherent in model inputs and evaluating its influence on the resulting outputs. Each model input selected were associated with epistemic or aleatory uncertainties, used to develop a design of experiments based on Latin Hypercube Sampling.

Simulation outputs included stent deployment diameters at three different levels (Inflow, Mid and Outflow), effective orifice area (EOA), and transvalvular pressure gradient (TPG). These outputs were used to create a surrogate model based on a Gaussian Regression Process, which was essential for performing MCS with 10000 Sobol samples. The surrogate model's accuracy was evaluated in terms of the mean relative error (MRE) between predictions and actual finite element results. MCS results supported a sensitivity analysis using Total Effect index to identify the most influential parameters in the simulations, mapped in terms of Pareto plots. CDFs were generated for simulation outputs and compared with clinical data CDFs, which also accounted for uncertainty. Validation was performed by quantifying differences between simulation and clinical CDFs using an area metric, ensuring rigorous evaluation of the model's agreement with clinical outcomes.

Results

The computational framework successfully replicated the deployment of the S3 THV in a patient-specific model. Surrogate modeling using GPR showed excellent accuracy for structural outputs (MRE < 1%) but struggled with fluid dynamics, particularly TPG (MRE = 12.1%), due to challenges in flow boundary conditions. Validation metrics based on CDF comparisons using area metric indicated strong agreement for structural outputs (area metric < 5%), but discrepancies were observed for fluid dynamics results (area metric > 30%).

Discussion and conclusions

This study demonstrates the application of the ASME V&V40 framework for validating patient-specific TAVR models, highlighting the influence of model input parameters on biomechanical and hemodynamic responses. Validation through CDF comparisons highlighted strong agreement for structural metrics but noted discrepancies in fluid dynamics due to inherent differences between in-silico and in-vivo conditions. The study underscores the need for prospective validations on new patient models and refined metrics to account for inter-patient variability. Despite challenges, this framework enhances the reliability of TAVR simulations and supports their integration into clinical decision-making.

References

1. Viceconti M et al, Methods, 185:120-7, 2021.
2. Catalano C et al, 18th International Symposium on Computer Methods in Biomechanics and Biomedical Engineering, 2023.

Acknowledgements

This project has received funding from Horizon 2020 under grant agreement No 101017523.

FLUTICASONE PROPIONATE DISTRIBUTION AND DEPOSITION IN CATS WITH BRONCHIAL AND NON-BRONCHIAL DISEASE

Carla Zamora (1), Mauro Malvè (2), Rocio Fernández-Parra (3)
[1]*Doctoral School, Catholic University of Valencia San Vicente Mártir, Valencia, Spain*
[2]*Public University of Navarre (UPNA), Pamplona, Spain*
[3]*Catholic University of Valencia San Vicente Mártir, Spain*

Introduction

Lower airway inflammatory diseases in cats, including asthma and chronic bronchitis, have a prevalence of 1–5% [1]. Computed tomography (CT) scans of cats with lower airway disease can reveal abnormalities such as bronchial wall thickening, patchy alveolar patterns, and bronchiectasis [2]. The primary treatment involves inhaled corticosteroids.
The aim of this study was to evaluate and compare the distribution and deposition of fluticasone propionate particles in client-owned cats presenting with a bronchial pattern on thoracic CT images and those with normal thoracic CT findings, using computational fluid dynamics (CFD).

Methods

Thoracic CT scans from client-owned cats were divided into two groups: non-bronchial disease (NBD, n=12) and bronchial disease (BD, n=12). For each case, a three-dimensional geometry of the trachea and seven lobar bronchi was reconstructed. The geometry of each model was discretised using a tetrahedral mesh, and simulations were conducted with ANSYS CFX. An unsteady, complete respiratory cycle was applied to each case. Imposed flow rates were 16.8 and 16.1 ml/s/kg for inspiration, and 13.9 and 12.7 ml/s/kg for expiration, for the non-bronchial and bronchial disease groups, respectively [3]. The analysis included aerosol particles measuring 1 µm and 10 µm in size, with a density of 1320 kg/m³. These particles, released from a simulated inhaler, travelled through the airways, where they either impacted the airway walls at different regions (trachea, bifurcation,
right cranial, middle or caudal bronchus, right accessory bronchus, left cranial or caudal bronchus), remained suspended, or exited through the model's outlets.

Results

The body weight of the NBD group ranged between 1.5 kg and 6.5 kg. In the BD group body weight ranged from 2.8 to 8.2 kg. Both groups exhibited a similar proportion of particles exiting the model (see Table 1).

Group	NBD		BD	
Particle	1µm	10µm	1µm	10µm
Outlet	97.67	95.05	98.00	95.62
Suspension	0.77	1.37	0.65	1.05

Table 1: Percentage of particles of 1 and 10µm through the outlets or remained in suspension. NBD: non-bronchial disease; BD: bronchial disease.

Particles measuring 10 µm tend to be trapped in greater numbers within the bronchial tree compared to 1 µm particles, although fewer are captured in the trachea, with a larger proportion remaining in suspension (see Table 1). No particles were observed on the bronchial walls of the right cranial and right accessory lobar bronchi (Figure 1). Conversely, the right mainstem and caudal bronchi were the regions with the highest number of trapped particles on their walls, with a median of 0.27% for both groups. The highest values were observed in the NBD group, reaching up to 1.1%.

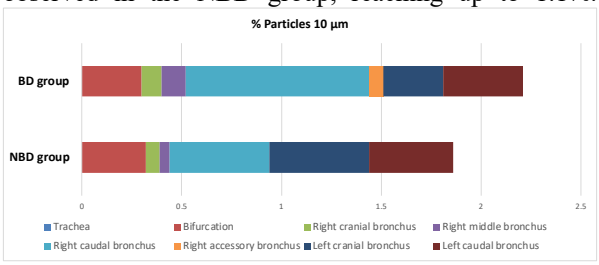


Figure 1: Percentage of 10µm particles deposited at the model. NBD: non-bronchial disease; BD: bronchial disease.

Discussion

This study presents a computational analysis of particle transport and deposition in the lower airways of feline patients exhibiting bronchial and non-bronchial patterns. Among the findings, the right accessory bronchus was identified as the region with the lowest particle deposition. This outcome is likely due to the bronchus being the narrowest and smallest region in the reconstructed model, which poses challenges for particle entry, particularly for larger particles. In contrast, the right mainstem and caudal bronchi, characterized by their larger diameters, were the regions where the highest number of particles were trapped. This suggests that a larger bronchial diameter may facilitate easier particle entry and increased deposition in these areas in cats.

References

1. Padrid P. Chronic bronchitis and asthma in cats. Philadelphia: WB Saunders; 2009.
2. Oliveira CR et al, Vet Radiol Ultrasound, 52(4):368–76, 2011.
3. Lin CH et al, J Feline Med Surg, 16(8):616-622, 2014.

Acknowledgements

This study is supported by the grant PID2021-125731OB-C31 and PID2021-125731OB-C33 from the Spanish Ministry of Science and Innovation MCIN/AEI/10.13039/501100011033/ and FEDER ('A way to build Europe`).

FSI MODELLING OF ASCENDING AORTIC ANEURYSMS WITH INVERSE IDENTIFICATION OF PATIENT-SPECIFIC MATERIAL PROPERTIES

Sabrina Nocerino (1), Chiara Catalano (2), Karol Calò (1), Sara Zambon (1), Salvatore Pasta (2), Umberto Morbiducci (1), Diego Gallo (1)

(1) Politecnico di Torino, Italy; (2) Università degli Studi di Palermo, Italy

Introduction

Biomechanical stimuli are crucial in the progression of ascending thoracic aortic aneurysm (ATAA) [1,2,3], with structural wall stress and strain playing a role in the risk of ATAA rupture [2,3], and with altered wall shear stress (WSS) playing a role in vascular degradation [1] and adverse remodelling [2]. Currently, biomechanical stimuli are typically obtained *in silico* through computational fluid dynamics (CFD) and computational solid mechanics (CSM) simulations. However, debate remains regarding CFD and CSM reliability due to (i) modelling assumptions and incomplete/uncertain input data derived from clinical sources, and (ii) the complex interplay between hemodynamic and structural stresses, which is often overlooked as these factors are studied separately. To address these challenges, this study introduces a semi-automatic fluid-structure interaction (FSI) framework that integrates the inverse identification of patient-specific aortic wall material properties, aiming at minimizing a primary source of uncertainty while enabling a comprehensive assessment of aortic biomechanics.

Methods

The proposed FSI framework is illustrated in Figure 1. Aortic geometries including the valve orifice plane, aortic root, and supra-aortic vessels are reconstructed at peak systole and at end-diastole from retrospectively-gated computed tomography angiography (CTA) [2]. Patient-specific transaortic jet velocity measured by Doppler echocardiography and pressure data obtained through brachial cuff measurements are used as input data. The vessel wall is modeled as a nonlinear isotropic hyperelastic Neo-Hookean solid with uniform thickness. To identify patient-specific material properties, an inverse method based on the volume of the ascending aorta (AAo) at peak systole is adopted [3]. After obtaining the diastolic tensional state through prestress simulations [4], the patient-specific systolic blood pressure is prescribed in CSM simulations using different Young's modulus values, within the previously reported range 0.8-8.0 MPa [3]. An exponential regression model is then used to find an analytical function linking the aortic Young's modulus with the simulated systolic AAo volume. Inverting this analytical function and knowing the measured systolic AAo volume, the patient-specific Young's modulus can be determined. Following a prestress simulation using the identified Young's modulus, FSI simulations are conducted with a two-way arbitrary Lagrangian-Eulerian (ALE) formulation. As for boundary conditions, homogeneous Dirichlet conditions are applied at the ring-shaped solid domain boundary sections in terms of null displacement. Doppler-derived flow rates are imposed in terms of flat velocity profile at the fluid inflow section. Zero-dimensional (0D) models are coupled to the 3D fluid domain outflow sections. The 0D parameters are tuned to match patient-specific cuff pressure measurements in coupled 0D and one-dimensional (1D) simulations. All simulations are performed using the finite element-based solver SimVascular.

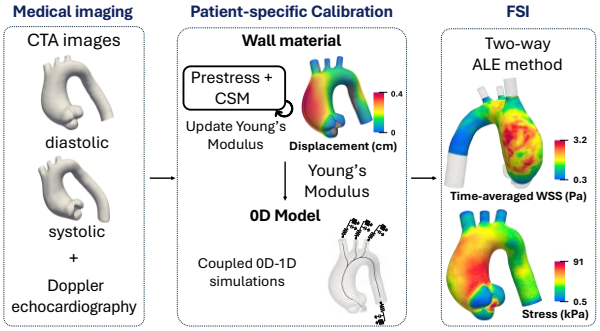


Figure 1: Workflow of the FSI framework.

Results

For a representative patient (Figure 1), the regression analysis AAo volume *vs*. Young's modulus shows an excellent goodness-of-fit, with an R^2 value of 0.99 and a sum of squared residuals equal to 0.43 cm^6. The CTA measured AAo volume at peak systole was 106.90 cm^3, resulting in a Young's modulus of 2.43 MPa. The AAo volume at peak systole obtained from the FSI simulation with patient-specific material properties was 104.34 cm^3, resulting in an error equal to -2.39%.

Discussion

By reconstructing the valve orifice, the FSI framework allows to simulate both tricuspid and bicuspid valve morphologies. The framework enables the exploration of the synergistic action of hemodynamic and structural stress, potentially revealing distinct or combined effects of these biomechanical stimuli on ATAA progression.

References

1. De Nisco et al., *Med Eng Phys*, 82 :119-129, 2020.
2. Pasta et al., *Ann Thorac Surg*, 110(5):1595-1604, 2020.
3. Trabelsi et al., *Ann Biomed Eng*, 44:84-98, 2016.
4. Bäumler et al., *Biomech Model Mechanobiol*, 5:7-28, 2020.

Acknowledgements

This study was carried out within the project "ASSOCIATE", (2022L7KK7L) funded by the EU – NextGenerationEU, MUR, PRIN 2022 program (D.D.104 02/02/2022).

CELL ENCAPSULATION INTO PROTEINOSOMES FOR SHIELDING FROM BIOPRINTING SHEAR STRESS

Sara Manzoli (1), Matteo Nifosì (1), Martina Piccoli (2), Stefano Valente (3), Nicoletta Braidotti (3), Pierangelo Gobbo (3), Piero G. Pavan (1,2), Silvia Todros (1)

1. Department of Industrial Engineering, University of Padova, Italy; 2. Fondazione Istituto di Ricerca Pediatrica Città della Speranza, Padova, Italy; 3. Department of Chemical and Pharmaceutical Sciences, University of Trieste, Italy.

Introduction

3D bioprinting is a highly promising technique for fabricating cell-loaded constructs for muscle tissue engineering. However, a major challenge associated to this technique is the high shear and compressive stresses exerted on cells during extrusion through the printer nozzles [1]. To overcome this issue, myoblasts are here encapsulated into soft, semipermeable, biocompatible microcompartments called proteinosomes [2], that may act as protective shells. Numerical analyses with the Finite Element Method (FEM) are adopted to estimate proteinosomes deformation during printing and their capability to ensure cell shielding.

Methods

Proteinosome microcompartments were produced, modifying a previously published protocol [3], forming a Pickering emulsion (PE) by mixing an aqueous solution of protein-polymer nanoconjugates (containing bovine serum albumin and poly(N-isopropylacrylamide)), myoblast laden cell proliferating medium and 2-ethyl-1-hexanol volumes. Different cell densities (1'000, 100'000 and 500'000 cells/total volume) were suspended into the cell culture medium to investigate the best cell localization and viability. To standardize the production, different PE techniques were compared such as manual PE [2] and vortex assisted PE (10Hz, 10 seconds). Myoblasts' spatial localization into capsules' inner cavity was evaluated by means of fluorescence microscopy imaging and capsules' diameter distribution was obtained. The stress shielding capability of the proteinosomes was evaluated through FEM models (ABAQUS, Simulia, Dassault Systemès, France), simulating their mechanical response to typical nozzle-related stresses. Proteinosome membrane constitutive parameters were deduced based on previously published literature [2].

Results and discussion

The preliminary results of myoblast encapsulation are shown through fluorescence images obtained at the confocal microscope, where encapsulated cells can be observed (Figure 1A). For all the cell densities tested, the number of myoblasts being effectively included in the proteinosomes was analyzed through *ImageJ* (NIH [4]) software plugin. The only condition allowing a homogeneous myoblasts distribution into proteinosome inner cavity (2-6 cells were encapsulated) corresponded to 100'000 cells/total volume. Vortexed emulsions were characterized by the narrowest proteinosome diameter distribution density (Figure 1B). It was also found that the cell density did not affect proteinosome morphological parameters. FEM analysis showed that the shear stresses associated with the printing process were distributed exclusively at the level of proteinosome membranes, leaving their inner volume unstressed (Figure 1C). This suggested proteinosomes could be effectively used as cell shielding during the printing.

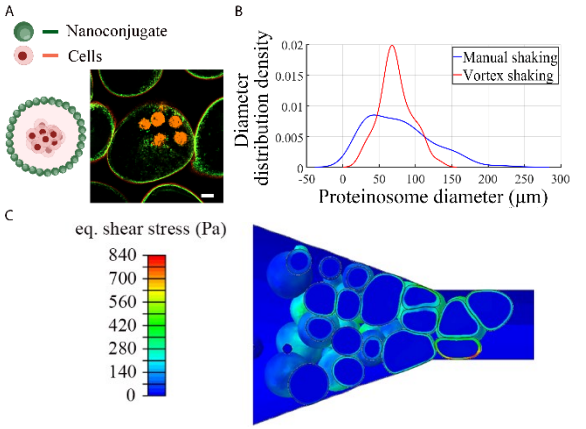


Figure 1: A) Graphical representation of a single cell-laden proteinosome and Z-stack fluorescence image of cell-loaded proteinosome (orange: cells; green: proteinosome membrane). Scalebar: 20 μm. B) Diameter distribution density of manually and vortexed produced proteinosomes. C) Equivalent shear stress (Pa) from FEM analysis of proteinosomes subjected to 3D extrusion printing.

References

1. Boularaoui et al, Bioprinting, 20, e00093, 2020.
2. Gobbo et al, Nat Mater, 17, 1145–1153, 2018.
3. Park et al, Eur. J. Org. Chem, 43, e202200968, 2022.
4. Schneider et al, Nature Methods, 9, 671–675, 2012.

Acknowledgements

This work was supported by the National Recovery and Resilience Plan, Mission 4, Component 2, Investment 1.1, by the Italian Ministry of University and Research, funded by the European Union Next Generation EU – Project Title "Novel visible light-degradable hydrogels embedded with cell-laden proteinosomes for the 3D bioprinting of diaphragm-like muscle tissues (3D-L-INKED)" (CUP C53D23008360001). The activity has been carried out in collaboration with Tissue Engineering Laboratory, Istituto di Ricerca Pediatrica Città della Speranza, Padova, Italy.

APPLICATION OF AN ELECTROSPUN SYNTHETIC MATERIAL FOR AN INNOVATIVE CARDIOVASCULAR GRAFT

Sara Ragusa (1,2), Emanuela Bologna (1), Mariano Licciardi (2), Massimiliano Zingales (3)

1. *Advanced Medical Engineering Devices s.r.l.,90141 Palermo, Italy;*
2. *Dipartimento di Scienze e Tecnologie Biologiche Chimiche e Farmaceutiche (STEBICEF), Università degli Studi di Palermo, 90123 Palermo, Italy;*
3. *Dipartimento di Ingegneria, Università degli Studi di Palermo, 90128 Palermo, Italy.*

Introduction

Graft materials are related to post-operative complications of aneurysm repair [1]. In the case of Endovascular Aneurysm Repair (EVAR), stent-graft (Nitinol frame and polymeric graft) is an artificial blood conduit, designed to act as a false lumen at the site of abdominal aneurysm. Polyethylene terephthalate (PET, Dacron) and expanded polytetrafluoroethylene (ePTFE) are used as graft materials. They result stiffer to diameter expansion than native vessel, perturbating the Windkessel effect [2]. The mechanical mismatch between aortic graft and native aorta leads to intimal hyperplasia, hemodynamic alterations in cardiovascular system and long-term cardiovascular morbidity. [3].
This work aims to investigate the Poly (1,4-butylene succinate) (PBS) as innovative graft materials by means electrospinning technology, to realize a biomimetic graft able to match the structure and mechanical features of aorta.

Methods

PBS is a biocompatible aliphatic polyester with interesting properties which makes it applicable in biomedical field [4,5]. To perform electrospinning, a solution of PBS and Ciprofloxacin (CPX) in 1,1,1,3,3,3-hexafluoroisopropanol (HFIP) was used. The electrospinning process parameters, such as applied voltage, needle-collector distance and flow rate, the concentration of polymer in solution and the effect of environmental conditions were studied to optimize the process and the fabrication. Scanning electron microscopy (SEM) was adopted as a method to study fibers morphology. In addition, uniaxial mechanical tests were performed to investigate the graft mechanical behavior in circumferential and longitudinal directions.

Results

Figure 1 shows the morphology of graft obtained by a solution of 22% of PBS in HFIP with CPX as a result of a optimization process. The diameter distribution of the fibers is not uniform with a values range of 100-300 nm The mechanical tests indicate the anisotropic properties of the sample. The Young Modulus of the longitudinal direction is larger than that of the circumferential direction (Figure 2).

Discussion

Electrospinning allows the fabrication of fibrous scaffolds with nanometric diameter, able to reproduce the structure of native vessel tissue. At the same time, environmental condition and process parameters have a major influence on the process, preventing the technology reproducibility. The morphology of electrospun fibers influences the physical and mechanical properties of the resulting grafts [6]. PBS can be considered an interesting material, characterized by easy processability. It could be used for the inner layer of a structured graft, as interface with blood flow. Due to its biodegradability, a non-biodegradable material is needed to provide long-term mechanical support.

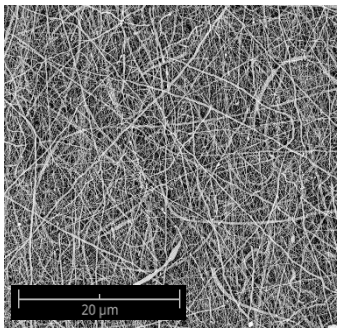


Figure 1: SEM image of graft morphology obtain by a solution of 22% of PBS.

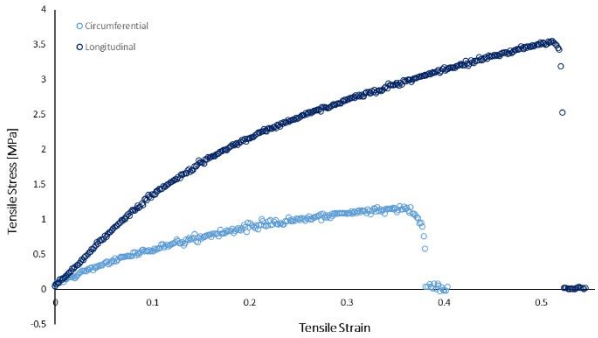


Figure 2: Uniaxial stress-strain curves for the PBS in longitudinal and circumferential directions.

References

1. Sun et al, J Funct Biomater, 15(9):248, 2024
2. Ferrari et al, J Biomech, 86:132-140, 2019
3. Bisacco et al, Eur J Vasc Endovasc Surg, 63(4):567-577, 2022.
4. Miceli et al., Polymers (Basel), 14(21), 2022.
5. Cicero et al, J Biomed Mater Res B Appl Biomater, 110(1):125-134, 2022.
6. Cooper et al, ACS Omega, 3(5): 5547-5557, 2018

FLUID-STRUCTURE INTERACTION STUDY POST-LEFT ATRIAL APPENDAGE INVERSION PROCEDURE ON PATIENT-SPECIFIC MODELS

Silvia Puleo (1), Roberta Scuoppo (1), Giuseppe Sausa (2), Stefano Cannata (3), Giovanni Gentile (4), Julius M. Guccione (5), Ghassan S. Kassab (6), Caterina Gandolfo (3), Salvatore Pasta (1,2)

1.Department of Engineering, University of Palermo, Palermo, Italy; 2. Department of Research, IRCCS ISMETT, Palermo, Italy; 3. Interventional Cardiology Unit, IRCCS ISMETT, Palermo, Italy; 4. Radiology Unit, IRCCS ISMETT, Palermo, Italy; 5. Department of Surgery, University of California San Francisco, San Francisco, USA; 6. California Medical Innovations Institute, San Diego, USA.

Introduction

Atrial fibrillation (AF) increases the risk of thromboembolic events due to clot formation in the left atrial appendage (LAA). Left atrial appendage inversion (LAAI) has emerged as a minimally invasive, device-free alternative to traditional LAA exclusion methods. Using a suction-based catheter, the procedure partially inverts the LAA into the atrium, leveraging the heart's natural tissue responses for occlusion without permanent implants [1]. To evaluate the biomechanical and hemodynamic outcomes of LAAI, patient-specific fluid-solid interaction (FSI) analyses were performed on four LAA morphologies (chicken wing, windsock, cactus, cauliflower) to assess hemodynamic changes and thrombogenic potential within the inverted LAA.

Methods

Following LAAI simulations carried out by Scuoppo et al. [2], one-way FSI analysis was performed by coupling ABAQUS (v2021hf7, Dassault Systèmes, USA) with XFlow (v2022, Dassault Systèmes, USA) to estimate left atrial hemodynamics [3]. The deformed LAAI configuration served as the initial geometry. The Ogden material model combined with isotropic thermal expansion simulated left atrial contraction via a virtual temperature profile, with a luminal pressure of 2.5×10^5 MPa applied. Boundary conditions included fixing distal ends of inlets and outlets and constraining the inverted portion to replicate the tissue glue used during LAAI. Restart analysis accounted for stress fields generated during LAAI simulations. Blood was modeled as an isothermal Newtonian fluid (37 °C, viscosity: 0.0037 Pa·s, density: 1,060 kg/m³). Temporal and spatial resolutions were 2×10^{-4} s and 4 mm, refined to 0.2 mm near the appendage. Pressure waveforms were imposed at pulmonary vein inlets, with a velocity outflow condition at the mitral valve. Outlet extensions ensured stable flow. Two cardiac cycles, each lasting 0.9 seconds, were simulated for each FSI analysis.

Results

Maps of the vorticity parameter on the LAAI wall at peak systole and diastole were categorized into risk levels to identify regions with potential thrombosis risk (Fig. 1). At end-systole, critical areas were observed near the LAAI apex in the cactus morphology, while the chicken wing morphology showed high-risk regions throughout the cycle. The windsock primarily exhibited low to mid-risk areas, whereas the cauliflower morphology showed pronounced critical vorticity areas. During diastole, the cactus morphology uniquely demonstrated a notable reduction in vorticity risk compared to other phenotypes.

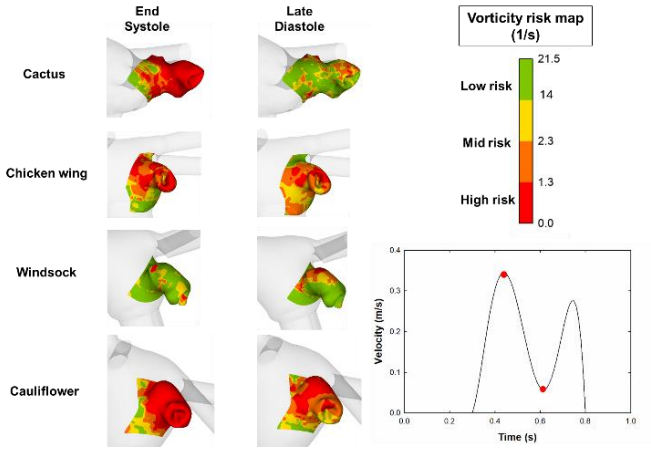


Figure 1: Vorticity risk maps indicating thrombogenic potential for each appendage morphology.

Discussion

Due to the LAA's tendency toward a low-flow state, FSI studies were performed in order to quantify vorticity and evaluate the thrombogenic potential for every appendage phenotype. The results of vorticity study showed that the windsock morphology minimizes the risk of thrombus formation and is most favourable to stable hemodynamic, instead the irregular shape of the cauliflower morphology presented serious hemodynamic issues. For this reason, the LAAI procedure for the cauliflower phenotype suggests to invert each of the lobes to remove the apex by multiple inversion. Although LAAI appears to be a promising therapeutic treatment for reducing clot formation, screening standards should be established to determine whether appendage morphologies are anatomically appropriate for the inversion procedure. Such measures could enhance patient outcomes and reduce the risk of recurrent AF following the procedure.

References

1. Wang et al, Front Bioeng Biotechnol, 11:10111121, 2023.
2. Scuoppo et al, ECCOMAS 2024, 9, 2024.
3. Puleo et al, Sensors, 24:5040, 2024.

NUMERICAL MODELING OF THE MECHANICAL BEHAVIOR OF HYDROGELS FOR CARTILAGE TISSUE ENGINEERING

Silvia Spadoni (1), Marta Confalonieri (1), Silvia Todros (1), Elena Stocco (2), Silvia Barbon (2), Andrea Porzionato (2), Piero G. Pavan (1,3)

1. Department of Industrial Engineering, University of Padova, Italy; 2. Department of Neurosciences, Section of Human Anatomy, University of Padova, Italy; 3. Fondazione Istituto di Ricerca Pediatrica Città della Speranza, Padova, Italy

Introduction

Articular cartilage can be affected by pathologies with different degrees of severity, including osteoarthritis, which often require surgical intervention to repair chondral defects. A possible therapeutic strategy includes the use of biomaterials able to promote cartilage regeneration and exhibiting mechanical properties comparable to native cartilage.

Native and partially oxidized polyvinyl alcohol (PVA) hydrogels have emerged as promising candidates for cartilage repair and regeneration, due to their excellent biocompatibility, high water absorption, customizable mechanical properties and low friction coefficient [1]. Among several aspects to be assessed in the performance of PVA scaffolds, the time-dependent compressive behavior is of particular importance to predict *in vivo* short-term mechanics.

Methods

PVA hydrogels are prepared in different concentrations (15, 20 and 25 wt% in water) according to a consolidated protocol [2], obtaining a physical cross-linking through three freeze-thawing (FT) cycles (F: − 20°C for 24 h; T: + 4°C for 24 h). Mechanical tests are performed on a Bose ElectroForce® Planar Biaxial Test Best instrument (TA Instruments, USA), in different loading conditions, including tensile and compressive, almost-instantaneous and long-term protocols. All the mechanical tests are carried out on samples soaked in PBS solution.

Finite element analyses (FEA) are performed using ABAQUS Standard (Simulia, Dassault Systèmes, France). An isotropic poro-visco-hyperelastic material model is adopted to account for the mechanical effect of both solid and liquid phases of PVA hydrogels, refining a previously adopted approach [3]. The instantaneous elastic response of the PVA is described by means of an isotropic hyperelastic model of Ogden form. The viscoelastic behavior of the solid phases is described through a Prony series with 4 terms:

$$g_R(t) = \frac{G_R(t)}{G_R(0)} = 1 - \sum_{i=1}^{4} g_i[1 - \exp(-t/\tau_i)] \qquad (1)$$

where $G_R(t)$ is the shear relaxation, $G_R(0)$ is the instantaneous modulus, and g_i and τ_i are the constitutive parameters obtained by a fitting to the tensile stress-relaxation data. The time-dependent volumetric response is obtained combining FEA with an optimization procedure in MATLAB (MathWorks) by fitting the model to indentation-consolidation data, in order to estimate permeability and compressibility of the hydrogels.

Results

Almost-instantaneous compressive tests show that the hydrogel stiffness increases with the wt% of PVA in water. The time-dependent behavior shows a stress relaxation of about 40% of the initial stress value. The compressive mechanical behavior of PVA hydrogel at concentration of 15 wt% is shown in Fig. 1, comparing experimental data and numerical results. A similar agreement between experimental and numerical data is obtained for PVA hydrogels at concentrations of 20 and 25 wt% (data not shown here for brevity).

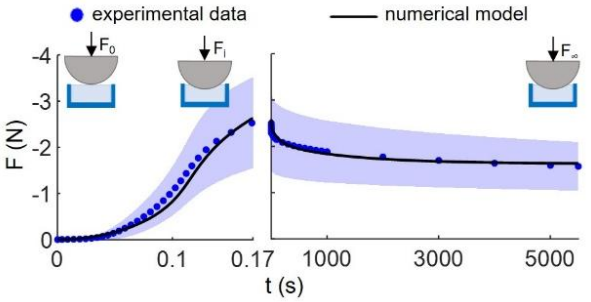


Figure 1: Experimental-numerical comparison for indentation and consolidation phases for PVA 15 wt%. Experimental data are represented as mean ± standard deviation; F_0, F_i, F_∞ represent, respectively, the force measured at the beginning of the test, at the end of indentation and at the end of consolidation phases.

Discussion

Among the hydrogels considered in this work, PVA 25% has a compressive stiffness close to the lower values in the range of human articular cartilage reported in the literature [4]. The assumed constitutive model and the optimization procedure enable to obtain suitable constitutive parameters to capture the time-dependent compressive mechanical behavior of PVA hydrogels. These constitutive models are adopted to describe the compressive behavior of PVA hydrogels compared to articular cartilage (healthy and osteoarthritic) based on literature experimental data on human subjects.

Future developments will be aimed at numerical analyses simulating *in vivo* loading conditions and patient-specific cartilage defects.

References

1. Barbon et al, Processes, 9:730, 2021.
2. Stocco et al, J.Tissue Eng.Regen.Med., 11: 2060–70, 2015.
3. Todros et al, Bioengineering, 9:789, 2022.
4. Belluzzi et al, Processes, 11: 1014, 2023.

SHAPE OPTIMIZATION OF TMJ PROSTHETIC FOSSA: A KINEMATIC-DRIVEN APPROACH

Talal Bin Irshad (1), Giulia Pascoletti (1), Elisabetta M. Zanetti (1)

1. *Department of Engineering, University of Perugia, ITALY*

Introduction

Custom temporomandibular joint (TMJ) prostheses focus heavily on bone (fossa) interface customization, yet the design of joint surfaces remains underexplored, with existing approaches ranging from hinge-like to planar or incongruent geometries [1]. There is no consensus regarding optimal joint shape, size, or the inclusion of anatomical stops, leading to significant variability in solutions. While advancements in materials, such as PEEK have been made [2], the geometric and kinematic alignment of TMJ prostheses remains inconsistent. This study is aimed at addressing this gap by introducing a patient-specific method for optimizing the fossa geometry.

Methodology

CT-based segmentation and mandibular tracking data were used to build a multibody model in ADAMS (Hexagon Software, rel. 17). Prosthetic components, including artificial condyles and fossae, were designed in SolidWorks and evaluated through simulations with recorded jaw movements, using the ITAKA system. Two fossa designs, Compact Design Fossa (CDF) and Enhanced Stability Fossa (ESF) were tested to assess the efficiency of the methodology through key metrics: the range of motion, the peak penetration and the interference volume, here analyzed as indices of performance. The design of the articular surface of the fossa is finally optimized through an iterative approach.

Results

The existing designs proved to be inadequate due to high penetrations and limited ranges of motion (13°), highlighting the need for improved geometry, also a dislocation of the condyle was observed with the CDF design (Fig. 1b) The Modified Enhanced Stability Fossa (MESF), resulting from the iterative design aimed to minimize the penetration volume when patient-specific kinematics are applied, offered reduced wear risks, and enhanced the full recovery of mandibular movements (20°).

Discussion

This study underscores the importance of optimizing fossa designs in TMJ prostheses to restore natural condylar kinematics effectively using mandibular tracking data taken on the patient. By addressing limitations in existing designs, the optimized design enhances stability, reduces wear risks, and aligns with natural mandibular function. This kinematic-driven approach highlights the potential for improving prosthesis performance and for articular surface personalization in TMJ rehabilitation.

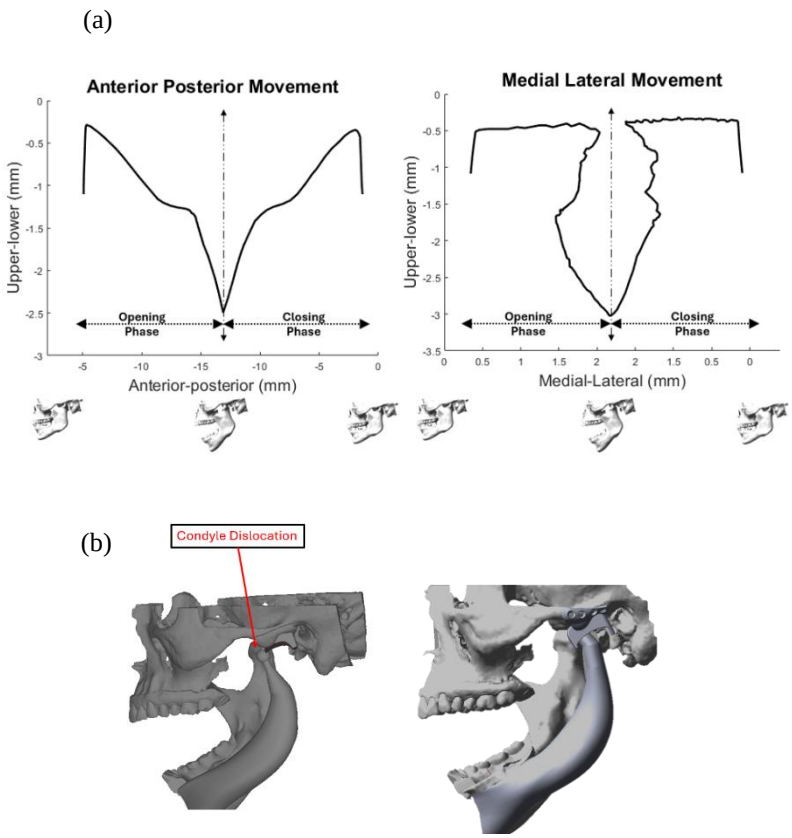


Figure 1: (a) Anterior-posterior and Medial-lateral movements (b) Prosthetised mandible movements at CDF and MESF

Reference

1. Valls-Ontañón *et al.*, *Journal of Cranio-Maxillofacial Surgery*, Jun. 2024, doi: 10.1016/J.JCMS.2024.06.011.

2. Genovesi, W., Comenale, I., Fernandes, M., & Filho, W. I. (2023). *Journal of Surgery*, *8*(16). https://doi.org/10.29011/2575-9760.001945

Acknowledgements

I would like to express my gratitude to 3DIFIC s.r.l. for their valuable support and knowledge, which greatly contributed to this work

NOVEL APPROACH FOR CHARACTERIZING VISCOELASTIC AND POROELASTIC PROPERTIES OF GELMA HYDROGELS

Marta Tosini[1,2], Eleonora Accili[1,2] ,Simona Villata[2,3], Marco Gaudiosi[2,3], Désirée Baruffaldi [2,3], Francesca Frascella[2,3], Fabrizio Pirri[2,3], Alberto Audenino[1,2], Diana Massai[1,2], Gianpaolo Serino[1,2]

1. Department of Mechanical and Aerospace Engineering; 2. Polito[BIO]MedLab, Politecnico di Torino, Italy; 3. Department of Applied Sciences, Politecnico di Torino, Italy.

Introduction

Cell behavior is significantly influenced by the mechanical properties of the microenvironment [1]. In particular, the viscoelasticity and poroelasticity of biological tissues, dependent on their time-dependent behaviors, have recently gained recognition for their crucial role in both healthy and pathological conditions. Thus, in case of *in vitro* models, it is essential to carefully design the mechanical properties of the materials employed for mimicking the cellular microenvironment. Gelatin-methacryloyl (GelMA) hydrogels are promising materials due to their tunable features, however their time-dependent mechanical properties remain underexplored. In this study, we developed a novel approach, based on nanoindentation tests, to investigate the load relaxation behavior of GelMA hydrogels. This enabled the characterization of viscoelastic and poroelastic parameters, providing a methodology for assessing the suitability of GelMA hydrogels in replicating the mechanical properties of healthy and pathological tissues.

Materials and Methods

Nine GelMA hydrogel compositions were synthesized [2], varying the methacrylation degree (Medium (M), High (H), and Very High (VH)) and the polymer concentration (7.5, 10, and 12.5%). Stress relaxation nanoindentation tests were performed in wet conditions (Phosphate Buffered Saline) at 37°C (Piuma nanoindenter, Optics11). Indentation depth (δ = 2000 nm) was reached in 1 s and held constant for 6 s before probe retraction. Each GelMA composition was tested in 3 batches, with 30-50 indentations per batch. The Hertz model [3] was used to assess the effective Young's modulus (E_{eff}) of the samples. Viscoelastic properties were analyzed with the generalized Maxwell model [4,5], described by the Prony exponential series (N = 2), enabling to obtain the shear moduli at maximum load (G_0) and at equilibrium (G_∞), with their difference indicating the degree of samples' viscoelasticity. The poroelastic properties analysis was performed using the Hu's model [6]. The drained Poisson's ratio and time constant were used to calculate the diffusivity coefficient (D) and intrinsic permeability (k). For fitting procedure carried out for the viscoelastic and poroelastic analysis, a genetic algorithm optimization was implemented to minimize risk of local minima (Matlab, R2023a).

Results

The effective elastic modulus of the samples ranged from 0.5 to 57 kPa, increasing with GelMA concentration and methacrylation degree (Table 1). Shear moduli showed a similar trend, spanning from 0.2 to 19 kPa (Table 2). Moreover, G_∞ was consistently lower than G_0, with a percentage decrease of 7–13%, reflecting different degrees of viscoelastic relaxation. For poroelastic analysis, the diffusivity coefficient was found in the order of magnitude of 10^{-11} m²/s for all samples, decreasing with higher methacrylation degrees. Intrinsic permeability decreased with increasing methacrylation and concentration (Table 3).

	7.5% E_{eff} (kPa)	10% E_{eff} (kPa)	12.5% E_{eff} (kPa)
M	0.9±0.4	4.7±1.1	12.1±9.0
H	2.0±1.1	5.3±1.5	28.9±11.0
VH	3.2±1.6	7.1±3.0	48±9.4

Table 1. Elastic analysis: Effective Young's modulus E_{eff}

	7.5%		10%		12.5%	
	G_0 (kPa)	G_∞ (kPa)	G_0 (kPa)	G_∞ (kPa)	G_0 (kPa)	G_∞ (kPa)
M	0.3±0.1	0.2±0.1	1.4±0.3	1.3±0.3	3.0±2.5	2.7±2.4
H	0.6±0.2	0.5±0.1	1.6±0.4	1.4±0.4	7.6±4.0	6.7±3.6
VH	0.8±0.3	0.7±0.2	2.3±1.0	2.0±1.0	16.0±2.8	14.1±2.6

Table 2. Viscoelastic analysis: Shear moduli G_0 and G_∞

	7.5% k (m^2)	10% k (m^2)	12.5% k (m^2)
M	$40.6 \pm 35.6 \cdot 10^{-18}$	$3.0 \pm 0.9 \cdot 10^{-18}$	$3.4 \pm 2.7 \cdot 10^{-18}$
H	$16.3 \pm 19.0 \cdot 10^{-18}$	$4.4 \pm 4.4 \cdot 10^{-18}$	$1.3 \pm 1.2 \cdot 10^{-18}$
VH	$11.6 \pm 7.8 \cdot 10^{-18}$	$3.2 \pm 3.5 \cdot 10^{-18}$	$0.48 \pm 0.3 \cdot 10^{-18}$

Table 3. Poroelastic analysis: Intrinsic permeability k

Discussion

This study presents a novel approach, based on nanoindentation tests, for characterizing the time-dependent mechanical properties of soft materials at the cell-scale. The effective elastic modulus values confirm the GelMA's effectiveness in mimicking, for example, the elastic properties of the lung tissue, both in healthy (0.5-3 kPa) and pathological (10-20 kPa) conditions. The viscoelastic model was utilised to derive the G_0 and G_∞ parameters, which offer immediate insight into the degree of relaxation exhibited by the samples. The poroelastic analysis showed that intrinsic permeability increases with softer samples. Overall, this work underscores the importance of reliable mechanical assessments for designing materials that closely replicate the properties of native tissues, with the final aim of advancing regenerative medicine applications.

References

1. Handorf et al, Organogenesis, 11(1), 2015.
2. Van Den Bulcke et al, Biomacromolecules, 31-38, 2000.
3. Hertz J, fur Reine Angew. Math, 156-171,1881.
4. Islam et al, J Biomech, 113, 2020.
5. Tosini et al, Appl Sci, 14(3), 2024.
6. Hu et al, Appl Phys Lett, 96, 2010.

CO-CULTURE CHAMBER PROTOTYPE TO DEVELOP A RETINA-ON-A-CHIP TO BE INTEGRATED IN A RETINA-BRAIN MULTIORGAN SYSTEM

Riccardo Tripputi (1) , Alessia Ciciriello (1), Asja Maggiore (1), Viviana Romano (1), Diego Albani (2), Carmen Giordano (1), Federica Boschetti (1)

1. Department of Chemistry, Materials and Chemical Engineering "Giulio Natta", Politecnico di Milano, Milan, Italy.

2. Istituto di Ricerche Farmacologiche Mario Negri IRCCS, Department of Neuroscience, Milan, Italy.

Introduction

Retinal diseases, such as age-related macular degeneration (AMD), are a major cause of blindness and a significant health challenge. A hallmark of AMD is the accumulation of drusen, similarly to beta-amyloid plaques buildup in Alzheimer's disease. The retina and brain in fact share several physiopathological features, such as inflammation and the glymphatic system's role in waste clearance [1], forming an interplay known as the "retina-brain axis. Moreover, recent evidence identifies the retina as a "window to the brain" offering a minimally invasive tool to study neurodegenerative diseases [2]. This work presents a Transwell-based co-culture chamber designed for a retina-on-a-chip system, which can be integrated into a multi-organ platform to better understand retinal pathologies and their link to the retina-brain axis.

Materials & Methods

The retina-on-a-chip housing is fabricated with Biomed Clear Resin using a Formlabs 3B+ 3D printer. It features a custom electrospun silk fibroin-PCL membrane mimicking Bruch's membrane [3], supporting RPE cells for photoreceptor function, while endothelial cells on the opposite side simulate choroidal tissue. Above the RPE layer, a 3D printable sodium alginate-gelatin (SA-G) bio-ink [4] creates a microenvironment for photoreceptor seeding (*Figure 1*).

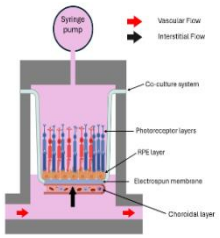


Figure 1. Illustration of the retina-on-a-

COMSOL simulations were conducted to analyse the velocity distributions under the Bruch's membrane and optimize the chamber geometry for uniform shear stress on cells. Hydraulic stability was tested by connecting the device to pumps and monitoring DMEM leakage under sterile conditions at 37°C and room temperature.

Results

The co-culture device consists of basal and apical chambers, interconnected by threading to securely hold the membrane in place. A dynamic-condition version supports the integration of fluidic systems to mimic in vivo retinal vascular flow, while a static-condition version compatible with 6-well plates was designed for simpler applications (*Figure 2*). An oval-shaped chamber was chosen because it provided a more uniform velocity distribution (with a variation of 5.36%, compared to the maximum velocity difference in the chamber) while minimizing vortex formation and recirculation. Hydraulic stability is ensured by a gasket placed in a dedicated housing, eliminating adhesive use and potential cytotoxicity.

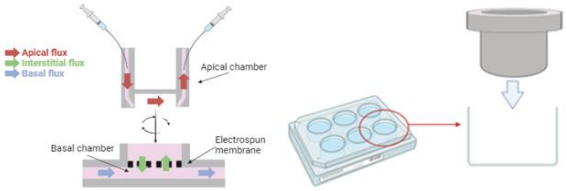


Figure 2. Dynamic and static versions of the co-culture chamber.

Discussion

The device features an innovative design ensuring secure membrane placement, reusability, and user-friendliness. Its versatility, supported by the integration of different membranes, makes it adaptable for various organ-on-chip models. Fluidic connections in both chambers recreate in vivo vascular flows, providing a valuable tool for advanced physiological modelling.

Conclusion

The 3D-printed co-culture chamber represents a promising platform for retinal studies, marking an initial step toward an in vitro retina-brain model. Ongoing studies are direct on evaluating sterilization efficacy and assessing endothelial cell viability under static and dynamic conditions. Additionally, a papain-based protocol is being tested to isolate photoreceptor cells from porcine retina [5] for seeding in SA-G bioink.

References

1. Delle C et al, Int J Mol Sci, 25:5734, 2024.
2. Alber et al, Alzheimer S & Dementia, 20:728-740, 2023.
3. Belgio et al, Bioengineering, 8:18, 2021.
4. Belgio et al, Applied Sciences, 14:6980, 2024.
5. Zayas-Santiago et al, Mol Vis, 15:1-9, 2009.

A DIGITAL TWIN FOR MYOCARDIAL BLOOD FLOW PREDICTION IN THE DIAGNOSIS OF CARDIAC PERFUSION DEFECTS

Viola Cusumano (1,2), Elisabetta Criseo (1,2), Andrea Baggiano (1), Giovanni Montino Pelagi (2), Guido Nannini (3), Alberto Redaelli (3), Gianluca Pontone (1), Christian Vergara (2)

1. Centro Cardiologico Monzino, Milano, Italy; 2. LaBS, Dipartimento di Chimica, Materiali ed Ingegneria Chimica "Giulio Natta", Politecnico di Milano, Italy; 3. Dipartimento di Elettronica Informazione e Bioingeneria, Politecnico di Milano, Italy

Introduction

Myocardial perfusion is vital for heart function, but it is often compromised by Coronary Artery Disease (CAD), leading to ischemic damage. Accurate assessment of myocardial blood flow (MBF) is crucial for the diagnosis and management of CAD. Currently, stress computed tomographic perfusion (stress-CTP) is the primary method for obtaining MBF data [1], but it carries drawbacks like radiation exposure and the use of stress agents. Digital twins, computational personalized models, offer a promising non-invasive alternative for estimating MBF, providing valuable insights for CAD patients. Computational studies on MBF prediction often use a single or multi-compartment Darcy model to represent microcirculatory flow but face challenges in some parameters' calibration due to patient-specific variability. This study introduces a digital twin with a group-based calibration that minimizes the error between computed MBF with stress-CTP MBF, highlighting its clinical predictive potential.

Methods

We retrieved both Coronary Computed Tomography Angiography (CCTA) and stress-CTP scans from 34 patients within the PERFECTION study dataset provided by the Monzino Cardiology Center, Milan. Coronary arteries and myocardium are automatically segmented [2] and processed to generate tetrahedral meshes. Myocardial perfusion regions are mapped to specific coronary outlets, as described in [3]. We employ a coupled mathematical model that integrates Navier-Stokes equations for large coronary flow with a three-compartment Darcy model for intramyocardial hemodynamics, incorporating vessel distensibility [3].
Accordingly, microcirculatory flow is assumed to occur within a porous medium, derived from a homogenization procedure. Personalized aortic inlet pressure [4] and customized intra-myocardial pressure are applied. Perfusion simulations are carried out in the generated domains. Calibration of the parameters is carried out by categorizing the PERFECTION cohort into six groups basing on stenosis degree and myocardium perfusion proportions across RCA, LCX, and LAD.
One patient per group (*calibration patients*) is used for calibration, yielding six distinct parameter sets. The calibration minimizes the global relative error between simulated and stress-CTP in-space-averaged MBF.
The calibrated model is applied to the remaining patients (*validation patients*) within their respective groups. Post-processed MBF maps are compared to stress-CTP maps using a validation error metric and statistical analysis to assess clinical agreement and diagnostic accuracy.

Results

In general, our model accurately captures pressure values and trends, reflecting physiological phasic flow and increased perfusion during diastole. Comparison with stress-CTP data shows a validation error of less than 10% in 20 out of 28 patients, with an error of less than 5% in 14 of them. Statistical analysis reveals a moderate correlation between clinical measurements and the model's predictions with a sensitivity of 0.77, specificity of 0.65, precision of 0.72 and accuracy of 0.7.

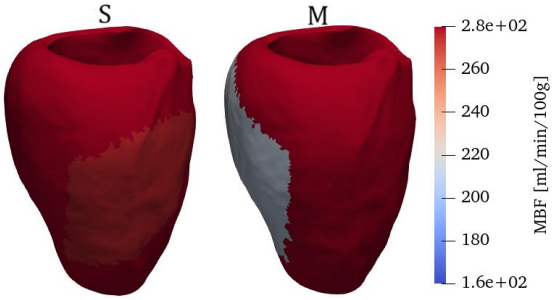


Figure 1: Digital twin simulated MBF (S) and stress-CTP measured one (M) of one validation patient.

Discussion

The study shows that the proposed digital twin accurately predicts average MBF in each region. Statistical analysis demonstrates the model's ability to distinguish between patients at risk and those not at risk. To our knowledge, this is the first study to achieve promising results in MBF prediction using a digital twin, calibrated independently of clinical measurements and validated on a cohort of 34 patients.

References

1. Pontone, G. et al.: JACC: Cardiovascular Imaging, 2019.
2. Nannini at al, APL bioengineering 8(1)- 2024.
3. Pelagi, G.M. et al.: Biomechanics and Modeling in Mechanobiology, 2024.
4. Pelagi, G.M. et al.: Annals of Biomedical Engineering, 2024.

APPLICATION OF CONSTITUTIVE MODELS FOR COMMERCIALLY AVAILABLE BIOPOLYMERS AND THEIR BLENDS

Vito Burgio (1), Martina Di Giacinti (1), Mariana Rodriguez Reinoso (1), Valentina Tuveri (1), Cecilia Surace (1)

1. Laboratory of BIO-MAterials and STructures, DISEG, Politecnico di Torino, Italy

Introduction

Medical-grade copolymers have been used in many biomedical applications, including tissue engineering scaffolds, implantable medical device manufacturing, textile-based medical solutions, and drug delivery platforms. These biomaterials, known as biodegradable polymers, enable a controlled degradation rate.

Polymeric medical devices are exposed to various strain states in-vivo, such as shear, creep and cyclic loading. Finite element modelling for testing these devices is the only way to show their performances during physiological and unphysiological stresses encountered in the implantation sites. Three different viscoplastic constitutive models were evaluated: the Three Network Model (TNM) [1], the Three Network Viscoplastic (TNV) Model [2], and the Flow Evolution Network (FEN) model [3]. This study aimed to assess the application of these three new constitutive models on commercially available biopolymers and their blends to explore their application for simulated medical devices.

Methods

The biodegradable medical-grade copolymers (Resomer® LC 703 S and Resomer® LR 704 S) used in this study were supplied in pellets by Evonik Industries. Specifically, the original polymers and the following blends combinations were tested: ratio 60:40, 40:60, and 50:50. Specimens were produced by compression moulding (CM) and injection moulding (IM).

The uniaxial tension tests were performed on dog bone-shaped specimens Type 5A (specimen design according to ISO 527-2 standard). The specimens underwent axial testing under displacement control with a displacement rate of 5 mm/min until failure. The tests were conducted at room temperature. Stress-strain curves were derived from the experimental data. The model fitting was performed in the MATLAB environment.

Results

The TNM and TNV material model gives accurate predictions of the mechanical behaviour of the biopolymers under investigation. The prediction of the mechanical behaviour is accurate up to 100% of logarithmic strain. After this value, at the end of the strain-hardening phase, both models become less accurate. In some cases, the models underestimate the true stress, while in others, they overestimate it. The FEN material model gives a good prediction of the biopolymer's strain-softening behaviour.

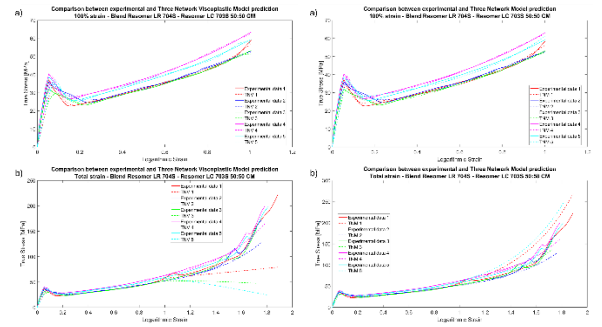


Figure 1: Results of the TNV calibration (Left) and TNM calibration (Right) on the experimental data on blend ratio 50:50 of Resomer® LR 704 S- Resomer® LC 703 S CM. a) prediction on data up to 100% logarithmic strain, b) TNV prediction considering the whole range of deformation.

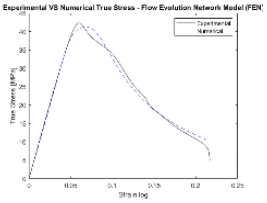


Figure 3: Results of the FEM calibration on the experimental data on blend ratio 60:40 of Resomer® LR 704 S- Resomer® LC 703 S CM.

Discussion

The TNM, TNV and FEN material models represent useful and powerful tools for predicting the behaviour of biopolymers. To perform high-reliability Finite Element Analysis, advanced constitutive models must be employed for the numerical validation and development of medical devices and implants.

This work represents the first application of these viscoplastic constitutive laws on biodegradable polymers. The future goal of this research involves applying advanced models to develop innovative devices for soft tissue repair, such as T-SURE (Tissue SUrgical REpair) and T-REMEDIE (Tendon REpair Medical DevIcE), which have been developed by the research group at the Politecnico di Torino.

References

1. Bergstrom, J. S., and Bischoff, J. E., 2010, “An Advanced Thermomechanical Constitutive Model for UHMWPE,” Int. J. of Structural. Changes in Solids, 2(1), pp. 31–39
2. J.S. Bergstrom, 2015. Mechanics of solid polymers: theory and computational modeling.
3. Dreher, M.L., Nagaraja, S., Bergstrom, J., Hayman, D., 2017. Development of a Flow Evolution Network Model for the Stress-Strain Behavior of Poly(L-lactide). J Biomech Eng 139. https://doi.org/10.1115/1.4037071